ATOMIC BEAM RESONANCE STUDY OF INDIUM

AN ATOMIC BEAM RESONANCE STUDY

OF

INDIUM-115m, INDIUM-117 AND INDIUM-117m

By

JOHN ALEXANDER CAMERON, B.A.

A Thesis

Submitted to the Faculty of Graduate Studies

in Partial Fulfilment of the Requirements

for the Degree

Doctor of Philosophy

McMaster University

October 1962

DOCTOR OF PHILOSOPHY
(Physics)

McMASTER UNIVERSITY
Hamilton, Ontario

TITLE: An Atomic Beam Resonance Study of Indium-115m, Indium-117 and Indium-117m

AUTHOR: John Alexander Cameron, B.A. (University of Toronto)

SUPERVISOR: Dr. R. G. Summers-Gill

NUMBER OF PAGES: viii, 117

SCOPE AND CONTENTS: It was the purpose of this research to investigate by the method of atomic beam magnetic resonance those isotopes of indium which may be recovered from neutron irradiated cadmium and to attempt to interpret the results in terms of existing nuclear theory. A description of the atomic beam method for the measurement of nuclear moments and of the apparatus used in the experiments will be given.

The results obtained for the three isotopes studied are:

In^{115m} $I = 1/2$ $a(^2P_{1/2}) = -904.348 \pm 0.016$ Mc/sec

$a(^2P_{3/2}) = -95.973 \pm 0.010$ Mc/sec

$\mu_I = -0.243707 \pm 0.000026$ nuclear magnetons

In^{117m} $I = 1/2$ $a(^2P_{1/2}) = (-) 931.5 \pm 2.0$ Mc/sec

$\mu_I = (-) 0.2510 \pm 0.0005$ nuclear magnetons

In^{117} $I = 9/2$

ACKNOWLEDGEMENTS

I should like to express my appreciation to all those who have made this research possible:

To Dr. R. G. Summers-Gill for his continual interest in the indium project and for helpful suggestions in many phases of the work;

To Mr. Keith Eastwood and the other members of the Atomic Beam Group for their willing cooperation in the maintenance and operation of the apparatus;

To the staff of the reactor for providing the many radioactive sources;

To my wife, Frances, for her unfailing patience and encouragement.

This research was supported through grants to the group by the National Research Council of Canada and through scholarships to the author by the Ontario Research Foundation and the National Research Council.

TABLE OF CONTENTS

LIST OF TABLES

LIST OF FIGURES

CHAPTER I

INTRODUCTION

Since the introduction of the magnetic resonance method of atomic beam spectroscopy (Rabi et al. 1938), the contribution of this field of research to the knowledge of atomic and nuclear properties has grown rapidly. Precise measurements can be made of atomic and nuclear multipole moments through their effect on the hyperfine structure of electronic states which live for periods in excess of 10^{-5} seconds. Measurements have been made to high precision using atoms whose nuclei are stable. Advances in technique have allowed the extension of the method to radioisotopes whose half-lives are quite short. Following the pioneer experiment on Na^{24} (Bellamy and Smith 1953) the method of detection using radioactivity has been used by a number of laboratories in Europe and North America. Groups presently active in this field are at the Argonne and Brookhaven National Laboratories, the University of California at Berkeley, Columbia University, and Princeton University in the United States, the University of Uppsala in Sweden, and McMaster University in Canada.

As the body of experimental data has grown, nuclear theory has been required to account for systematic trends which become clear. Ground state spins are fairly well accounted for by the shell model, while the collective model is required to explain the behaviour of dipole and

quadrupole moments in some groups of nuclides. The increasing complexity of nuclear theory results both from the need to account better for this increasing fund of nuclear data and from the desire to deal in a more realistic way with the forces which are thought to exist within nuclei.

The study of the indium isotopes In^{115m} and In^{117m}, and the preliminary investigation of In^{117} in this laboratory stems from the prospect of making such a detailed study of trends in nuclear moments within the large group of indium nuclei. In all, some 16 isotopes of indium and their 15 isomers have been produced and identified. Of these, 11 have now been studied by the method of atomic beams. The stable isotopes In^{113} and In^{115} were thoroughly investigated by a group at Columbia. The light isotopes In^{109}, In^{110m}, and In^{111} were cyclotron produced and studied by the atomic beam group at the University of California. The isotopes In^{113m}, In^{114m}, and In^{116m} were studied at the Argonne National Laboratory. The remaining isotopes are formed in very low abundance in energetic particle reactions or as fission products. Their half-lives range from an hour to a few seconds.

CHAPTER II

NUCLEAR MODELS AND THE COMPUTATION OF NUCLEAR MOMENTS

The interaction of an atomic nucleus with the electromagnetic field is most easily described in terms of electric and magnetic moments. These are assumed to originate in the nuclear charge and current distribution. Although a detailed knowledge of the nuclear wave function would be required in order to evaluate all the multipole moments, it is possible on the basis of fairly simple considerations to draw some conclusions regarding the moments.

The electric and magnetic multipole operators of order 2^λ are

$$Q_\lambda^\mu = e\, g_L\, r^\lambda\, Y_\lambda^\mu$$

$$M_\lambda^\mu = \mu_N\, \nabla(r^\lambda\, Y_\lambda^\mu) \cdot \left(g_L \frac{2}{\lambda+1} \underline{L} + g_S \underline{S}\right)$$

where $Y_\lambda^\mu(\theta,\phi)$ is the spherical tensor of rank λ and projection μ, (r,θ,ϕ) are the nuclear coordinates, g_L and g_S are the orbital and spin gyromagnetic ratios, e is the proton charge and μ_N is the nuclear magneton $e\hbar/2Mc$. Thus Q_λ^μ and M_λ^μ have parities $(-1)^\lambda$ and $(-1)^{\lambda+1}$ respectively. Therefore, the static moments, which contain the diagonal matrix elements of these operators, will be zero for odd λ in the electric case and for even λ in the magnetic case. This is premised on the fact that parity is a good quantum number for nuclear states. If this were not so, then diagonal matrix elements would arise due to mixing terms of opposite parity by the odd-parity operator. In view of the recent experiments

(Wu et al. 1957) indicating the non-conservation of parity in weak interactions, the absence of such degeneracies cannot be assumed a priori. It may be shown that if such an effect does occur, it must arise from the spin contributions of the nucleons and not from their convection currents in the nucleus.

Purcell and Ramsey (Ramsey 1950; Lee and Yang 1956) have found that the electric dipole moment of the neutron is less than e(5×10^{-20}cm). This implies that the mixing of states of different parity into a nuclear state is 3×10^{-13} at most. It may therefore be taken that no odd electric or even magnetic multipole moments exist in the nucleus.

Classically, the charge and current distribution gives rise to an infinite sum of multipole moments. Quantum mechanical effects related to the observability of the moments cause the expansion to terminate with only a finite number of terms. The diagonal matrix element for the moment of order 2^λ is

$$\langle I\, M' \,|\, Q_\lambda^\mu \,|\, I\, M \rangle = (I\, \lambda\, M\mu \,|\, I\, M') \langle I \| Q_\lambda \| I \rangle$$

where $\langle I \| Q_\lambda \| I \rangle$ is the reduced diagonal matrix element and $(I\, \lambda\, M\mu \,|\, I\, M')$ is a Clebsch-Gordan coefficient which is zero unless I, I, and λ satisfy a triangular relationship. That is,

$$\lambda \leq 2I \quad .$$

That is, the highest order multipole whose expectation value is non-vanishing is the 2^{2I}-pole. Hence, the magnetic dipole moment is observable only for nuclei of spin equal to or greater than 1/2. The electric quadrupole moment is observable only when the spin is equal to or greater than unity, and so on.

Whether a moment may in fact be measured under given experimental conditions depends on the nature of the field imposed on the nucleus by these conditions. In the atomic beam method, the field is imposed by the orbital electrons. This field is subject to the same type of multipole expansion and the interaction with the nucleus takes the form

$$\mathcal{H} = \sum_{\mu\lambda} (-1)^{\mu} Q^{\mu}_{\lambda}(\underline{r}_e)\, Q^{-\mu}_{\lambda}(\underline{r}_n)$$

where $\underline{r}_e$ and $\underline{r}_n$ are the electronic and nuclear coordinates respectively. The sum is therefore terminated at a value λ which is the smaller of 2I or 2J, where I and J are the nuclear and electronic angular momenta respectively.

Theoretical values of the nuclear moments Q_λ are obtained by calculating the diagonal matrix elements $\langle I\ I \mid Q_\lambda \mid I\ I \rangle$ from the nuclear wave function $\mid I\ M{=}I \rangle$. Here the spin quantum numbers have been shown explicitly and all other quantum numbers necessary to describe the state have been suppressed. In the exact nuclear wave function, these are many in number and in all but a few simple cases of low mass nuclei are too difficult to treat. The result of introducing assumptions which reduce the number of quantum numbers to reasonable proportions is a nuclear model. Several such models have been proposed which account for nuclear properties in various regions of nuclear mass. Some of those which have proved successful in dealing with nuclear moments will be discussed below.

1. THE SINGLE PARTICLE SHELL MODEL

The extreme single particle model assumes that many of the nuclear properties are vested in single nucleons outside an inert even-even core. The potential in which these extra particles move is a self-consistent potential of all the nucleons. It is a central well to which a spin-orbit term is added to account for the empirical "magic numbers" of neutrons or protons which give rise to particular stability of the nucleus.

The shell model energy levels which arise from the potential of Mayer and Jensen (Mayer and Jensen 1955) are shown for protons in Figure 1 and for neutrons in Figure 2, for Z and N, the proton and neutron numbers, up to 82. The angular momentum notation follows the spectroscopic form, the letter labelling the orbital angular momentum and the subscript giving the total angular momentum. Shell closure at the magic numbers 8, 20, 28, 50, and 82 is apparent. Also clear are the neighbouring levels of widely differing angular momenta near 50 and 82 which are used to explain the existence of nuclear isomerism in these regions.

The predictions of this model regarding the spins and parities of many ground and low-lying excited states of nuclei are borne out by experiment, although several notable examples of disagreement do exist. The single particle shell model makes a definite prediction regarding the nuclear multipole moments of odd-mass nuclei. The moments are assumed to arise from the vector coupling of the spin and orbital angular momenta of the single unpaired nucleon. The magnetic dipole moment is therefore given in nuclear magnetons by

Figure 1. Shell model energy levels of a single proton.

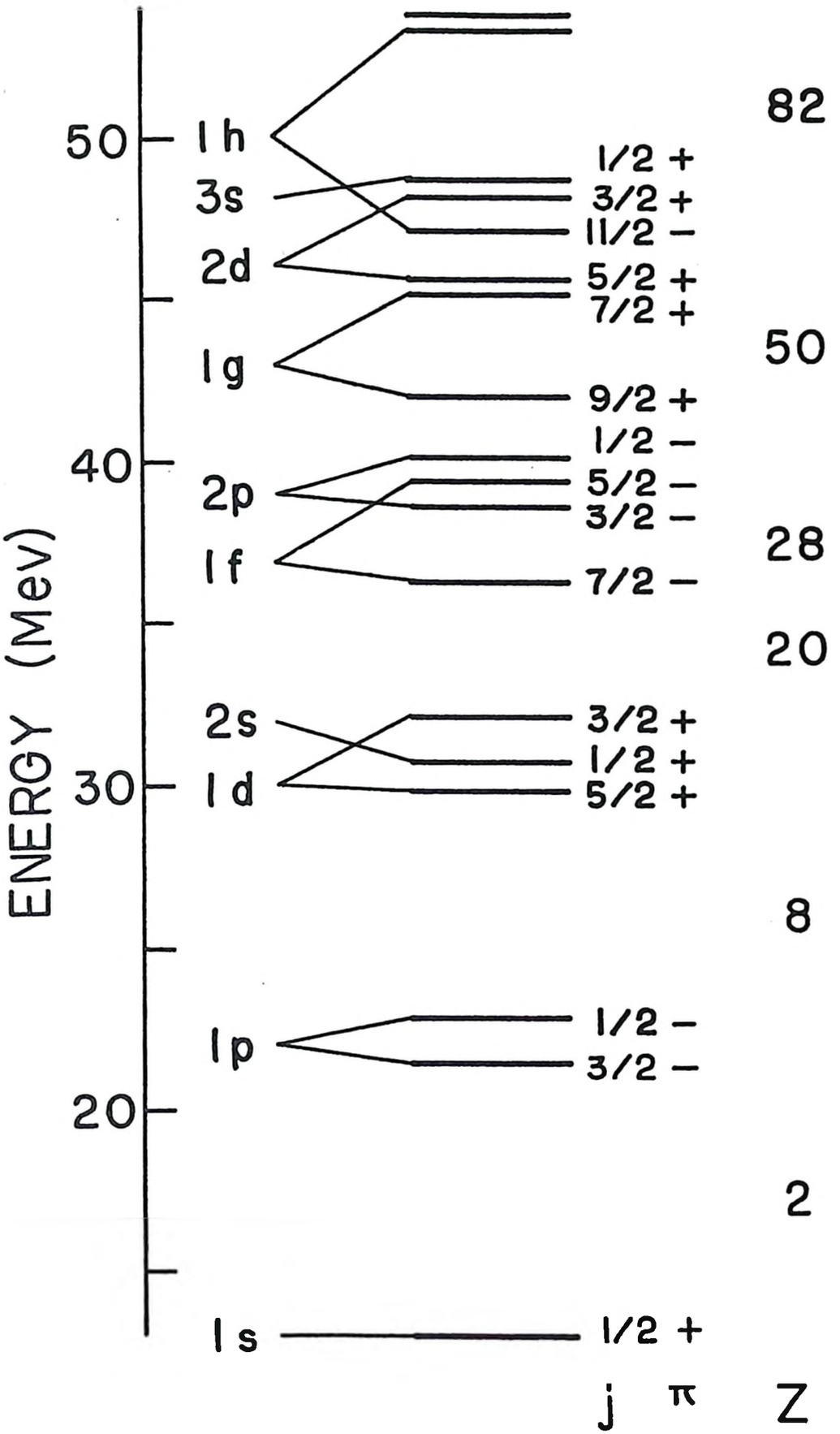
ENERGY (Mev)
50
40
30
20
1h
3s
2d
1g
2p
1f
2s
1d
1p
1s
1/2 +
3/2 +
11/2 −
5/2 +
7/2 +
9/2 +
1/2 −
5/2 −
3/2 −
7/2 −
3/2 +
1/2 +
5/2 +
1/2 −
3/2 −
1/2 +
82
50
28
20
8
2
j π
Z

Figure 1

Figure 2. Shell model energy levels of a single neutron.

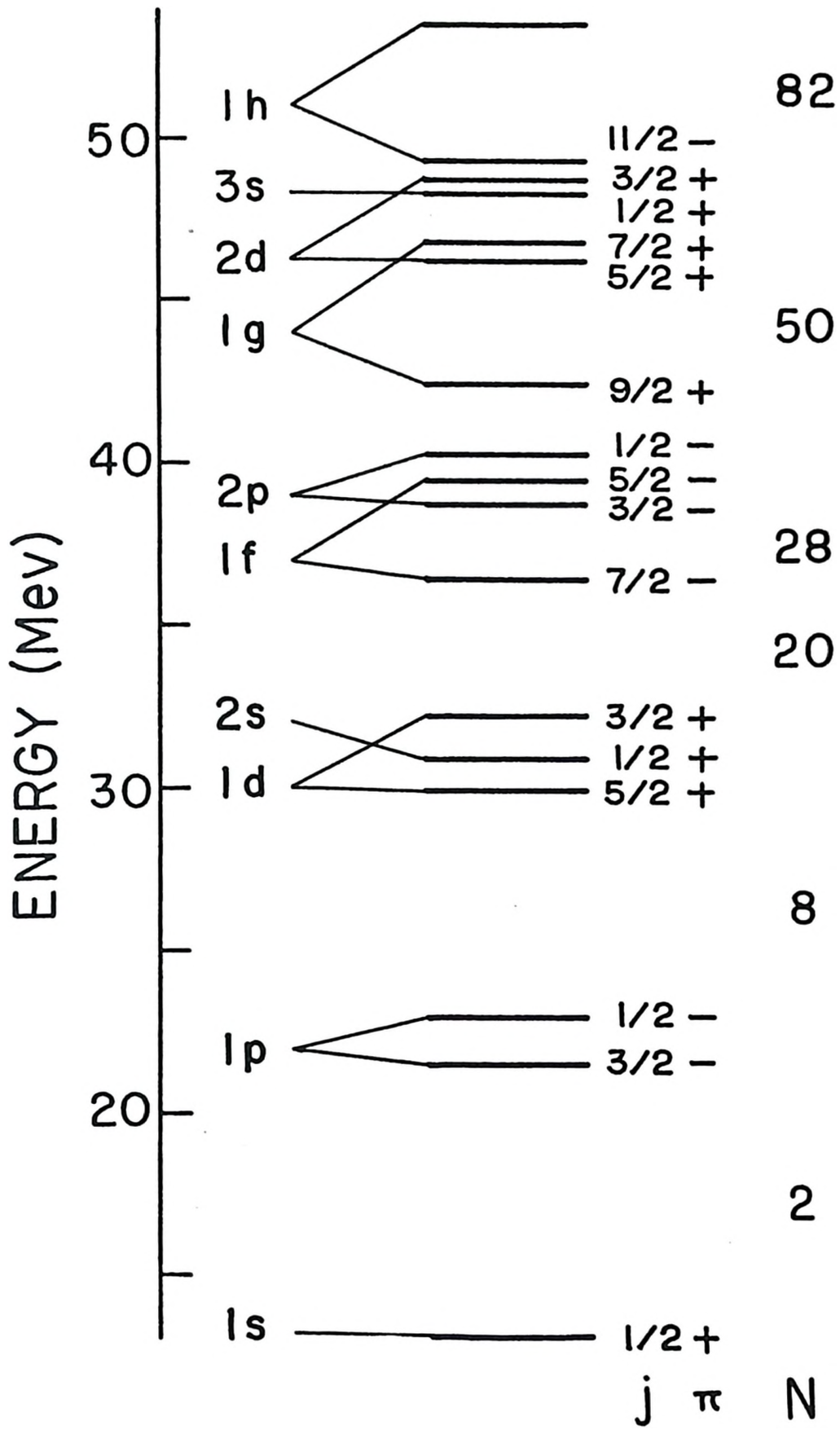
ENERGY (Mev)
50
40
30
20
1h
3s
2d
1g
2p
1f
2s
1d
1p
1s
11/2 −
3/2 +
1/2 +
7/2 +
5/2 +
9/2 +
1/2 −
5/2 −
3/2 −
7/2 −
3/2 +
1/2 +
5/2 +
1/2 −
3/2 −
1/2 +
82
50
28
20
8
2
j π N

Figure 2

$$\mu_{SP} = g_I j = \frac{1}{2} j \left[(g_\ell + g_s) + (g_\ell - g_s) \frac{\ell(\ell+1) - 3/4}{j(j+1)} \right]$$

where the nuclear spin I is equal to j, the total angular momentum of the unpaired particle. The spin and orbital gyromagnetic ratios g_s and g_ℓ are usually taken to have the free nucleon values

$g_s = 5.586$	$g_\ell = 1$	for protons
$g_s = -3.826$	$g_\ell = 0$	for neutrons.

The values of the nuclear moments obtained according to the above prescription are the Schmidt moments (Schmidt 1937) and are shown in Table I. With a few exceptions among light nuclei, magnetic moments for any given spin are found to fall roughly into two groups corresponding to, but lying between, the Schmidt values.

To improve the agreement with experiment, two modifications are possible without abandoning the general principles of the model. These involve revision of the gyromagnetic ratios, g_s and g_ℓ. Modification of both factors is expected on the basis of meson field theory, although this theory is not sufficiently developed to give accurate corrections. Miyazawa has shown (Miyazawa 1951) that the "quenching" of the anomalous spin magnetic moments from their free particle values toward the Dirac values of 2 and 0 for the proton and neutron can give results in close average agreement with experimental values. Modification of g_ℓ results if the effective charges of the proton and neutron are changed from their free particle values. These effects are expected to vary only slowly with nucleon number.

TABLE I

Schmidt Values of Magnetic Moments

Spin I	Odd Proton		Odd Neutron	
	$I = \ell + 1/2$	$I = \ell - 1/2$	$I = \ell + 1/2$	$I = \ell - 1/2$
1/2	2.793	- 0.264	- 1.913	0.638
3/2	3.793	0.124	- 1.913	1.148
5/2	4.793	0.862	- 1.913	1.338
7/2	5.793	1.716	- 1.913	1.488
9/2	6.793	2.533	- 1.913	1.565
11/2	7.793	3.559	- 1.913	1.619

The single particle shell model deals somewhat less successfully with the spins and magnetic moments of odd-odd nuclei. In this case, empirical coupling rules have been found (Nordheim 1951; Brennan and Bernstein 1960) for the spins of such nuclei. Given the form of coupling, the magnetic moments may be inferred roughly using the Schmidt moments, or to a higher degree of accuracy using the moments of neighbouring odd-mass nuclei to determine empirical g-values.

The nuclear quadrupole moment according to the shell model is that of the unpaired particle. For an odd proton of angular momentum j, it is

$$Q_j = -e^2 \frac{2j - 1}{2(j + 1)} \langle r^2 \rangle$$

where $\langle r^2 \rangle$ is the mean square radius of the proton orbit. For odd neutrons, no quadrupole moment is predicted. Although the shell model calculation can be modified to allow polarization of the even core, it is still not possible to quantitatively reach the experimental values of quadrupole moments in all nuclei. The most notable failure of the shell model occurs in the mass regions $150 < A < 190$ and $A > 225$. In these nuclei, the large observed quadrupole moments require the assumption of permanent nuclear deformation.

The model also predicts values, similar to the Schmidt values in form, for nuclear octupole moments (Schwartz 1955). The few octupole moments which have been measured lie between the extremes predicted by the model.

2. THE INDIVIDUAL PARTICLE MODEL

A natural extension of the above model is to take into account the separate motions of all the nucleons outside closed shells, the doubly magic core being considered inert. However, the calculations based on this model are quite involved for nuclei with more than a few extra-core particles. Simplifying assumptions which involve the concepts of isobaric spin and seniority aid in computation but fail above mass 40. This model has successfully treated cases of spin anomalies, such as that of Na^{23} where three $d_{5/2}$ protons couple to give a spin of 3/2.

3. CONFIGURATION MIXING

In spite of the obvious oversimplification of the single particle shell model in dealing with nuclear states, the single particle wave functions form a convenient basis for a representation. The approximate validity of the model suggests that the real nuclear wave function can be closely approached by the use of only a few single particle wave functions. The mixing coefficients are determined by the form of two-body interaction assumed to exist between extra-core particles. Due to the short range of nuclear forces, this is often assumed to be a contact interaction. Nuclear properties then become averages over a number of single particle states whose amplitudes must be calculated. The work of Arima, Horie and others (Arima and Horie 1954) has shown that many of the trends in moments may be accounted for by allowing small admixtures to occur in the nuclear wave function. Of particular importance are contributions from the spin-orbit partner of the dominant wave function.

4. THE COLLECTIVE MODEL

A small residual part of the two-body nuclear force has a longer range and leads to another class of nuclear motion. As the number of nucleons outside closed shells increases, the nucleus becomes increasingly deformable, with the result that collective surface oscillations of low energy become possible.

The surface oscillations, when expanded in a spherical harmonic series, begins with a monopole term. The virtual incompressibility of nuclear matter makes this oscillation one of very high energy. The following terms involve dipolar motion. The simplest such motion of the whole surface requires a motion of the centre of mass of the nucleus. Its coefficient in the expansion must therefore be set to zero. A dipole term which preserves the centre of mass is that in which the neutron and proton surfaces move in the opposite sense. It is this motion which is observed in the nuclear photoeffect as the "giant dipole" resonance at 15 to 20 Mev.

The oscillation of lowest energy is the next in the harmonic series, namely the quadrupole oscillation, in which the nucleus undergoes ellipsoidal deformation from its spherical equilibrium shape. Associated with a single quantum (phonon) of such an oscillation is an angular momentum of $2\hbar$ and positive parity. The energy of such an oscillation is, for spherical nuclei, between 0.5 and 2 Mev and depends primarily on the rigidity of the nuclear surface. Higher order oscillations exist at higher energies. Octupole vibrational levels have been observed in inelastic nucleon-nucleus scattering at energies of several million volts.

Far from closed shells, the two-body pairing force makes permanent deformation energetically favourable so that collective rotation becomes

possible. The loss of spherical symmetry removes the degeneracy of the magnetic substates of the shell model levels. The energies and decay modes of low-lying excited states provide a sensitive measure of the degree of nuclear deformation. This deformation in turn may be used to calculate dipole and quadrupole moments for the nucleus. The good agreement obtained with experimental values of these moments is one of the great successes of the model.

The collective motions of vibration and rotation may couple with particle excitation giving rise to nuclear states reminiscent of the electronic states of vibrating or rotating molecules. Indeed, much of the terminology of the collective model is similar to that used in molecular spectroscopy. In particular, it should be noted that the interaction of the particle excitations with the collective motion of lowest energy allows configuration mixing involving states of the same parity whose angular momenta differ by no more than two units. The theory of such interactions and its effect on nuclear properties such as the nuclear moments has been worked out in detail by Bohr, Mottelson, and others (Bohr and Mottelson 1953; Nilsson 1955). Treating the particle-surface coupling by perturbation theory, Bohr and Mottelson derive the expression

$$\mu = \mu_{SP} + \chi^2 \sum_{j'} \left\{ \left[-\alpha_{jj'}(\varepsilon_j - \varepsilon_R) + \beta_{jj'}(\varepsilon_{j'} - \varepsilon_R) \right] \left(\frac{\hbar\omega}{\hbar\omega + \Delta_{jj'}} \right)^2 \right\}$$

$$\pm \delta_{ll'} \chi^2 (\varepsilon_S - \varepsilon_L) \frac{3}{4(2l+1)} \frac{(2j-1)(2j+3)}{(j+1)^2} \frac{\hbar\omega}{\hbar\omega + \Delta_{jj'}}$$

where the mixing coefficients $\alpha_{jj'}$ and $\beta_{jj'}$ are given by

$$\alpha_{jj'} = 2j^2(2\ j\ 0\ 1/2 \mid j'\ 1/2)^2$$

$$\beta_{jj'} = \alpha_{jj'}\,\frac{j(j+1) + j'(j'+1) - 6}{2j(j+1)}$$

The energy terms contain the phonon energy $\hbar\omega$ and the energy difference $\Delta_{jj'}$ between the states j and j'. The collective gyromagnetic ratio g_R is usually taken to have the hydrodynamical value Z/A. The coupling strength is K^2. The term preceded by $\delta_{ll'}$ is non-zero only for the members of a spin-orbit doublet. The positive and negative signs are to be taken for a particle and hole state respectively.

5. TWO-NUCLEON FORCES

Recently, the treatment of two-nucleon correlations by methods similar to those used in the theory of superconductivity (Belyaev 1959) has led to a reinterpretation of the collective and particle motions in these terms. The principal result is a smoothing out of the Fermi surface of the nucleus. This means that the nuclear ground state is no longer a pure single particle state but consists of a distribution of states with amplitudes dictated by the shape of the Fermi surface and the requirements of conservation of angular momentum and particle number. Kisslinger, Sorensen, and others have considered the effect of such a model on nuclear properties, including the magnetic moments (Kisslinger and Sorensen 1960; Freed and Kisslinger 1961). Their results are similar to those of Bohr and Mottelson for the phonon mixing case. Freed and Kisslinger consider further the effects of core excitations but do not include collective motions in this.

6. SUMMARY

In the interpretation of nuclear moment data, the above theories should be considered complementary rather than in opposition to one another. The work mentioned above has shown a strong connection between configuration mixing and the collective motions in a common source, the nuclear correlations. Mesonic effects, both the quenching of nucleon moments due to suppression of recoil states by the Pauli exclusion principle and the additional electric and magnetic effects of meson exchange currents, have been shown to be large enough to account for appreciable changes in magnetic moments from the Schmidt values.

Since most of the more sophisticated models are able to account approximately for the values of nuclear moments, it is of interest to compare within neighbouring nuclei, isotopes or isotones, the trends in the nuclear moments as observed experimentally and predicted theoretically.

CHAPTER III

THE MEASUREMENT OF NUCLEAR MOMENTS

The spins and multipole moments of atomic nuclei have been measured under a number of experimental conditions. Such measurements may be classed under two general headings -- non-resonance methods and resonance methods.

The former grouping includes the early experiments involving the observation of hyperfine structure in atomic spectra, both optical and microwave, and the alternation of intensities in molecular band spectra. The experiments of Stern and Gerlach (Stern 1921) and others (Frisch 1933; Rabi 1933) on the focusing of atomic and molecular beams by inhomogeneous magnetic fields belong to this category. Recent additions to the non-resonance family are the nuclear alignment experiments at low temperatures. For radioactive species, the measurements of transition rates, internal conversion coefficients, angular correlation between radiations, and beta-ray spectrum shapes give information leading to nuclear spins and moments.

Resonance experiments have led to the most precise measured values of nuclear moments. Examples in this category are the nuclear absorption and induction experiments (Purcell 1946; Bloch 1946), paramagnetic resonance absorption, and the various double resonance techniques, as well as the methods of atomic and molecular beams. For measuring the effects of the microscopic environment on the nuclear

resonance, and in order to establish an absolute scale of magnetic moments, the nuclear magnetic resonance method is invaluable. However, the largest body of precise nuclear moment data has been obtained through relative measurements in atomic beam resonance experiments.

The great advantage of the atomic beam method for the measurement of nuclear moments is its high sensitivity and selectivity. Whereas the other methods outlined above require samples containing at least 10^{13} nuclei of the type being studied and an isotopic abundance of 0.1% or more, the atomic beam method can be applied to samples containing as few as 10^{11} atoms and to isotopes which occur in abundances of 10^{-9} or less. The requirement in the solid state resonance methods of crystal formation prevents the study of radioisotopes whose half-lives are shorter than several hours. Advances in techniques of beam production and detection have allowed the study in atomic beam experiments of isotopes whose half-lives are as short as 18 seconds. In the following sections the theoretical basis of the atomic beam method will be outlined as it applies to the experiments to be reported here.

1. THE ATOMIC HYPERFINE INTERACTION

The method of atomic beam radiofrequency spectroscopy depends on the interactions of the nuclear and electronic electromagnetic fields with each other and with externally applied magnetic fields. In the absence of such external fields, the total atomic Hamiltonian may be written as

$$\mathcal{H}_{total} = \mathcal{H}_{nuclear} + \mathcal{H}_{electronic} + \mathcal{H}_{hyperfine}$$

Since the nuclear energy levels are widely spaced compared to the electronic energies of the atom, that part of the wave function can, in

most cases, be assumed to separate from the rest. That is, in what follows, it will be assumed that the nucleus is in a single eigenstate of $\mathcal{H}_{nuclear}$, usually the ground state or a metastable isomeric state. The term $\mathcal{H}_{electronic}$, in which the nucleus is treated as a point charge, gives rise to the gross and fine structure of the atomic optical spectrum, with energies of the order of one electron-volt being typical. Such terms arise from the electrostatic interactions of the electrons with the nucleus and with each other, and from the magnetic interactions with each other through the spin and orbital magnetic moments. The final term gives rise to the hyperfine structure splitting of the electronic levels, with energies of the order of 10^{-5} to 10^{-6} electron-volts. Separation of the wave functions of $\mathcal{H}_{electronic}$ and $\mathcal{H}_{hyperfine}$ is usually possible. However, a small residual interaction occurs between hyperfine states of close-lying electronic levels, notably in fine structure multiplets.

In Chapter II, the form of the hyperfine interaction was written

$$\mathcal{H}_{hyperfine} = \sum_{\lambda\mu} (-1)^{\mu} \, Q^{\mu}_{\lambda}(\Sigma_e) \, \tilde{Q}^{\mu}_{\lambda}(\Sigma_n).$$

That is, the hyperfine interaction consists of a series of terms in which the 2^{λ}-pole of the nucleus interacts with the 2^{λ}-pole component of the electronic field. These terms are, in increasing order:

the magnetic dipole

$$\mathcal{H}_{M1} = h \, a \, \underline{I} \cdot \underline{J}$$

the electric quadrupole

$$\mathcal{H}_{E2} = h \, b \, \frac{3(\underline{I}\cdot\underline{J})^2 + \frac{3}{2}(\underline{I}\cdot\underline{J}) - I(I+1)J(J+1)}{2I(2I-1)J(2J-1)}$$

and the magnetic octupole

$$\mathcal{H}_{M3} = h\, c\, \frac{10(\underline{I}\cdot\underline{J})^3+20(\underline{I}\cdot\underline{J})^2+2(\underline{I}\cdot\underline{J})[-3I(I+1)J(J+1)+I(I+1)+J(J+1)+3]-5I(I+1)J(J+1)}{I(I-1)(2I-1)J(J-1)(2J-1)}$$

Higher order multipole interactions are of course present but they are small effects and have so far not been observed. The constants a, b, and c, whose units are those of frequency, are related to μ, Q, and Ω, the nuclear magnetic dipole, electric quadrupole, and magnetic octupole moments respectively. A detailed account of these relationships may be found, for example, in Kopfermann's Nuclear Moments (Kopfermann 1958). It is sufficient for the present work to note that they have the approximate form

$$a = \frac{\mu_I}{I} \times \text{electronic factor}$$

$$b = Q \times \text{electronic factor}$$

$$c = \Omega \times \text{electronic factor.}$$

Hence, the Fermi-Segrè formula

$$\frac{a_1}{a_2} = \frac{(\mu_I/I)_1}{(\mu_I/I)_2}$$

and corresponding relationships for the higher moments

$$\frac{b_1}{b_2} = \frac{Q_1}{Q_2}$$

$$\frac{c_1}{c_2} = \frac{\Omega_1}{\Omega_2}$$

follow for two isotopes in the same electronic state.

The above equations are exact only for a point nucleus and their failure to be borne out experimentally reflects this simplifying assumption. The breakdown of the assumption becomes particularly apparent in the study of atoms with S-state electrons. Here "hyperfine anomalies" of the form

$$\frac{a_1}{a_2} = \frac{(\mu_I/I)_1}{(\mu_I/I)_2}(1 + {}_1\Delta_2)$$

have been found in which ${}_1\Delta_2$ is 0.001 or larger. In other cases, where the electronic wave function vanishes at the origin, the hyperfine anomaly is much smaller.

The separation of $\mathcal{H}_{\text{electronic}}$ and $\mathcal{H}_{\text{hyperfine}}$ is not always a valid procedure, especially when the electronic level is part of a fine structure multiplet. The perturbing effect of a second electronic state causes a net repulsion between levels of the same total angular momentum and shifts such levels by an amount δW given approximately by

$$\delta W \approx \frac{1}{\Delta E}(\Delta W)^2.$$

If the separation ΔE between electronic levels is of the order of 1 e.v. and the hyperfine interval ΔW is of the order of 10^{-5} e.v., this effect is of order 10^{-10} e.v. It is clearly seen that the above perturbation is most appreciable for atoms having a small fine structure interval and large hyperfine splittings. The calculations have been made to second order by Schwartz (Schwartz 1955) for a number of cases in which experiments have been performed to sufficient accuracy to yield a value for the octupole interaction constant c. One such case is that of In^{115} in which the correction to c due to the perturbation is 0.0011 Mc/sec, a hundred times the value of c deduced from the uncorrected data.

The hyperfine Hamiltonian may be diagonalized by noting that

$$\underline{I}\cdot\underline{J} = \frac{1}{2}\left[F(F+1) - I(I+1) - J(J+1)\right] = \frac{1}{2}K$$

where

$$\underline{F} = \underline{I} + \underline{J}$$

is the total angular momentum of the atom. Thus the energy in a state of given F is a linear combination of a, b, and c:

$$W_o(F) = ha\frac{K}{2} + hb\frac{\frac{3}{4}K(K+1) - I(I+1)J(J+1)}{2I(2I-1)J(2J-1)} +$$

$$+ hc\frac{K^3+4K^2+\frac{4}{5}K\left[-3I(I+1)J(J+1)+I(I+1)+J(J+1)+3\right]-4I(I+1)J(J+1)}{I(I-1)(2I-1)J(J-1)(2J-1)}$$

The final term contributes very little to $W_o(F)$ due to the smallness of the interaction constant c. Extensive tables and graphs have been prepared by the atomic beam group at the University of California, Berkeley, in which only the dipole and quadrupole terms are considered (Baker 1960). In such graphs, $W_o(F)/ha$ is plotted as a function of b/a. An example is shown in Figure 3 for the case J = 3/2, I = 9/2, which is appropriate to indium isotopes of spin 9/2 in the $^2P_{3/2}$ electronic state. The equations of the straight lines are

$$\frac{W_o(6)}{ha} = \frac{27}{4} + \frac{1}{4}\frac{b}{a}$$

$$\frac{W_o(5)}{ha} = \frac{3}{4} - \frac{5}{12}\frac{b}{a}$$

$$\frac{W_o(4)}{ha} = -\frac{17}{4} - \frac{5}{24}\frac{b}{a}$$

$$\frac{W_o(3)}{ha} = -\frac{33}{4} + \frac{11}{24}\frac{b}{a}$$

Figure 3. Zero field spacing of the hyperfine energy levels of an atom with $J = 3/2$, $I = 9/2$.

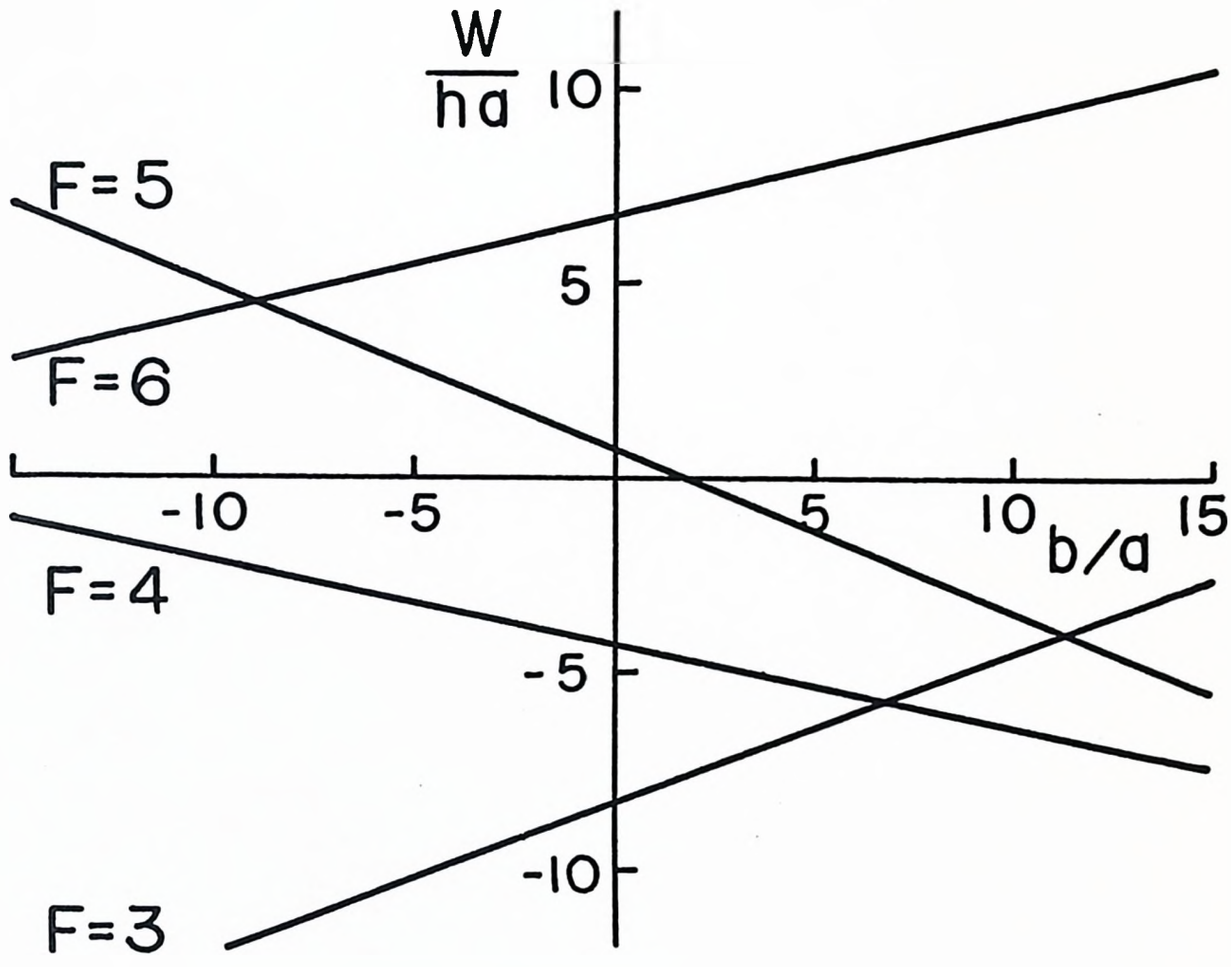

Figure 3

The hyperfine Hamiltonian may be diagonalized by noting that

$$\underline{I}\cdot\underline{J} = \frac{1}{2}\left[F(F+1) - I(I+1) - J(J+1)\right] = \frac{1}{2}K$$

where

$$\underline{F} = \underline{I} + \underline{J}$$

is the total angular momentum of the atom. Thus the energy in a state of given F is a linear combination of a, b, and c:

$$W_0(F) = ha\,\frac{K}{2} + hb\,\frac{\frac{3}{4}K(K+1) - I(I+1)J(J+1)}{2I(2I-1)J(2J-1)} +$$

$$+ hc\,\frac{5}{4}\,\frac{K^3+4K^2+\frac{4}{5}K\left[-3I(I+1)J(J+1)+I(I+1)+J(J+1)+3\right]-4I(I+1)J(J+1)}{I(I-1)(2I-1)J(J-1)(2J-1)}$$

The final term contributes very little to $W_0(F)$ due to the smallness of the interaction constant c. Extensive tables and graphs have been prepared by the atomic beam group at the University of California, Berkeley, in which only the dipole and quadrupole terms are considered (Baker 1960). In such graphs, $W_0(F)/ha$ is plotted as a function of b/a. An example is shown in Figure 3 for the case J = 3/2, I = 9/2, which is appropriate to indium isotopes of spin 9/2 in the $^2P_{3/2}$ electronic state. The equations of the straight lines are

$$\frac{W_0(6)}{ha} = \frac{27}{4} + \frac{1}{4}\frac{b}{a}$$

$$\frac{W_0(5)}{ha} = \frac{3}{4} - \frac{5}{12}\frac{b}{a}$$

$$\frac{W_0(4)}{ha} = -\frac{17}{4} - \frac{5}{24}\frac{b}{a}$$

$$\frac{W_0(3)}{ha} = -\frac{33}{4} + \frac{11}{24}\frac{b}{a}$$

Figure 3. Zero field spacing of the hyperfine energy levels of an atom with J = 3/2, I = 9/2.

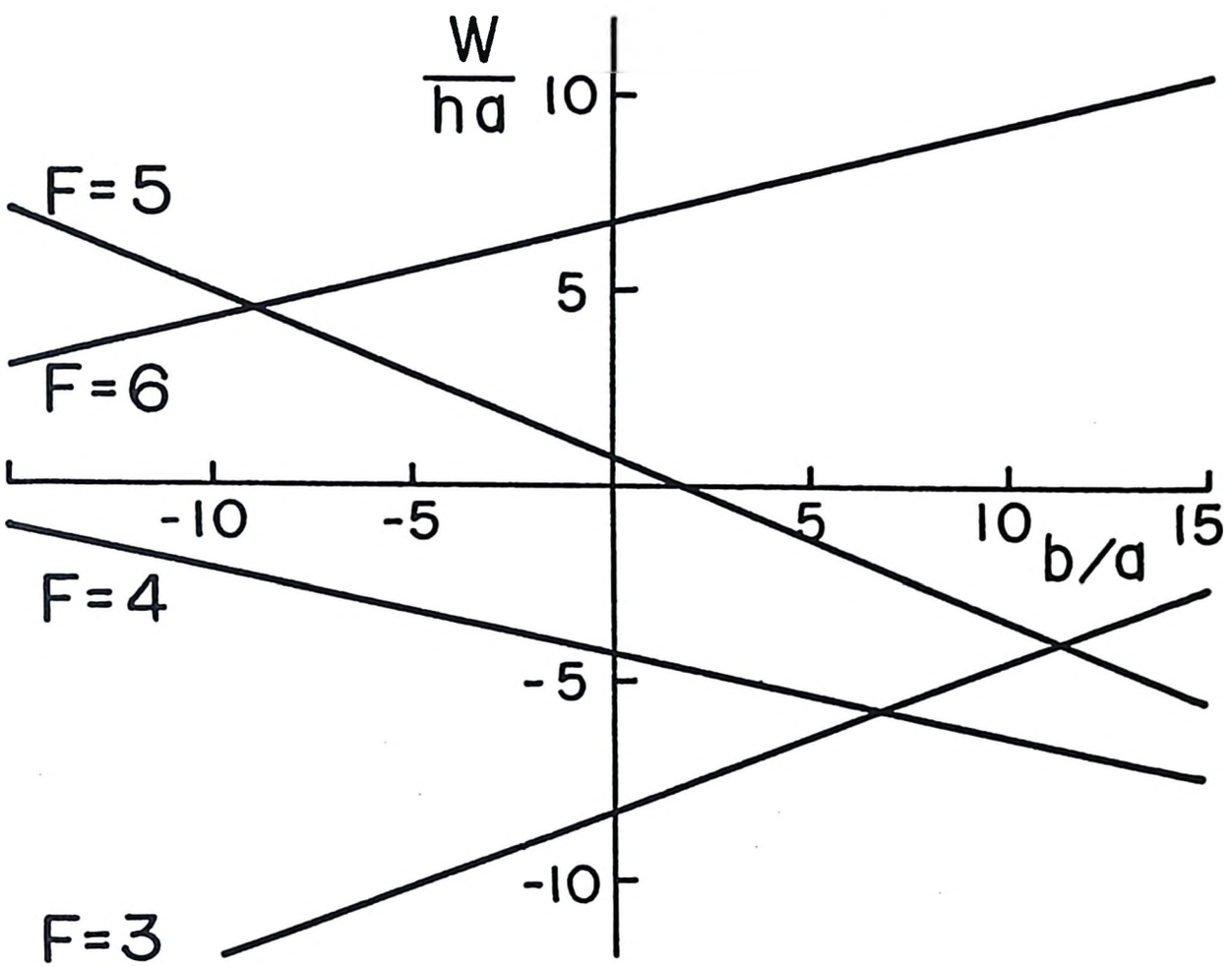

Figure 3

From the above it may be seen that for b = c = 0, the level spacing displays the Landé interval rule

$$W_0(F) - W_0(F-1) = a F.$$

The effect of the quadrupole interaction, as may be most easily seen from the diagram, is to change first the spacing, then, for large b/a, the ordering of the hyperfine energy levels. It is also clear that a change in the sign of a, occasioned by a reversal of the sign of μ_I, causes an inversion of the energy levels.

In the presence of an external magnetic field $\underline{H}$, the hyperfine Hamiltonian is modified by the addition of a term giving the energy of the electronic and nuclear magnetic dipole moments in the field. The additional term is

$$\mathcal{H}_M = -\underline{\mu}_J \cdot \underline{H} - \underline{\mu}_I \cdot \underline{H}$$

The largest part of $\mathcal{H}_M$ is the electronic one since $\mu_I/\mu_J \approx M_e/M_p \approx 1/2000$. A further term involving the octupole moment and the second derivative of the field has been ignored due to the smallness of c.

In the magnetic interaction, the field felt by the nuclear moment is reduced by diamagnetic shielding due to the atomic electrons. This reduction is proportional to the applied field and may be calculated from the electronic wave function. Kopfermann tabulates the field reduction factor 1/K (K > 1) calculated from Hartree wave functions (Kopfermann 1958). An equivalent correction is the multiplication of the nuclear magnetic moment by 1/K to obtain the "shielded" moment. In the

remainder of this chapter, the nuclear moment is to be taken as the shielded moment. In the preceding account of the relationship between the nuclear moment and the hyperfine interaction constant, the shielded moment may also be used provided a suitable correction factor is included.

It was shown above that $\mathcal{H}_{\text{hyperfine}}$ is diagonal in the (F,m) representation, where $\underline{F}$ is the total atomic angular momentum and m is its component along the quantization axis. The eigenvalues $W_o(F)$ were found to be independent of m. With the application along the z-axis of an external magnetic field of magnitude H, non-diagonal terms are introduced, in addition to further diagonal terms. Thus in general a secular equation must be solved for the eigenvalues W(F,m). To examine some of the properties of this equation and its solutions we write

$$\mathcal{H}_M = -\underline{\mu}_J \cdot \underline{H} - \underline{\mu}_I \cdot \underline{H}$$

$$= -\left(\frac{\mu_J}{J} J_z + \frac{\mu_I}{I} I_z\right) H.$$

In the (F,m) representation chosen, $J_z + I_z$ (= F_z) has eigenvalues m. Therefore,

$$\langle F,m \mid I_z \mid F',m' \rangle = m\delta_{FF'}\,\delta_{mm'} - \langle F,m \mid J_z \mid F',m' \rangle$$

where $\delta_{FF'}$ and $\delta_{mm'}$ are Kronecker δ's. As a result

$$\langle F,m \mid \mathcal{H} \mid F',m' \rangle = W_o(F) - \frac{\mu_I}{I} mH\,\delta_{FF'}\,\delta_{mm'} - \left(\frac{\mu_J}{J} - \frac{\mu_I}{I}\right) H \langle F,m \mid J_z \mid F',m' \rangle .$$

The only non-zero matrix elements of J_z are

The case J = 1/2 is of particular interest since in this case the highest order determinant is 2 x 2 and all the eigenvalues W(F,m) may be obtained in a simple closed form. The solution, due to Breit and Rabi (Breit and Rabi 1931), is usually written

$$W(F=I\pm\frac{1}{2},m) = -\frac{h\nu}{4} - \frac{\mu_I}{I} H m \pm \frac{h\nu}{4}(2I+1)\left[1 + \frac{4m}{2I+1}x + x^2\right]^{1/2}$$

where

$$x = -2\frac{\left(\frac{\mu_J}{J} - \frac{\mu_I}{I}\right)}{h\nu(2I+1)} H \quad .$$

Experimentally, this case is of interest since it applies to all $S_{1/2}$ and $P_{1/2}$ ground states, including, for example, sodium and indium.

Since the Hamiltonian is formally symmetric with respect to exchange of I and J, the above treatment may be extended to the case of I = 1/2, with J remaining arbitrary. Then

$$W(F=J\pm\frac{1}{2},m) = -\frac{h\nu}{4} - \frac{\mu_J}{J} H m \pm \frac{h\nu}{4}(2J+1)\left[1 + \frac{4m}{2J+1}y + y^2\right]^{1/2}$$

where

$$y = -2\frac{\left(\frac{\mu_I}{I} - \frac{\mu_J}{J}\right)}{h\nu(2J+1)} H \quad .$$

This case may be applied, for example, to indium isotopes of spin 1/2 in the $^2P_{3/2}$ metastable atomic state.

The energy levels W(F,m) are plotted for I = 1/2, J = 1/2 and 3/2 in Figure 4 as functions of the field H. Such a graph is called a Breit-Rabi diagram.

Figure 4. Energy level diagrams for (a) $J = 1/2$, $I = 1/2$, $\mu_I < 0$ and (b) $J = 3/2$, $I = 1/2$, $\mu_I < 0$. Transitions of the type $\Delta F = 0$, which may be focused in the "flop-in" configuration, are indicated by the double-ended arrows.

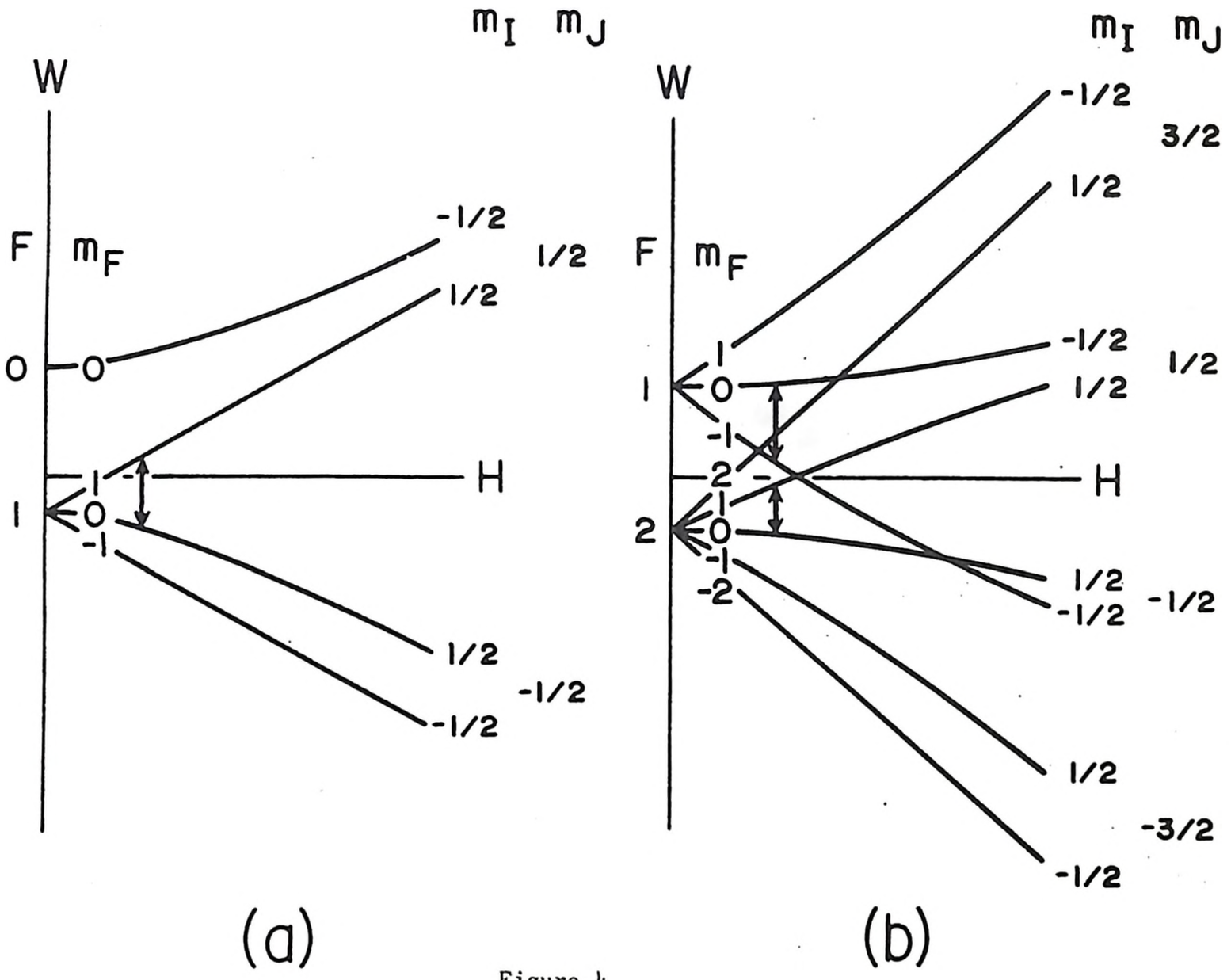

Figure 4

For values of I and J greater than 1/2, submatrices of higher order than two are involved and the solution of the secular equation becomes more laborious. A number of approaches are possible. The simplest of these is the perturbation theory, where the perturbation is taken as $\mathcal{H}_M$. The solutions to zero order are therefore simply the zero-field eigenvalues $W_o(F)$. The first order solution includes the diagonal matrix elements of $\mathcal{H}_M$ and consequently corresponds to the linear Zeeman splitting of the hyperfine levels:

$$W_1(F,m) = W_o(F) + \langle F,m|\mathcal{H}_M|F,m\rangle$$

$$= W_o(F) - \left[\frac{\mu_J}{J}\frac{F(F+1) + J(J+1) - I(I+1)}{2F(F+1)} + \frac{\mu_I}{I}\frac{F(F+1) + I(I+1) - J(J+1)}{2F(F+1)}\right] m H .$$

The second order perturbation includes the interactions between states of the same m-value in neighbouring hyperfine levels, and is of the form

$$W_2(F,m) = W_1(F,m) + \sum_{F' \neq F} \frac{\langle F,m|\mathcal{H}_M|F',m\rangle \langle F',m|\mathcal{H}_M|F,m\rangle}{W_o(F) - W_o(F')} .$$

From the properties of $\mathcal{H}_M$ outlined above, the only terms contributing to the sum are those in which $F' = F \pm 1$. Hence,

$$W_2(F,m) = W_1(F,m) + \frac{|\langle F,m|\mathcal{H}_M|F-1,m\rangle|^2}{\Delta W_{F-1,F}} - \frac{|\langle F,m|\mathcal{H}_M|F+1,m\rangle|^2}{\Delta W_{F,F+1}}$$

where $\Delta W_{F,F'} = h\Delta\nu_{F,F'} = W_o(F') - W_o(F)$ is the zero field separation between the states F and F'. Clearly, the effect of the second order terms is quadratic in the field.

The third order correction again connects only neighbouring F levels, but these terms are cubic in the field and the energy denominators are the squares of the hyperfine intervals. These and higher order terms are tedious to calculate. Therefore, in fields sufficiently large that third and higher orders must be taken into account, it is generally simpler to use other techniques of diagonalization of the Hamiltonian. The commonest procedure, and the one of most general application, is the use of successive numerical approximation methods with high-speed electronic computers. The atomic beam group at the University of California has been particularly active in this regard. The theses of L. L. Marino and V. J. Ehlers (Marino 1959; Ehlers 1960) contain descriptions of the programs and notes on their convergence properties.

In cases where one of J or I is less than or equal to 3/2, the m-submatrix of highest order is 4 x 4. Hence the secular equations to be solved are quartic at most. Closed solutions for such equations, although quite complicated, do exist.

Two applications of the above hyperfine structure theory are of interest in the atomic beam experiment. These concern the behaviour of atoms in strong inhomogeneous magnetic fields and in relatively weak homogeneous fields. The former are used to deflect the atomic beam while the latter are used as regions in which to induce atomic transitions.

2. THE DEFLECTION AND FOCUSING OF ATOMIC BEAMS

An atom in an inhomogeneous magnetic field experiences a force $\underline{F}$ given by

$$\underline{F} = -\nabla W = -\frac{\partial W}{\partial H} \nabla H = \mu_{eff} \nabla H \quad .$$

If the gradient is parallel to the direction of the field H, then it is clear from examination of the Hamiltonian that, for sufficiently strong fields,

$$\mu_{eff} \approx \frac{\mu_J}{J} m_J \ .$$

This property suggests that such strong inhomogeneous fields may be used to deflect beams of neutral atoms. Thus the single transverse inhomogeneous field used by Stern and Gerlach divided atomic beams into 2J+1 components according to m_J. Two such deflecting fields traversed successively by the beam can be arranged to act as polarizer and analyzer. The pioneer atomic beam resonance experiments of Rabi, as well as some present-day molecular beam experiments, use two deflecting fields, A and B, oriented in opposite senses. This arrangement provides a measure of velocity focusing for a beam of atoms. That this is so may be seen by considering A and B magnets of equal length and gradient. Since the deflecting force is small and transverse to the direction of the beam axis, the time spent by an atom in each magnet is the same and the two deflections cancel, independent of atomic velocity. For magnets of different lengths, the strengths may be adjusted to give the same effect. A transition which causes a change of the effective magnetic moment μ_{eff} of the atom in the region C between the deflecting magnets is observed as a decrease in the intensity of the beam on the axis at the exit of the B deflecting magnet.

The magnet configuration introduced by Zacharias for the study of K^{40} is similar in principle (Zacharias 1942). In this arrangement, the two deflecting fields A and B are in the same sense so that an atom deflected in one direction in the A magnet suffers a further deviation

in the same direction in the B magnet unless the sign but not the magnitude of its effective magnetic moment is changed in the region C between them. The magnet arrangement and some typical trajectories are shown in Figure 5. Fast-moving atoms from the source S are essentially undeviated by the magnet system, but are prevented from reaching the detector D by placing an obstacle, or "stop-wire", O, in the B magnet aperture at the point of maximum excursion of the beam from the machine axis, defined by the straight line from the source to the detector.

A resonance is thus observed as an increase in the signal level at the detector above a normally low background. This "flop-in" arrangement has the obvious advantage of an increased signal-to-background ratio over that of the earlier experiments. This feature has made possible the study of atomic species of extremely low abundance.

3. ATOMIC BEAM RESONANCES

Transitions in atoms in the beam are induced by applying in the C region a weak homogeneous magnetic field together with an oscillating magnetic field of the appropriate frequency. The A, C and B magnetic fields are all in the same direction as indicated in Figure 5. Atoms passing from the A to the C and hence to the B magnet do so adiabatically, that is, without changing the spatial quantization of their angular momentum. Their low velocity and the comparatively slow variations of the magnetic field due to fringing effects allow this to occur.

The price paid for the use of the flop-in technique is a reduction in the number of transitions observable with a given ratio of A to B magnetic fields. This is the reason for maintaining the flop-out arrangement in molecular beam studies where more transitions are observed

Figure 5. Beam trajectories in a "flop-in" atomic beam apparatus. The solid lines denote typical paths of atoms that undergo transitions in the C-field region in which the sign of m_J changes; the dotted lines, the paths of atoms which fail to make these transitions. The transverse scale, and hence the curvature of the trajectories, is exaggerated. Principal components of the apparatus are designated as follows: O - source oven, A - first deflecting magnet, C - homogeneous magnet, B - second deflecting magnet, S - stop wire, and D - detector.

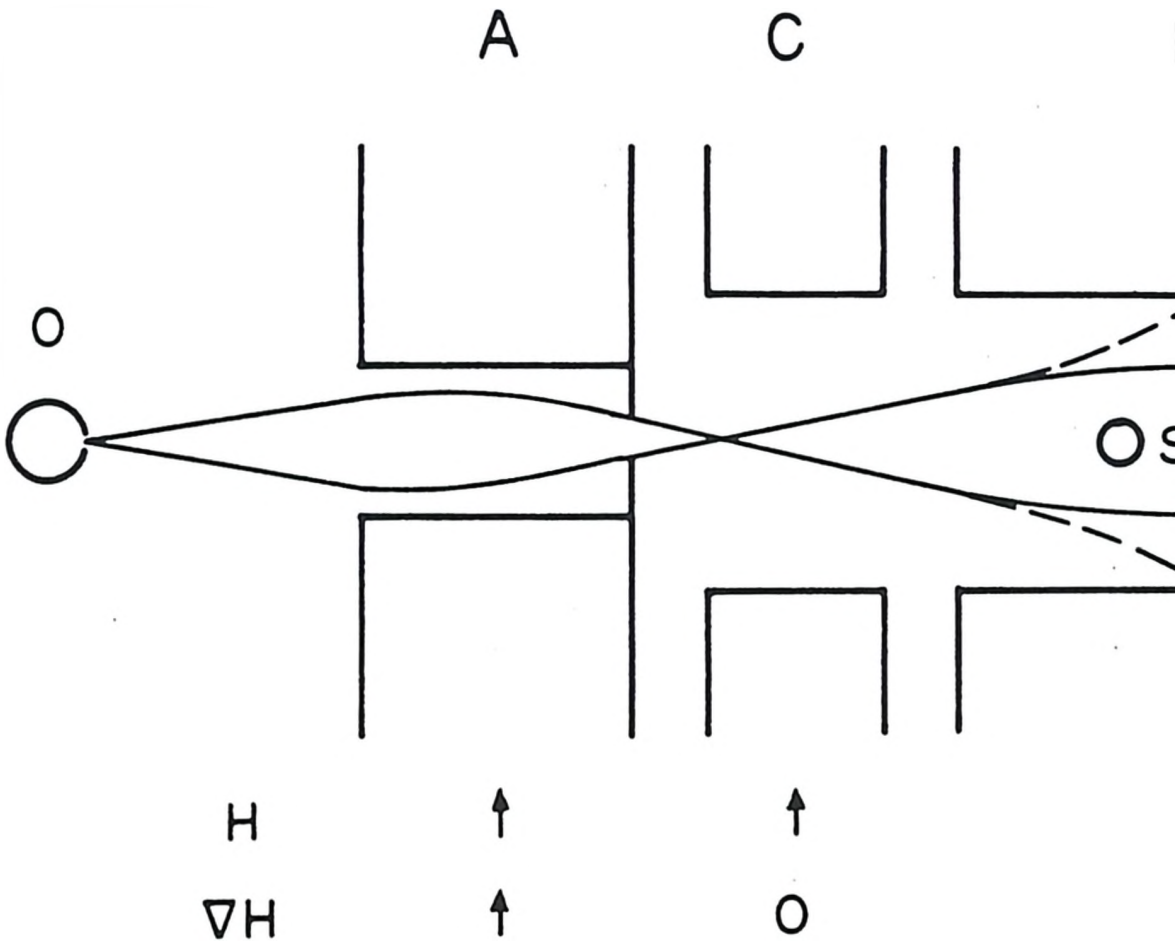

Figure 5

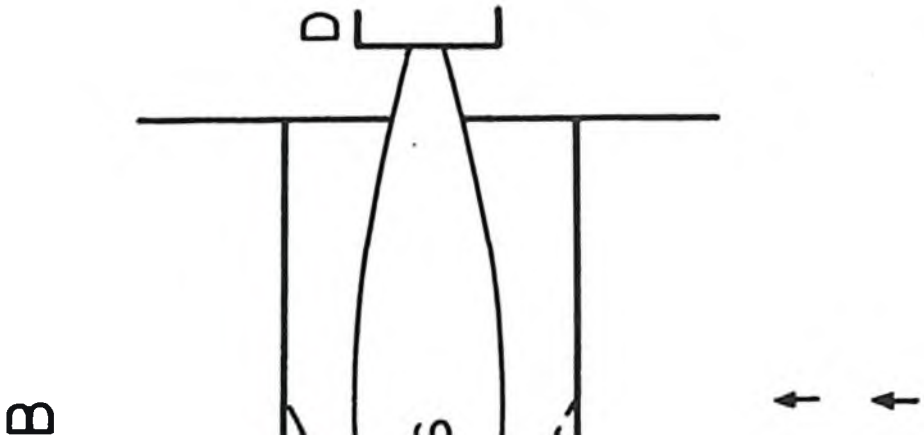
D
B

and further information on molecular structure is obtained. In addition, the requirement of reversal of μ_{eff} implies that the focusing fields must be sufficiently strong to decouple the electronic and nuclear spins. Examination of the Hamiltonian shows that this occurs when

$$\mu_J H \gtrsim ha,\ hb$$

When this condition is fulfilled, the observable transitions are seen to be of several forms. These may be subdivided according to the selection rules which govern them. For magnetic dipole transitions, these are

$$\Delta F = 0 \qquad \Delta m = \pm 1$$

$$\Delta F = \pm 1 \qquad \Delta m = \pm 1,\ 0$$

The π transitions, in which m changes, are induced by an oscillating magnetic field whose direction is perpendicular to that of the static or quantization field. The σ transitions, in which m does not change, are produced when the oscillating field is parallel to the static field direction.

a. <u>The Case $\Delta F = 0$, $\Delta m = \pm 1$</u>

The frequency of $\Delta F = 0$ transitions increases from zero at zero field where the magnetic states are degenerate, through the linear Zeeman region. At higher fields, quadratic and higher order terms become important. For the case $J = 1/2$, the single observable transition of this type is

$$(I+\tfrac{1}{2}, -I+\tfrac{1}{2} \leftrightarrow I+\tfrac{1}{2}, -I-\tfrac{1}{2})$$

$$(I+\tfrac{1}{2}, I+\tfrac{1}{2} \leftrightarrow I+\tfrac{1}{2}, I-\tfrac{1}{2})$$

for positive and negative magnetic moments respectively. The frequency

may be derived from the Breit-Rabi equation and is

$$\nu = -\frac{\mu_I H}{hI} + \frac{|a|}{4}(2I+1)\left[\left(1 - 2\frac{2I-1}{2I+1}|x| + x^2\right)^{1/2} - (1 - |x|)\right]$$

where

$$|x| = -\frac{(2\mu_J - \mu_I/I)H}{h\,|a|\,(I+\frac{1}{2})} .$$

The above formula is correct for either sign of μ_I. Note that the frequency is the same for both signs of the magnetic moment except for the small terms involving μ_I. The frequency may be expanded in a power series in H corresponding to the perturbation theory, with the result, correct to second order in the field:

$$\nu = -\frac{2(\mu_J + \mu_I)}{h(2I+1)}H + \frac{4I}{(2I+1)^3}\frac{(2\mu_J - \mu_I/I)^2}{h^2}\frac{H^2}{|a|} .$$

For the case $J = 3/2$, $I \geq 1/2$, two resonances of the type $\Delta F = 0$ are possible. These are at frequencies ν_+ and ν_-. The transitions are, for a positive magnetic moment,

$$\nu_+: \quad (I+3/2, -I+1/2 \longleftrightarrow I+3/2, -I-1/2)$$

$$\nu_-: \quad (I+1/2, -I+3/2 \longleftrightarrow I+1/2, -I+1/2) .$$

For a negative magnetic moment, the corresponding transitions are

$$\nu_+: \quad (I+3/2, I+1/2 \longleftrightarrow I+3/2, I-1/2)$$

$$\nu_-: \quad (I+1/2, I-1/2 \longleftrightarrow I+1/2, I-3/2) .$$

From the perturbation theory, the frequencies of these transitions are, to second order in H,

$$\nu_+ = -\frac{2}{2I+3}(\mu_J+\mu_I)\frac{H}{h} + \frac{6I^2}{(2I+3)^2(I+1)}\frac{(2/3\mu_J - \mu_I/I)^2}{|\Delta\nu_{I+1/2,I+3/2}|}\frac{H^2}{h^2}$$

$$\nu_- = -\frac{2}{(2I+1)(2I+3)}\left(\frac{2I+9}{3}\mu_J + \frac{2I^2+3I-3}{I}\mu_I\right)\frac{H}{h} +$$

$$+\left[\frac{2(2I-1)(I-1)(2I+3)}{(2I+1)^2I(I+1)}\frac{1}{|\Delta\nu_{I-1/2,I+1/2}|} - \frac{6I(I-1)}{(2I+3)^2(I+1)}\frac{1}{|\Delta\nu_{I+1/2,I+3/2}|}\right]\times$$

$$\times\left(\frac{2\mu_J}{3} - \frac{\mu_I}{I}\right)^2\frac{H^2}{h^2}.$$

b. <u>The Case $\Delta F = \pm 1$, $\Delta m = \pm 1, 0$</u>

The largest contribution to the $\Delta F = \pm 1$ transitions comes from the hyperfine interval itself. Thus a precise measure of this interval results from the observation of such resonances. In general, a number of σ and π resonances are observable. Often, certain of these turn out to have frequencies which are independent of the field to first order at some value of the field, so that knowledge of the field need not be precise in order to obtain a precise value of the hyperfine interval.

Examples of such "field independent" resonances are those of the σ transitions in the cases $I = 1/2$, $J = 1/2$ and $3/2$. These frequencies have minima at zero field, and at weak fields are given to order H^2 by

$$\nu_{1/2} = |a_{1/2}|\,(1+x^2)^{1/2} \approx |a_{1/2}| + \frac{2(\mu_J-\mu_I)^2}{|a_{1/2}|}\frac{H^2}{h^2}$$

$$\nu_{3/2} = 2|a_{3/2}|\,(1+y^2)^{1/2} \approx 2|a_{3/2}| + \frac{(\mu_J/3-\mu_I)^2}{4\,|a_{3/2}|}\frac{H^2}{h^2}.$$

At small values of the magnetic field H, the quadratic terms can be made very small. Errors in field calibration then do not strongly affect the values of $|a|$ derived from the σ transition frequencies.

In the $J = 3/2$ case, no other $\Delta F = \pm 1$ transition is observable for equal A and B magnet deflections, as may be seen from the Breit-Rabi diagram, Figure 4. However, for the case $J = 1/2$ there is a π resonance whose frequency, to second order in the field, is given by

$$\nu_{1/2'} = |a_{1/2}| - (\mu_J + \mu_I)\frac{H}{h} + \frac{(\mu_J - \mu_I)^2}{|a_{1/2}|}\frac{H^2}{h^2}.$$

Since this is field dependent, it does not lead to as precise a value of $|a_{1/2}|$.

c. Resonance Shapes

The resonance frequency corresponding to transitions between states of energies W_1 and W_2 is well defined by the Bohr condition,

$$\nu = \frac{W_2 - W_1}{h}.$$

Furthermore, the natural lifetime of the states involved in hyperfine transitions is extremely long due to the small energy differences and to the M1 character of the transitions, so that the natural width of the level is negligibly small. However, the perturbation due to the oscillating magnetic field in the C region acts for only a short time on any one atom of the beam as it passes through. As a result, the atomic beam resonance occurs over a distribution of frequencies characterized by a width

$$\delta\nu \approx \frac{1}{\delta t}$$

where $\delta t = L/v$ is the time spent by atoms of velocity v in the oscillating field of length L.

The shape of the resonance peak depends on the details of the spatial distribution of the oscillating field and, to a certain extent, on the velocity distribution of atoms in the beam. Calculations have been made by a number of authors for certain distributions of the oscillating field. Ramsey (Ramsey 1956) has derived expressions for transition probabilities in single and separated oscillating fields. In other cases of interest such calculations, based on first order perturbation theory, become very difficult.

Woodgate has shown (Woodgate and Hellwarth 1956) that a process involving Fourier transformation of the oscillating field about the transition frequency yields the same result as the perturbation theory in the single field case and gives results which are consistent with experiment in more complicated cases. According to the prescription set out by Woodgate, we let the oscillating field be given by

$$h(x)e^{i\omega t} = h(vt)e^{i\omega t}$$

where the time dependence of the complex amplitude arises from the atom's motion through the space-dependent field. The Fourier transform is then taken

$$g_v(\omega) = \int h(vt)e^{i(\omega-\omega_o)t}dt \ .$$

This procedure assumes that the actual atomic resonance occurs at a frequency ω_o which is narrowly defined compared to the final line-width. The transition probability for atoms with velocity v is then

$$P_v(\omega) = |g_v(\omega)|^2 \ .$$

If the velocity distribution in the beam is given by $y(v)$, then the transition probability averaged over the distribution is, except for a constant normalizing factor,

$$P(\omega) = \int P_v(\omega) y(v) dv \ .$$

In the results given below, the velocity distribution was assumed to take the simple form appropriate for a free parallel beam of atoms of mass m emerging from a source at temperature T:

$$y(v) = v^3 \, e^{-mv^2/2kT} \ .$$

This form follows if the source is assumed to contain a Maxwell-Boltzmann distribution of velocities,

$$N(v) \propto v^2 \, e^{-mv^2/2kT}$$

and the probability of escape through the source slit with velocity v and in the direction of the beam is simply proportional to v. In this way the integral $P(\omega)$ may, for the cases studied, be reduced to a sum over integrals of the form

$$I(p) = \int_0^\infty q^3 \, e^{-q^2} \cos \frac{p}{q} \, dq$$

$$K(p) = \int_0^\infty q^3 \, e^{-q^2} \sin \frac{p}{q} \, dq \ .$$

These have been tabulated by Kruse and Ramsey (Kruse and Ramsey 1951; Ramsey 1956).

Figures 6, 7 and 8 show the results of calculations and experiments for the oscillating fields used in this work. Part (a) of each Figure

shows the assumed spatial dependence of the field, h(x), while part (b) shows the calculated resonance distribution P(ω). The points are experimentally observed values.

The treatment of Woodgate and Hellwarth corresponds roughly to first order perturbation theory. As a result, the line shape at low radiofrequency power is probably satisfactory; however, as might be expected, the dependence of the transition probability at a given frequency on the amplitude of the oscillating field is not given correctly at high power. The result of the calculation is

$$P(\omega) \propto (\text{amplitude})^2$$

$$\propto (\text{power}) \quad .$$

Deviations from this dependence can be expected when the energy density becomes sufficiently large that some atoms undergo a second transition in the oscillating field region. In the linear Zeeman region of the hyperfine structure where the magnetic substates are equally spaced, this transition can be to a third quantum state, giving rise to "two-quantum transitions" in which the magnetic quantum number changes by two units. Alternatively, the second transition can be such that the atom returns to its original state. At higher fields and for $\Delta F = \pm 1$ transitions, the energy levels are not equally spaced and the second transition must lead back to the initial state.

The calculation outlined above assumes rather idealized experimental circumstances. The assumed distribution of the oscillating field amplitude only approximates the actual experimental situation. Furthermore, the velocity distribution used for the atoms in the beam

Figure 6. Resonance line shape calculation for a simple π solenoid. The assumed radiofrequency field amplitude distribution is shown in (a). The resulting line shape is compared in (b) with an experimental resonance.

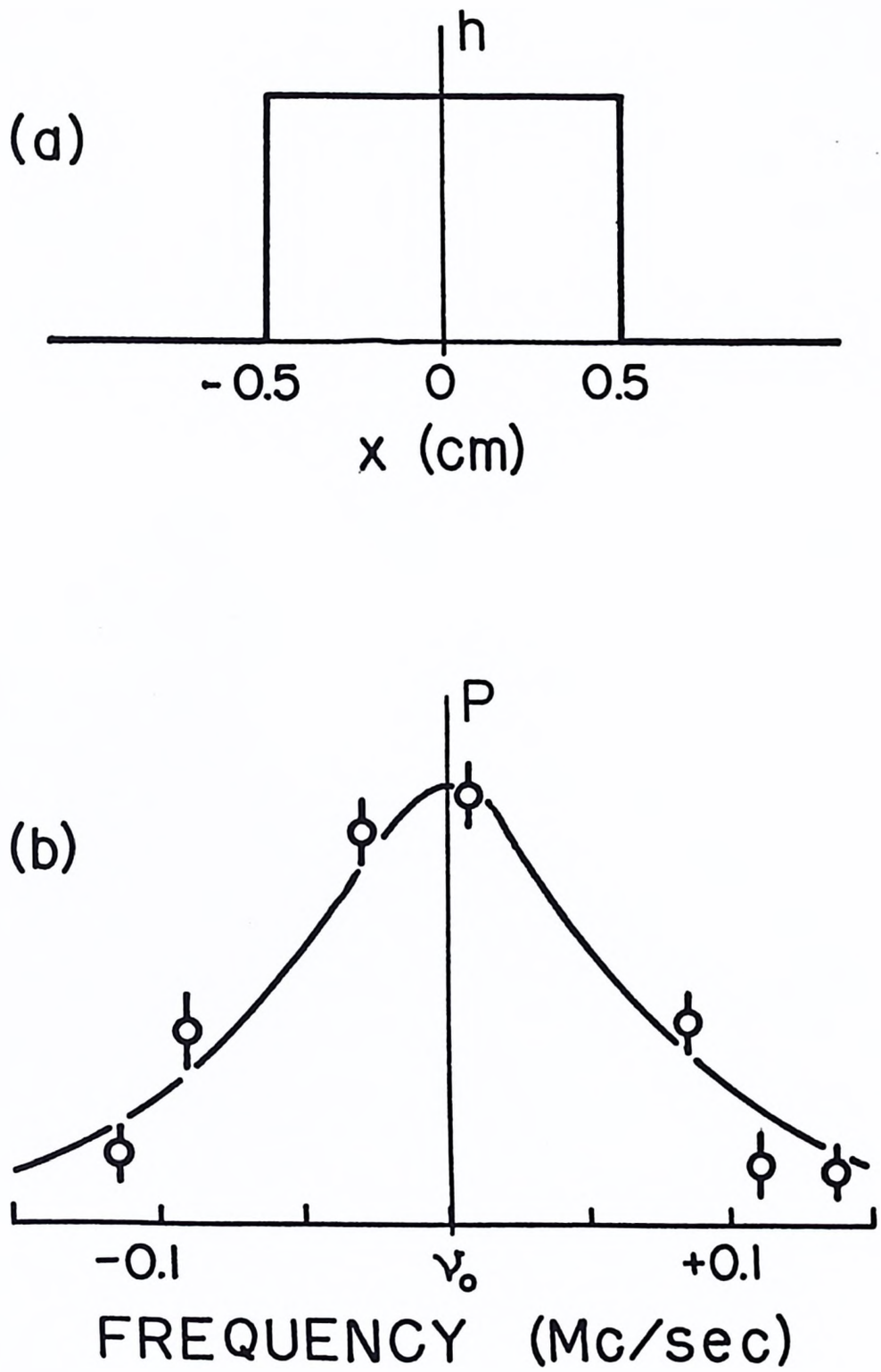

Figure 6

Figure 7. Results of a similar calculation for the first σ loop constructed.

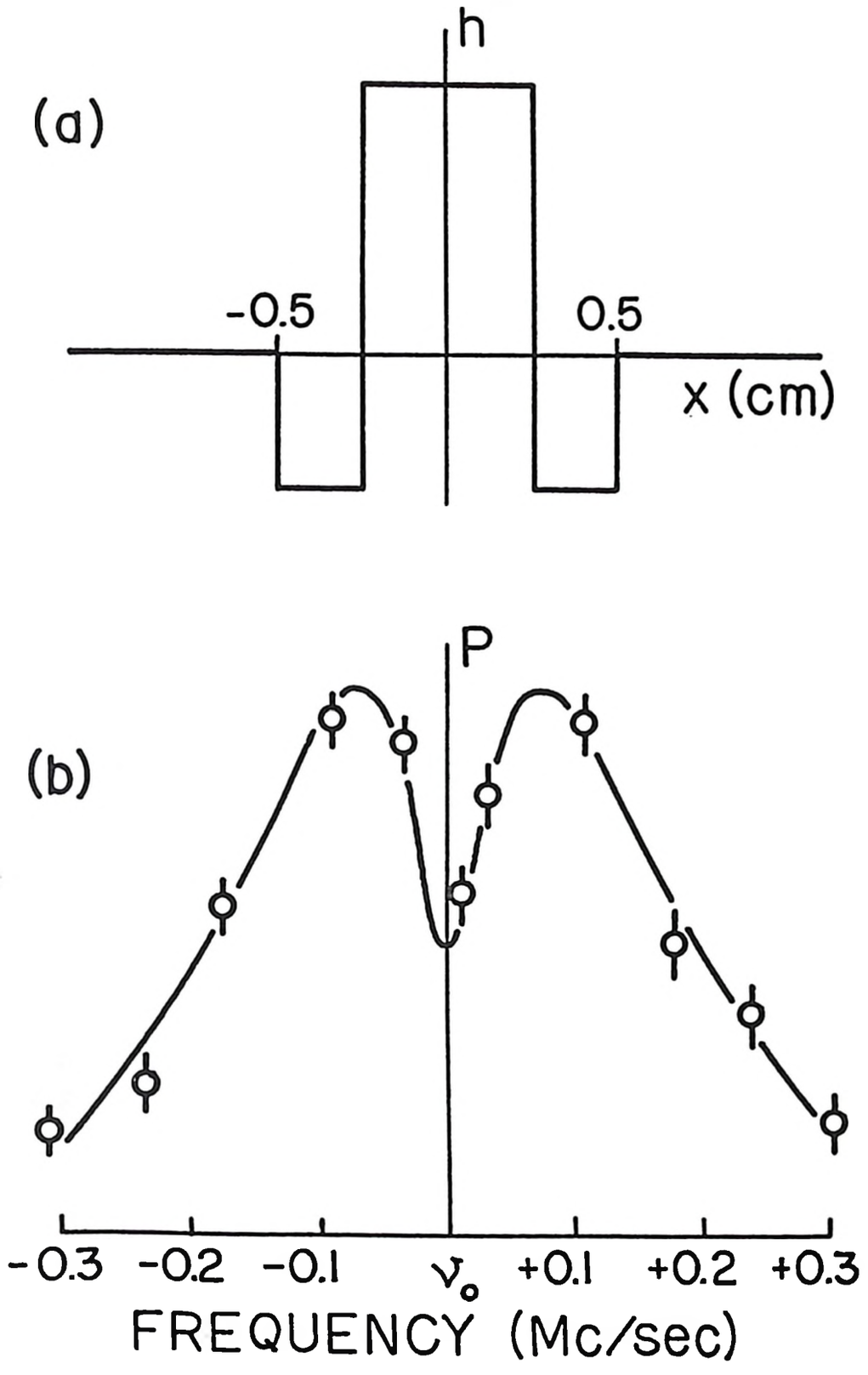

Figure 7

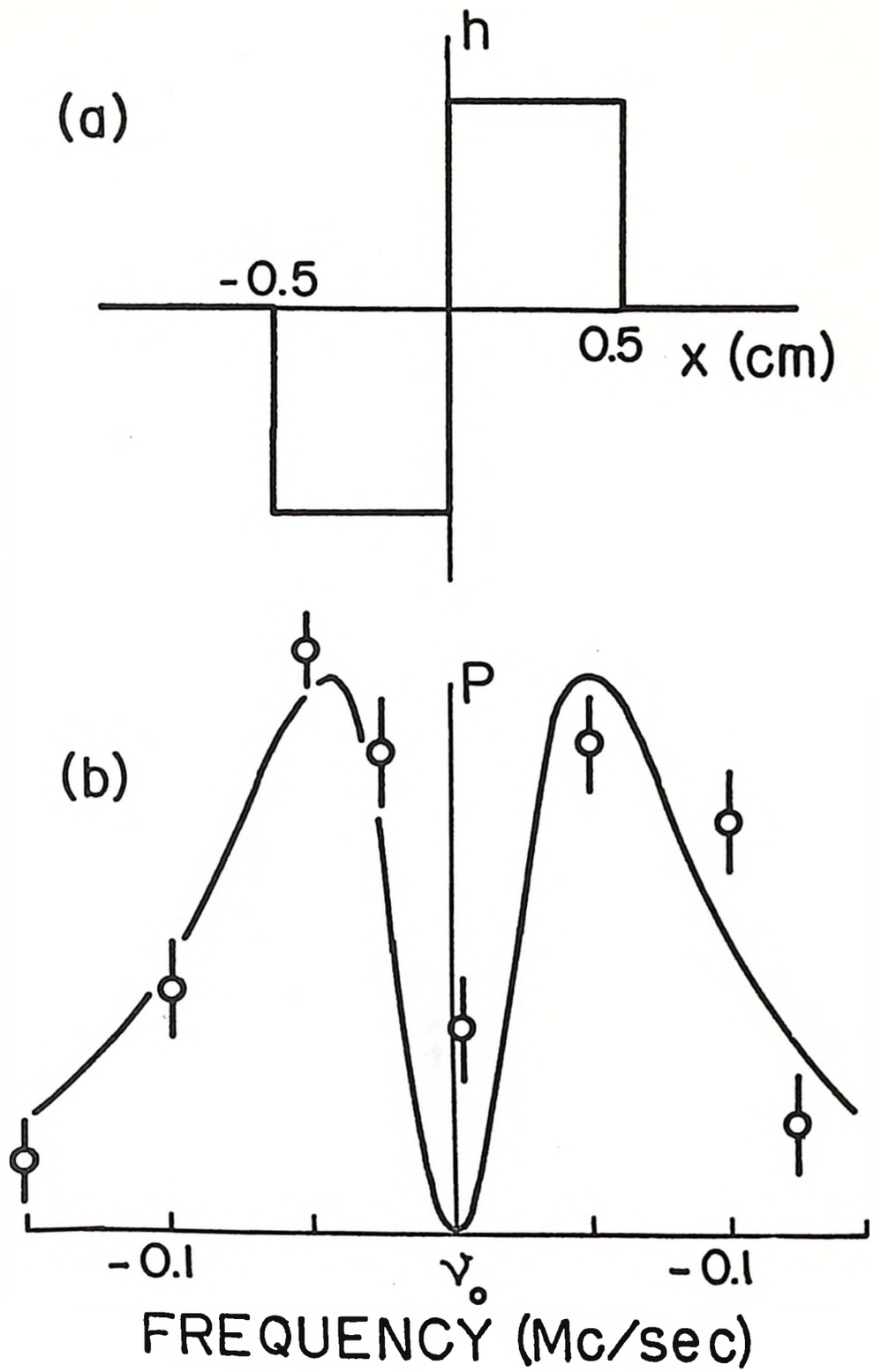

Figure 8

makes no allowance for cut-off due to the finite aperture of the magnet and collimating system. These effects are small however, and do not affect the general nature of the results obtained. The most important way in which the real experimental situation differs from that assumed is in the nature of the C-magnet field. In practice, it is extremely difficult to maintain a steady homogeneous weak C field in close proximity to the strong inhomogeneous deflecting fields. The result of both field inhomogeneity and drift is a broadening and distortion of the observed resonances with consequent loss of precision in determining the transition frequency.

It is difficult to give a quantitative analysis of these effects. However, some conclusions may be drawn on a very general basis. If the resonance frequency increases with field, and the field versus position curve is convex upward in the transition region, then the observed resonance will be shifted to the high frequency side and have a low-frequency "tail". Conversely, if the field-position curve is convex downward, the situation is reversed and the tail appears on the high frequency side. If the frequency decreases with increasing field, the cases are simply reversed. If the field possesses a gradient but no "curvature" in the transition region the resonance is broadened, but its centre is not shifted.

Field drifting provides further problems, particularly in the study of species of low abundance where considerable time is required to sweep the frequency through a resonance. Here the same arguments apply to the field-time curve as were used in the preceding paragraph for spatial inhomogeneity. If the resonance is obtained by measuring

signal intensities at a number of fixed frequencies, rather than by continuous sweeping of the frequency, the distortion or centroid shift due to field drifting can be reduced by arranging the frequencies in random order.

4. SENSITIVITY OF THE ATOMIC BEAM METHOD

In the study of radioisotopes, the problem of sensitivity is a particularly serious one. Aside from the health hazard present with strong sources of radiation, there are often limitations in source production. The magnitude of the signal observed at a detector is simply the product of the source strength, the apparatus transmission, and the detector efficiency. Since in an atomic beam experiment the deflecting force of the inhomogeneous fields is very small, only small departures of the atomic beam from its axis occur. The result is that even when all conditions are optimized, the transmission of the apparatus is small, ranging from 10^{-4} to 10^{-5} for most machines of the type considered here.

For a given machine then, the sensitivity is most strongly dependent on the means of detection. When trace isotopes are to be studied, the detector must be highly selective. In addition, random fluctuations in its background, which might mask variations in actual beam intensity, must be minimized. Several means of detection have been developed which meet these requirements in different applications. For the study of radioactive isotopes however, the method first used by Bellamy and Smith (Bellamy and Smith 1953) for Na^{24} has been most widely used. The beam is collected under fixed conditions for a period of time on a suitable surface. This is then removed from the beam and examined for its radioactivity using conventional low-background counting techniques.

Considerable effort has been spent by many workers to examine and systematize the problem of beam collection (Wexler 1950; Baker and Brink 1962). However, the number of combinations of beam and collector materials and conditions is large and the absolute measurement of collection efficiencies is difficult. As a result, the selection of suitable collection surfaces is largely a hit or miss matter.

In detection by radioactive counting, the background fluctuations referred to above are simply the variations in counter background which are possible over the counting period. The background may be counted for a long period before and after the experiment to obtain an "exact" average background counting rate b. If however the beam sample is counted for a short time T during the experiment, there will be an uncertainty $(bT)^{1/2}$ in the actual background, and hence in the net result, due to the randomness of the times of occurrence of the background counts. It is therefore important to reduce the background rate b to a minimum. At the same time, of course, it is necessary to maintain the maximum possible sample counting rate. When more than one active species is present in the beam, selectivity of the counter for the activity of interest is also desirable. In general, it is not possible to adjust all these parameters independently. Thus for a given experiment, an optimum compromise must be made.

An additional source of undesirable background is the "machine background" which arises from non-ideal operating conditions in the apparatus. Although the operating pressure of the atomic beam machine provides a classical mean free path many times the length of the flight path of the atoms of the beam, small angle scattering by residual gas

provides the largest portion of the background. That a single scattering at any part of the beam path could allow an atom to reach the detector with no change in magnetic moment may be seen from an examination of Figure 5. The atom need only be scattered in the opposite direction to its magnetic deflection.

A further contribution to the background can arise from atoms which undergo non-resonant transitions in the region between the focusing magnets. Such transitions can occur in two ways. In a region of zero field, the magnetic substates of a level of given F are degenerate and reorientation of the spin can occur. Such "zero field flops" are prevented if care is taken to avoid the occurrence of a null field at any position in the C region. The second source of undesirable transitions lies in non-adiabatic time variation of the magnetic field experienced by atoms of the beam. This may be caused by rapid spatial variation of the magnetic field such as occurs at the ends of the focusing fields. Such transitions were investigated theoretically by Majorana (Majorana 1932) who showed that the field step must contain Fourier components whose frequency is greater than the Larmor precession frequency of the atom. For the fields found in atomic beam machines, this effect is slight, even when quite complex magnet configurations are used.

CHAPTER IV

THE ATOMIC BEAM APPARATUS

The previous chapter has dealt with the theory which underlies the atomic beam magnetic resonance method for determining nuclear spins and moments -- namely the interaction of an atom with magnetic fields. In this chapter a brief review of the overall experimental situation will precede a more detailed description of the apparatus.

The atoms to be studied must travel collision-free through a series of three magnets from source to detector. To achieve such a situation, a highly evacuated path is required. For atoms which form solids at room temperature the source consists of a small oven. When this is heated to an appropriate temperature the material effuses from a slit in its side. Further slits define an aperture and it is the atoms emerging from the oven in this small solid angle which are studied. The atoms pass through two strong inhomogeneous magnets, A and B, in which they suffer transverse deflections by virtue of their atomic magnetic moment. Atoms are only able to negotiate the magnet and slit system and reach the detector if the sign of this moment is altered by a suitable Zeeman or hyperfine transition in the region between the A and B magnets. In this region a homogeneous magnet, C, of variable strength, and an oscillating field are provided. The frequency which allows a maximum flux of atoms to reach the detector and the corresponding C-field strength are related to the nuclear properties being studied.

Because the force on an atomic moment is weak and the resultant deflection is small, the permissible solid angle of the apparatus is seriously limited. Consequently, when radioactive materials are to be studied, appreciable signals are observed at the detector only for relatively large quantities of source material in the oven. The handling of such sources requires precautionary measures.

The important components of the atomic beam apparatus are therefore a high vacuum, a source of atoms, a detector, two strong deflecting fields, suitable collimating slits, a variable homogeneous magnetic field, and a radiofrequency field. To the extent that the nuclear parameters to be determined depend quantitatively only on the latter two, the principal requirement of the others is consistent performance sufficient to allow the detection of signals.

The principal design features of the McMaster atomic beam apparatus and its performance have been described previously (King 1960). Therefore, this chapter will deal mainly with the modifications which have been made to the apparatus and the consequent improvement of its performance, particularly in relation to the indium experiments.

1. LABORATORY

The experiment was performed in three rooms of the Nuclear Research Building adjoining the McMaster Reactor. The atomic beam machine itself is housed in a walk-in fume hood with the major part of the electronic controls outside a shielding wall. A counting room adjoins the control room. The counters are separated from the source end of the machine by about 25 feet, including four concrete block walls. In the experiments reported here, no increase in background counting rate was observed with sources present in the beam apparatus.

The chemistry and source preparation were performed in the "hot" laboratory of the building in a heavily shielded glove box. A new laboratory in a room adjoining the apparatus and connected to it by small "pass-through" ports was used in the latter part of the work. One of the connections passes directly into a glove box. In this way, sources can be loaded in the chemistry box and passed directly to the atomic beam apparatus with a minimum of delay and little danger of spreading radioactive contamination.

2. VACUUM

The vacuum enclosure of the apparatus itself consists of a dural base-plate on which welded aluminum boxes rest. The seal is made by two neoprene gaskets, with differential pumping. The source and main cases are interconnected by a buffer chamber and a flexible bellows. The system is evacuated to a pressure of less than 2×10^{-6} mm of mercury by means of four water-cooled oil diffusion pumps, together with appropriate fore-pumps and liquid nitrogen vapour traps. To facilitate rapid access to the interior of the machine, the pumps may be isolated from the vacuum enclosure by closing quarter-swing valves between the traps and the cases.

A separate mechanical pumping system is used for obtaining a rough vacuum when pumping down the apparatus. Under operating conditions, this pump is used as a first stage in pumping out source ovens and collector buttons as these are passed into the machine through their vacuum locks.

Sources of pressure rise in the apparatus were many. The most persistent of these was due to faulty welding of the main case. A further cause of high pressure in the apparatus was the outgassing of

accumulated beam materials, particularly the alkali metals. To maintain an operating pressure less than 2×10^{-6} mm of mercury, it was necessary to attend frequently to the above problems. The availability of a helium leak detector greatly facilitated the work of leak hunting.

3. THE MAGNET SYSTEM

Figure 9 is a view of the apparatus with the main chamber case removed to show the magnets. All three are fabricated from Armco iron and are energized by high impedance windings from power supplies electronically regulated to $1:10^4$. The pole tips of the deflecting magnets (1) and (3) are circularly cylindrical conforming to the equipotentials of two-wire fields whose equivalent wires are separated by 0.75 and 1.50 inches respectively. This form of field is chosen for the uniformity of its magnetic gradient, allowing the large useful beam cross-section shown in Figure 10. The B magnet (3), 15 inches in length, is twice as long as the A magnet (1). This proportion was selected for high transmission over a large range of atomic velocities. At an energizing current of 1 ampere, the field on the beam axis in the B magnet is 10,000 gauss. It was originally hoped to run with about 1.5 amperes of magnet current. However, excessive outgassing and high voltage breakdown in the separately pumped magnet windings prevents this.

The C-magnet pole faces are 5 inches long and 3 inches high, flat and parallel to 0.0002 inches at a nominal separation of 0.51 inch. Although the yoke provides a degree of shielding from the fringing fields of the deflecting magnets, considerable fringing into the C magnet was observed at low C fields, as may be seen in Figure 11. The values of the

Figure 9. A schematic view of the magnet system and the other main features of the apparatus as seen with the vacuum enclosure removed. 1 - A-magnet, 2 - C-magnet, 3 - B-magnet, 4 - oven interlock, 5 - button interlock, 6 - stop wire mechanism. Not visible are the beam defining slits located on the far ends of the deflecting magnets and the r-f loop in the pole gap of the C-magnet.

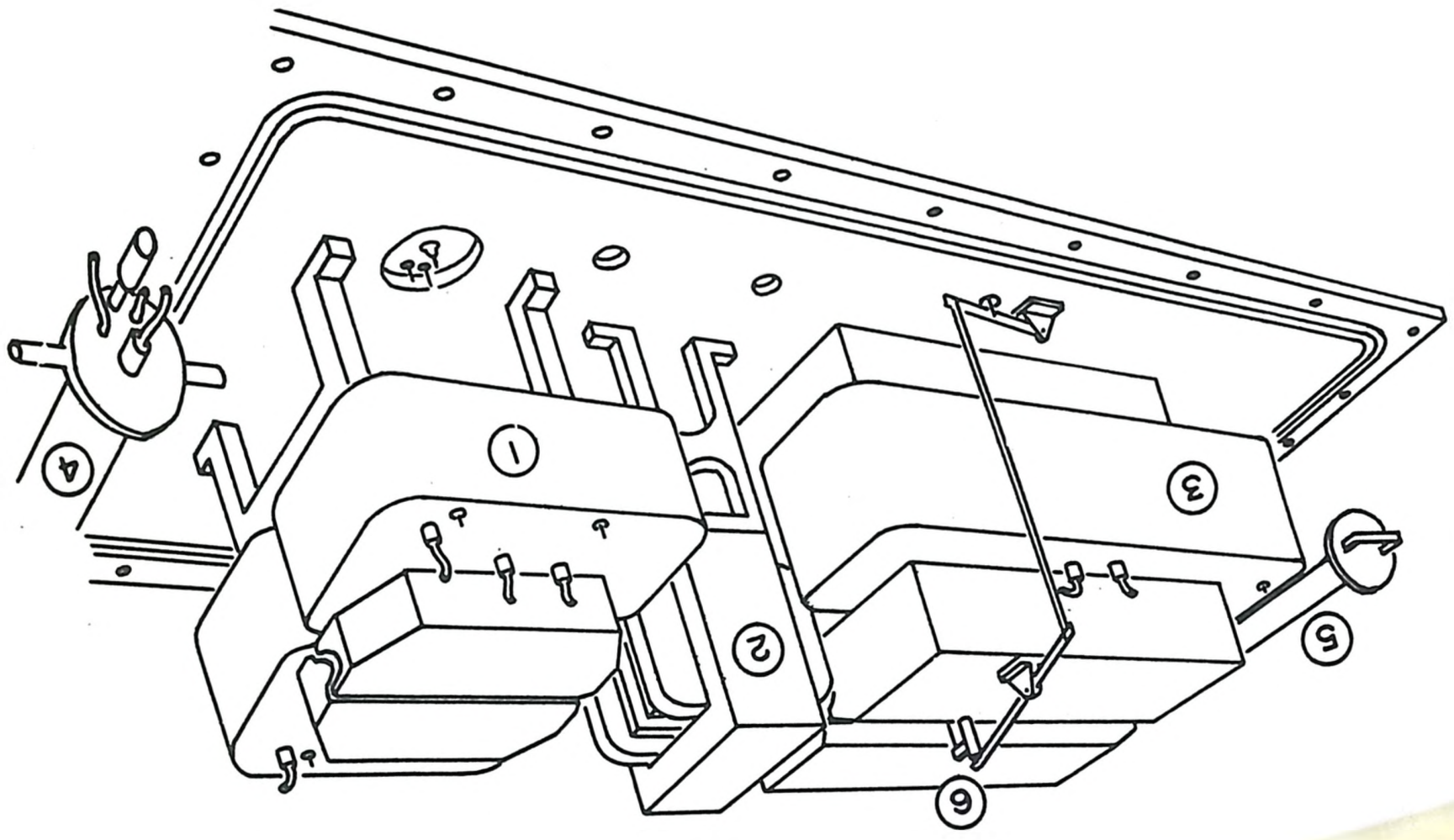

Figure 9

Figure 10. The profile of the pole tips of the deflecting magnets. The scale refers specifically to the A-magnet. The B-magnet is twice as large.

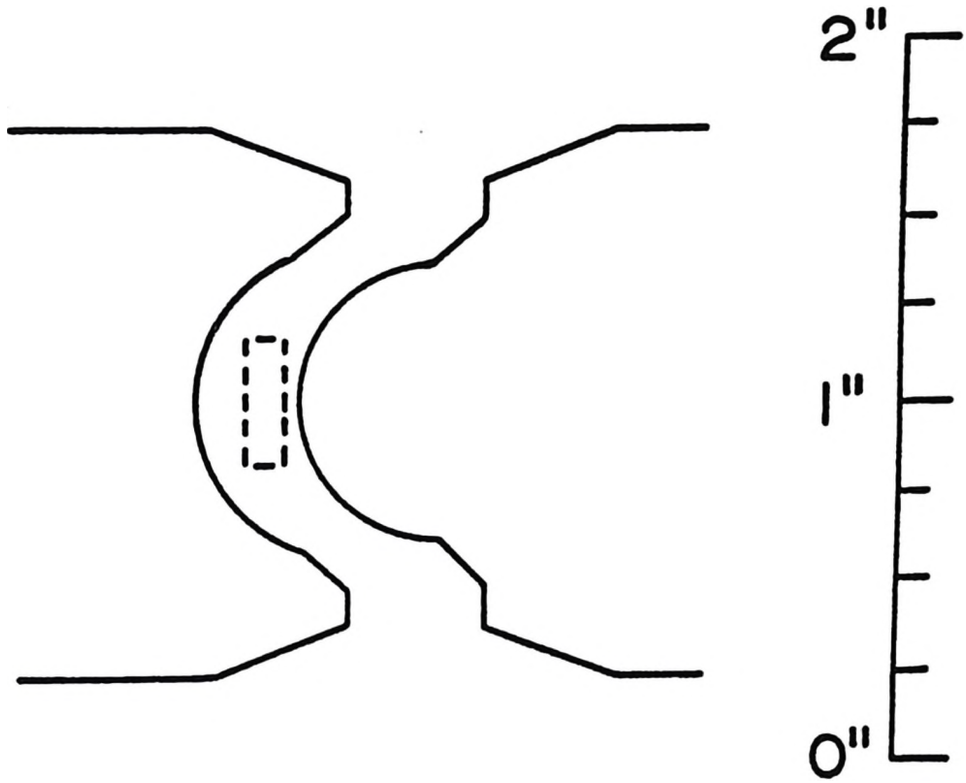

Figure 10

Figure 11. Results of a measurement of the transverse magnetic field strength at a number of positions on the beam axis. The limits of the A, C and B magnets are shown.

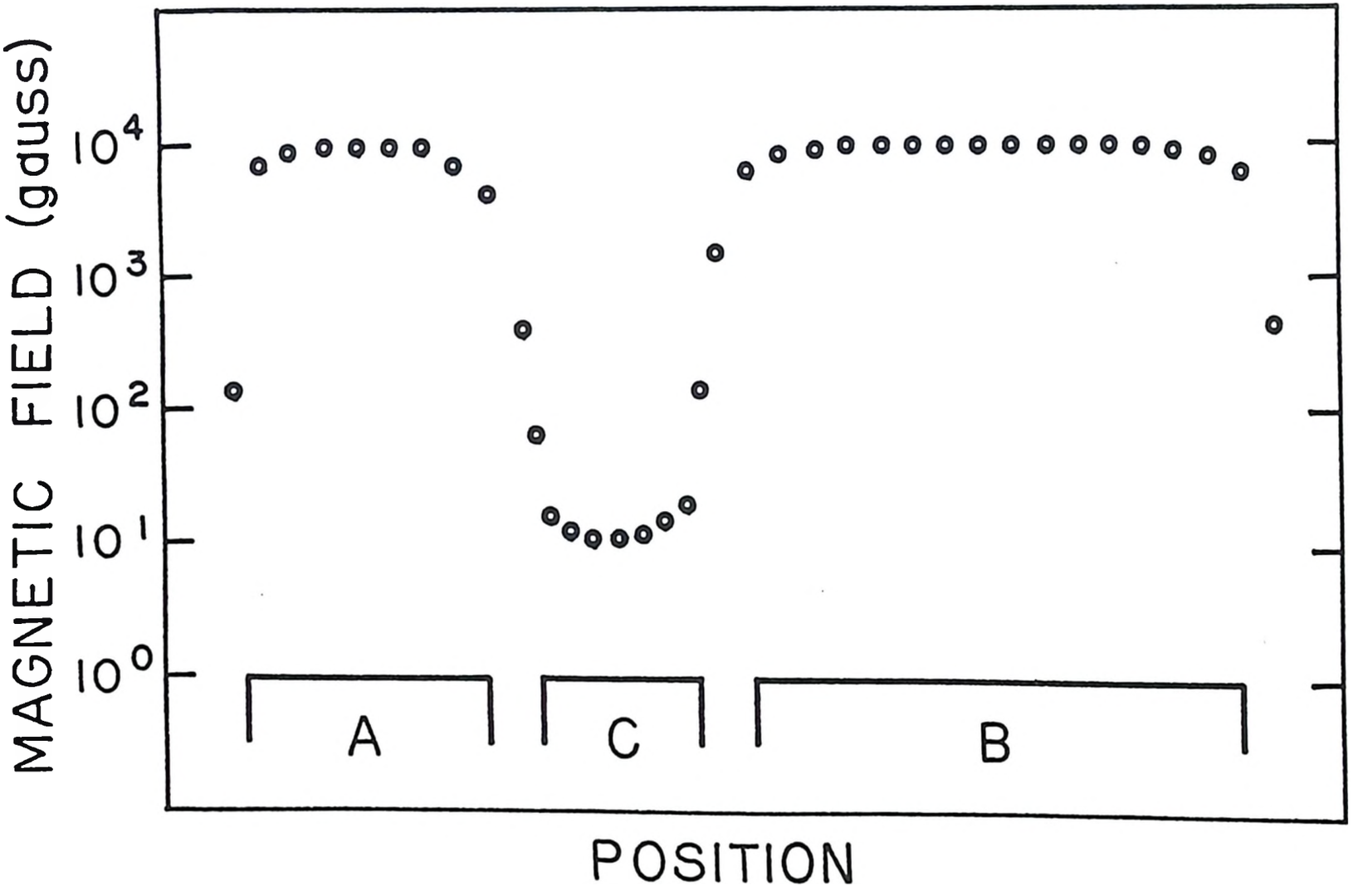

Figure 11

field in the deflecting magnets were measured using a flip coil while those in the C magnet were calculated from the $\Delta F = 0$ resonance in a sodium beam. At high C fields, fringing out of the C magnet occurs. In addition to these effects, considerable variation could be induced by hysteresis which appeared to vary with position in the magnet. Since the construction of the present apparatus a means of reducing these difficulties has been devised (Goodman 1960).

During the course of the indium experiments, the C field in the transition region was measured by observing the field-dependent $\Delta F = 0$ transition $(2,-1 \leftrightarrow 2,-2)$ in a beam of Na^{23}. Using the previously measured atomic and nuclear properties of this isotope (Ramsey 1956) and the Breit-Rabi equation, the field may be deduced with a precision limited only by the resonance line width.

4. THE COLLIMATING SYSTEM

The beam collimating system consists of a number of baffles and slits, and a central obstacle. Two baffles placed between the oven and the A magnet limit the beam to the A-magnet gap and prevent serious radioactive contamination of the magnet chamber. Beam scattering from the A-magnet pole faces is likewise precluded.

The beam defining slits are placed at the exit of each deflecting magnet. The obstacle wire is positioned at the point of maximum excursion of the beam from the machine axis. This arrangement of constraints on the atomic beam trajectories is consistent with high transmission at resonance over a wide range of velocities. The optimum aperture of the collimating system depends on the velocity, mass, and magnetic moment of the atoms comprising the beam, and on the attainable fields in the deflecting magnets.

Since most of the experimental optimization of conditions was carried out using beams of sodium and caesium, the results were scaled to give values appropriate for indium:

Stop-wire diameter	0.020 inch
A-magnet exit slit	0.010 inch
B-magnet exit slit	0.026 inch

Initial alignment of the collimating system was made by means of a cathetometer. Final adjustment was made using the atomic beam itself. Movement under vacuum of the A-magnet slit assembly and separately of each of the jaws of the detector slit was effected by means of slow motion screw drives through rotating vacuum seals in the apparatus base-plate. The over-all reduction of the motion was such that the slit movement was 1/1600 inch per turn. The positions of the moving slit parts were monitored using dial gauges mounted inside the vacuum chamber and viewed through lucite windows.

5. SOURCE OVENS

The source ovens were tantalum cylinders 5/8 inch in outside diameter and 1 inch high, with screw-on lids and adjustable slits 1/4 inch high and 1/8 inch thick. This is illustrated by Figure 12. A carbon lining helped to prevent the source material alloying with the oven. Electron bombardment heating at a power input of 120 watts maintained an oven temperature of 1100°C. Figure 13 shows the variation of temperature and indium vapour pressure with power input. The temperature was monitored during the course of the experiment using a Leeds and Northrup model 8622-C

Figure 12. The parts of a source oven showing the body of the oven, the slits, the lid and the carbon lining.

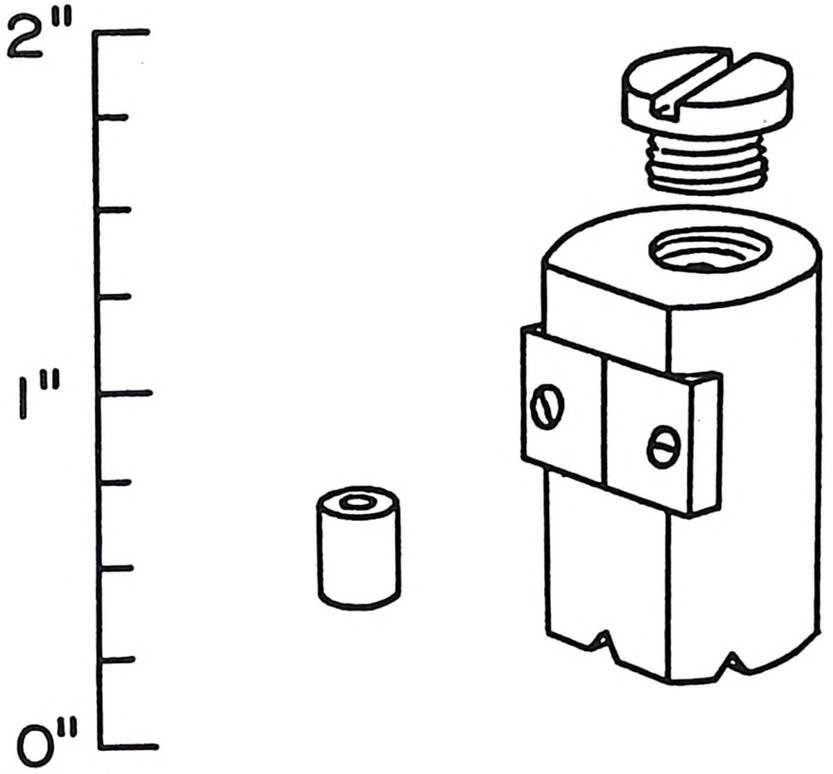

Figure 12

Figure 13. The dependence of the oven temperature and indium vapour pressure on the electron bombardment heating power.

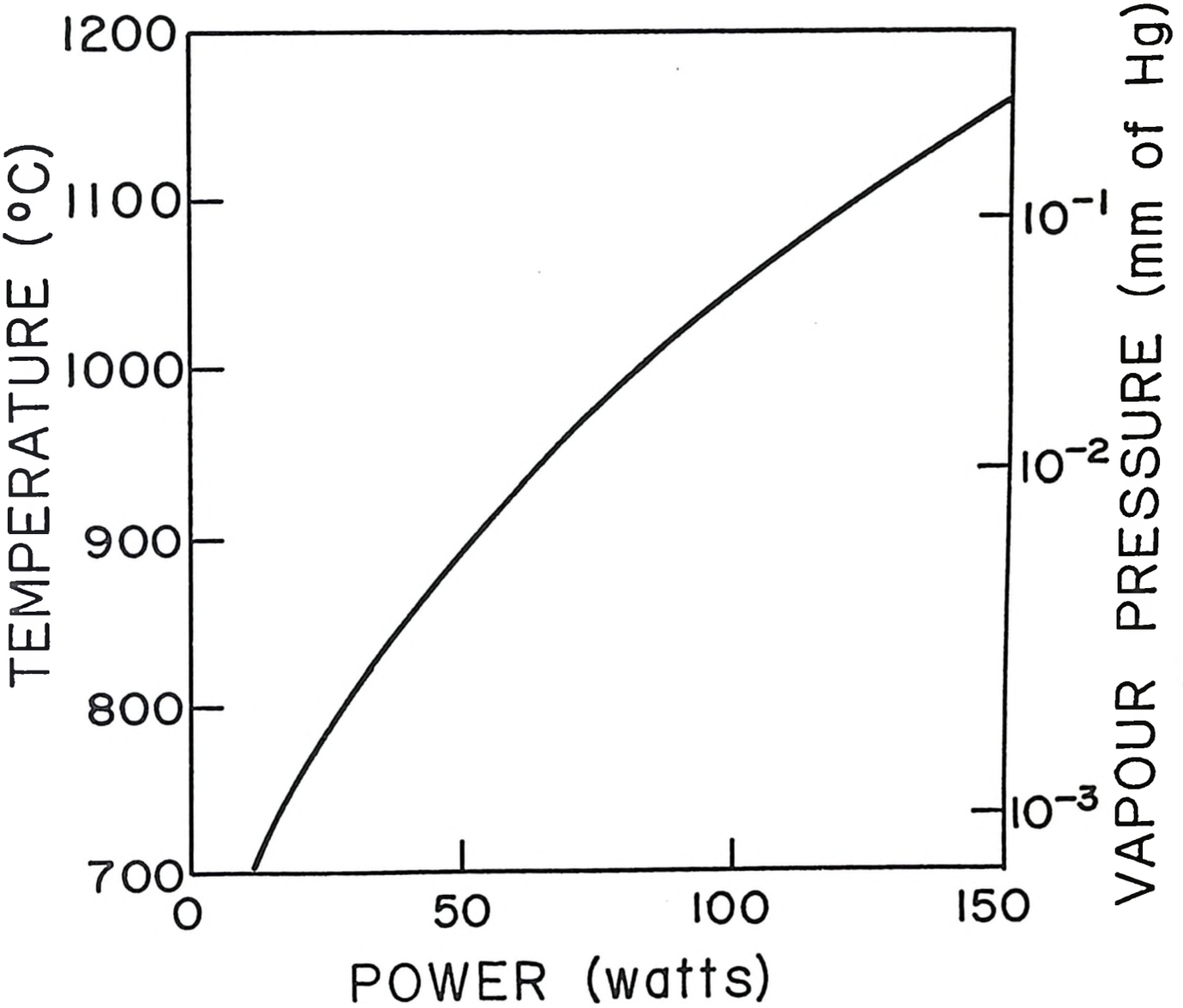
1200
1100
1000
900
800
700
TEMPERATURE (°C)
0
50
100
150
POWER (watts)
10^{-1}
10^{-2}
10^{-3}
VAPOUR PRESSURE (mm of Hg)

Figure 13

optical pyrometer. Temperature measurements were found to be reproducible by independent observers to within a few degrees Centigrade. By fine adjustment of the filament temperature and accelerating voltage, it was possible to regulate the oven temperature to a range of five or ten degrees.

It is possible to introduce the ovens to the vacuum system with a minimum of delay by the use of a vacuum lock provided with two stages of prepumping. A second oven is mounted in the same interlock and provides an alkali beam for alignment of the apparatus and calibration of the C-magnet field. This oven is similar in design to those described above but it is made of steel and heated directly by tungsten filaments.

6. RADIOFREQUENCY EQUIPMENT

For the provision of the oscillating magnetic field in the C magnet, generators are available which cover the frequency spectrum from 0.35 to 960 Mc/sec at a power level greater than one watt. This equipment is summarized in Table II. After a short warm-up period, the drift of all oscillators used was 5 kc/sec or less for a ten-minute period. The frequency jitter was less than 0.5 kc/sec so that the frequency could be adjusted to stay within 1 kc/sec of any given value for the duration of a button exposure.

Frequency measurements were carried out using a Beckmann Model 1610 10 Mc/sec counter and appropriate frequency transfer units. The gate timing of the counter and the standard frequencies of the transfer units were derived from the internal 1 Mc/sec crystal oscillator of the counter. This frequency in turn was monitored periodically by measuring the beat frequencies of its fifth and tenth harmonics with the 5 Mc/sec

TABLE II

Radiofrequency Oscillators

Manufacturer	Model No.	Frequency Range (Mc/sec)
Tektronix	190 A	0.35 - 50
Wandel and Goltermann	LMS 68/LO 40	40 - 110
Wandel and Goltermann	LMS 68/LMS 681	75 - 165
Wandel and Goltermann	LMS 68/LO 170	165 - 330
Wandel and Goltermann	LMS 68/LO 325	325 - 625
Wandel and Goltermann	LMS 68/LO 610	610 - 980

and 10 Mc/sec standard frequency transmissions of WWV. The comparisons were made by mixing on the antenna of a sensitive and selective short-wave receiver. After preliminary adjustment of the crystal oscillator, the beats with the standard transmissions were found to remain at a few cycles per second over a period of months. This corresponds to frequency errors of about one part per million. Errors in the received WWV frequencies are much smaller than this and may be neglected.

The radiofrequency power is carried by coaxial cable type RG 8/U to the atomic beam apparatus where it passes through a sealed coaxial bulkhead into the vacuum and terminates in a "loop" in the C-magnet gap. The early experiments were performed using the loops shown in Figure 14 (a) and (b) for π and σ transitions respectively. At frequencies above 300 Mc/sec these were found to be inadequate. Consequently, a new loop was designed consisting of a shorted air-dielectric coaxial line with a slot cut for the beam. This is illustrated in Figure 14 (c). Because the loops present a badly mismatched impedance to the 50-ohm transmission line, it was necessary to tune the line near the point where it passes into the vacuum. At low frequencies, this may be accomplished by using a tuned air-core transformer. At high frequencies, two tuning stubs, separated by a variable-length coaxial line, were used to match impedances. With the C-magnet field adjusted to bring the $\Delta F = 0$ resonance in a sodium beam into the desired frequency range, the circuit could be tuned to maximize the observed signal. The measurement of the voltage standing wave ratio in a slotted line was a less reliable criterion. At the frequencies employed, the tuning was sufficiently broad that a resonance search over 1 Mc/sec could be made with no further adjustment.

Figure 14. Radiofrequency loops used for (a) π transitions, (b) low frequency σ transitions, and (c) high frequency σ and π transitions. In (a) and (b), the beam passes through the loop parallel to the connector. In (c), the beam passes through the slots and the cut-away portion of the centre conductor.

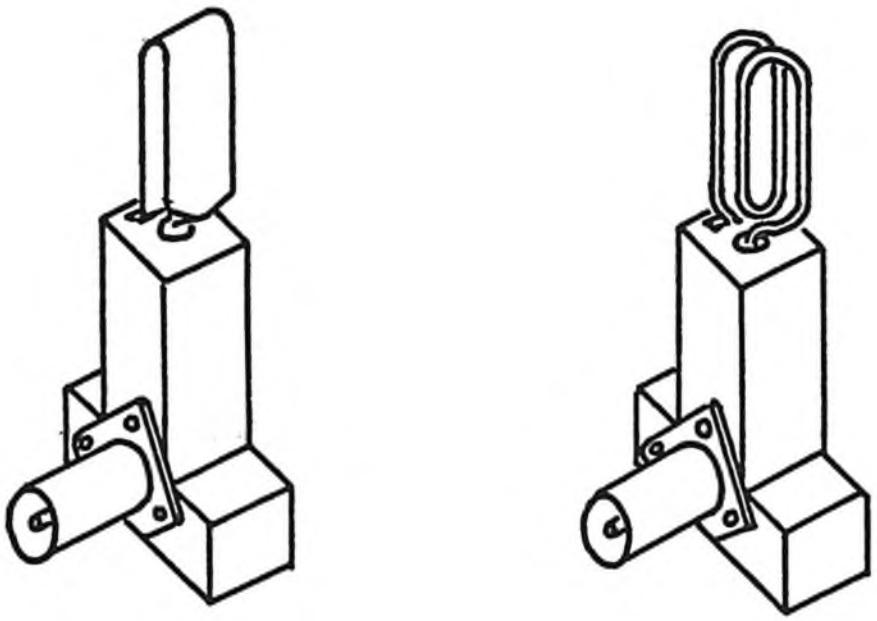

Figure 14

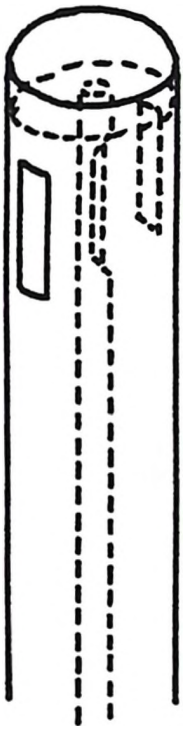

(c)

7. BEAM DETECTION

The principal method of beam detection is that of collection and counting of radioactivity. Suitable surfaces are exposed to the beam for a short time interval, then removed through a vacuum lock and transferred to the counting room. Scintillation and geiger counting systems are available for the study of the activity of the collector buttons.

Large sodium iodide crystals and photomultipliers, together with amplifiers and pulse-height selectors, allow preferential counting of gamma rays in a preset energy range. Details of the scintillation counting equipment have been given by King (King 1960). Thin anthracene and sodium iodide crystals with the same photomultipliers and pulse height analysers allow the counting of beta rays and X-rays. Finally, low-background Geiger counters allow counting of beta rays and conversion electrons. Four such Geiger counters are presently available. The counting tubes are halogen quenched end-window tubes, Philips type 18515. The matching anti-coincidence guard tubes, type 18517, were mounted over them inside lead castles of 2-inch wall thickness. The electronic circuitry is shown in block form in Figure 15. Details of the circuit are shown in Figure 16. Transistorized versions of the anticoincidence unit are being constructed for eight more counting channels.

An alternative method of detection is that of surface ionization. For a surface of work function ϕ and absolute temperature T, the ratio of ions to atoms leaving the surface is given by

$$\frac{N_+}{N_0} = \exp\left[-\frac{e(I-\phi)}{kT}\right]$$

where e is the electronic charge, I is the ionization potential, and k is

Figure 15. Block diagram of the circuitry for the anti-coincidence Geiger counters.

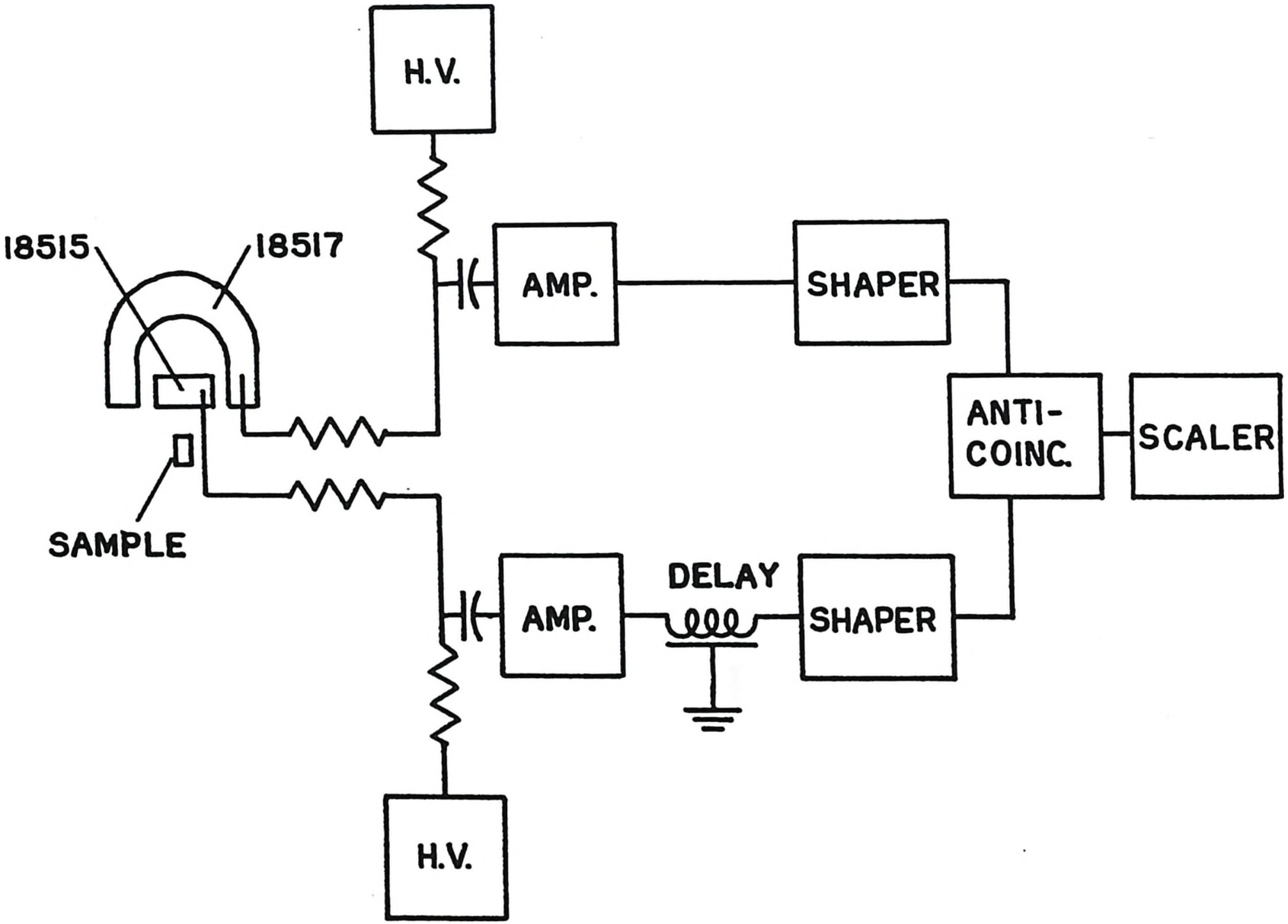
H.V.
18515
18517
AMP.
SHAPER
ANTI-
COINC.
SCALER
SAMPLE
DELAY
AMP.
SHAPER
H.V.

Figure 15

Figure 16. Schematic diagram of the anti-coincidence counting circuit. The blocked areas correspond to the amplifiers (left), pulse shapers (centre) and anti-coincidence circuit (right) of Figure 15.

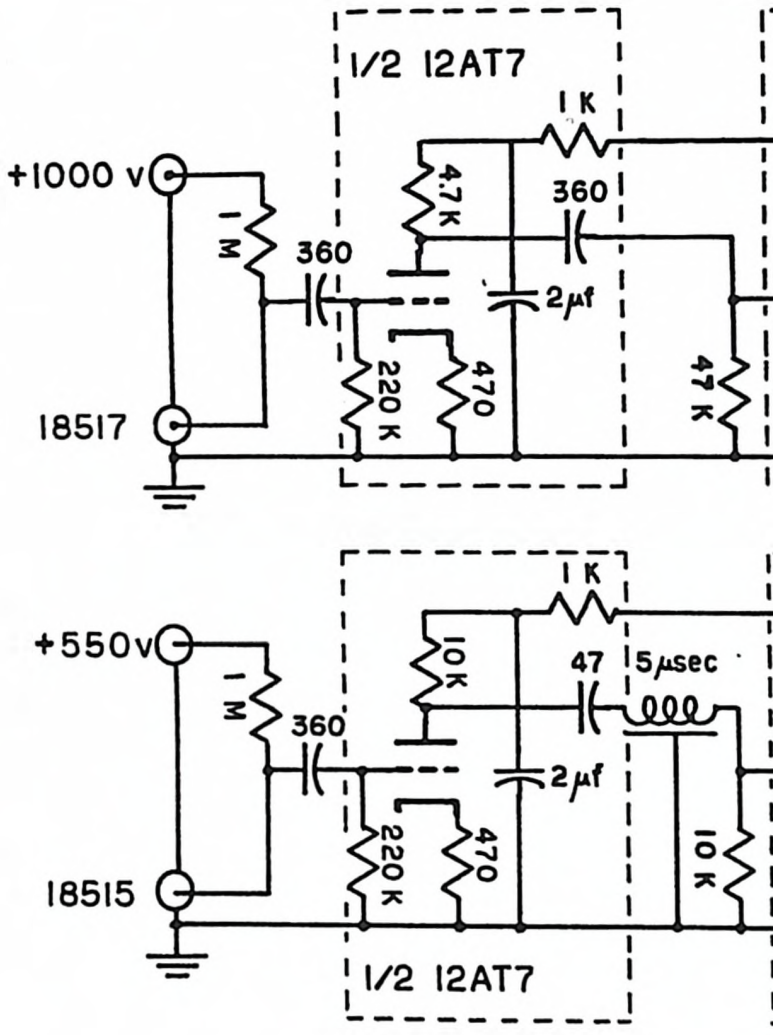
1/2 12AT7
1 K
+1000 v
4.7 K
360
1 M
360
2μf
220 K
470
47 K
18517
1 K
+550v
10 K
47
5μsec
1 M
360
2μf
220 K
470
10 K
18515
1/2 12AT7

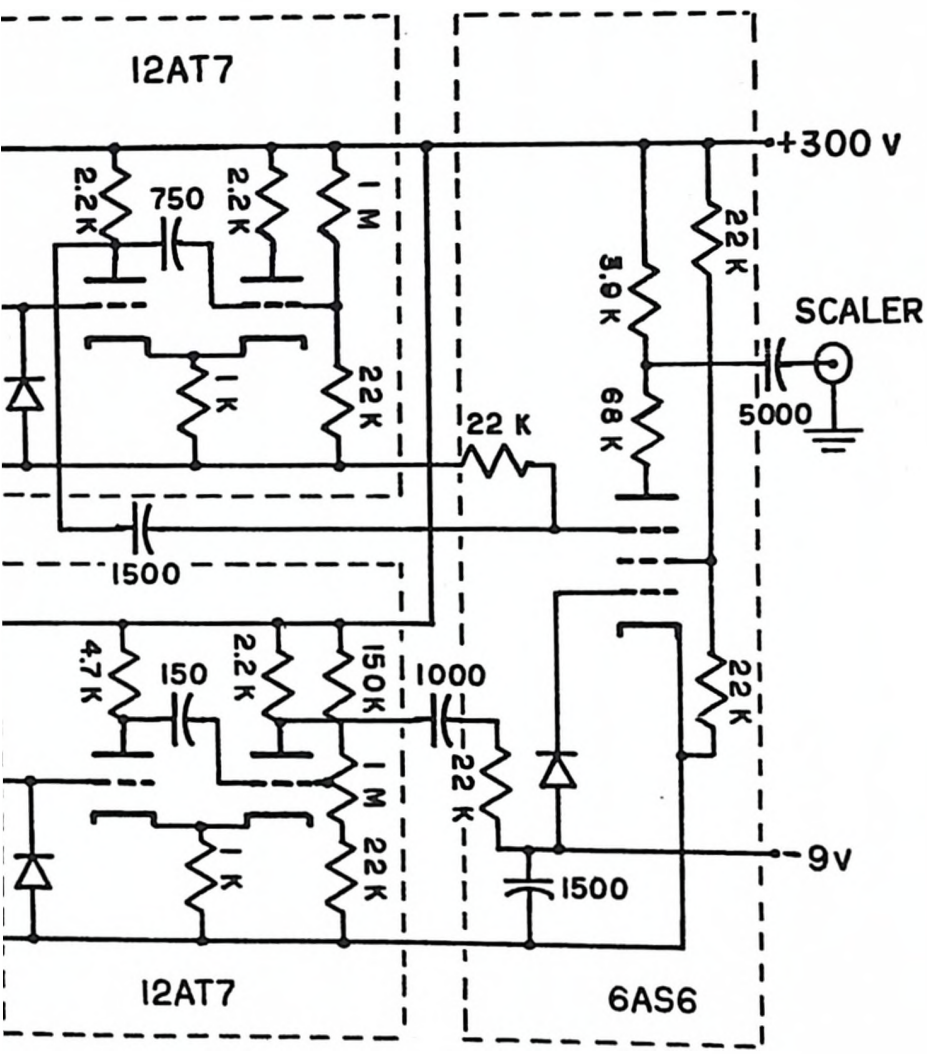
12AT7
+300 v
2.2K
750
2.2K
1 M
22K
1K
22 K
3.9 K
22 K
68 K
SCALER
5000
1500
4.7K
150
2.2K
150K
1000
22 K
1 M
22K
1K
22 K
22K
9v
1500
12AT7
6AS6

Figure 16

Boltzmann's constant. The alkali metals, whose ionization potentials are low, are therefore easily detected on hot tungsten. Materials with higher ionization potentials may be detected on oxidized tungsten or platinum. The detector consists of a tungsten ribbon which may be positioned at the exit slit of the B magnet, replacing the button holder. It may be maintained at orange heat by a current of 2 amperes. The ribbon is held at a positive voltage and the ions are collected on a grid grounded through a large resistance at the input stage of a Victoreen Tullamore Model VME-2 electrometer. The background ion current from a potassium-free tungsten wire depends strongly on temperature and apparatus pressure. Background currents of 10^{-12} amperes or less are normally encountered.

CHAPTER V

THE INDIUM EXPERIMENTS

The three indium isotopes involved in this study presented differing experimental problems. Similarities in the chemical procedures and beam production reflect the isotopic similarity, but because of differences in the nuclear properties other aspects of the experiments had to be altered radically.

1. ISOTOPE PRODUCTION

The indium isotopes studied, In^{115m}, In^{117m}, and In^{117}, were produced by the beta-decay of neutron irradiated cadmium. Natural cadmium consists of the stable isotopes shown in Table III. Listed there are the natural isotopic abundances, cross-sections, and products of thermal neutron capture. In addition, the half-lives and the principal decay daughters are shown. The Table gives an indication of the possibilities and difficulties of producing indium isotopes from cadmium by neutron irradiation.

The problem of the small cross-sections of Cd^{114} and Cd^{116} is aggravated by the very large cross-section of Cd^{113}. This isotope causes a considerable depression of the neutron flux in the region of the cadmium sample and limits the quantity of cadmium which may usefully be irradiated in a single reactor core position. The flux depression has been calculated for a number of flux distributions and absorber configurations (Westcott 1958; Case 1953). The source configuration selected

TABLE III

Indium Isotope Production

Mass	Abundance (%)	Cross-Section (10^{-24} cm^2)	Reaction Product	Half-Life	Principal Daughter
106	1.215	1	Cd^{107}	6.7 h	Ag^{107}
108	0.875	?	Cd^{109}	470 d	Ag^{109}
110	12.39	0.2	Cd^{111m}	49 m	Cd^{111}
		?	Cd^{111}	Stable	-
111	12.75	?	Cd^{112}	Stable	-
112	24.07	0.03	Cd^{113m}	14 y	In^{113}
		?	Cd^{113}	Stable	-
113	12.26	19300.	Cd^{114}	Stable	-
114	28.86	0.14	Cd^{115m}	43 d	In^{115}
		1.1	Cd^{115}	54 h	In^{115m}
116	7.58	$\sim$0.1	Cd^{117m}	2.9 h	In^{117}
		$\sim$1.	Cd^{117}	50 m	In^{117m}

was a hollow circular cylinder of height 1.5 inches, diameter 0.65 inches, and wall thickness 0.005 inch. This form fits neatly to the inside surface of a standard irradiation capsule of the Hallaster reactor and contains about two grams of cadmium. For such a configuration, the calculated average flux in the sample is 10 to 15 per cent of the undisturbed flux. This result is in agreement with the activities of cadmium produced and with measurements of the flux using cobalt-bearing aluminum monitors which were irradiated with a cadmium sample and compared against similar monitors irradiated at the same core position when no cadmium was present.

The long half-life of Cd^{115} compared to that of Cd^{117} and to Cd^{117m} allows the production of sources of In^{115m} with high activity and high purity. The shorter-lived In^{117} isotopes are necessarily produced in smaller quantity and are contaminated by considerable In^{115m} activity. This complicating background can be minimized by advantageous selection of irradiation and separation times. The growth and decay of any of the isotopes may be calculated for any duration of irradiation, provided the formation cross-sections, half-life, and decay mode are known for the parent isotope. The decay rate of the daughter isotope in question must also be known. This calculation has been performed using the best available data for the isotopes In^{115m}, In^{117m}, and In^{117}. The cross-sections for the formation of Cd^{117} and Cd^{117m} are not well known, but are estimated to be of the same size as those for formation of Cd^{115} and Cd^{115m}. The isomeric cross-section ratio of the latter pair is in agreement with theoretical values (Bishop 1961). Figure 17 shows the growth and decay in cadmium of the indium isotopes for irradiation times of (a) 100 hours, (b) 2 hours, and (c) 6 hours. The activities of In^{115m}

Figure 17. Growth and decay of indium activities in cadmium of natural isotopic constitution for irradiation times of (a) 100 hours, (b) 2 hours and (c) 6 hours. The solid, dashed and dotted lines represent the In^{115m}, In^{117m} and In^{117} activities respectively.

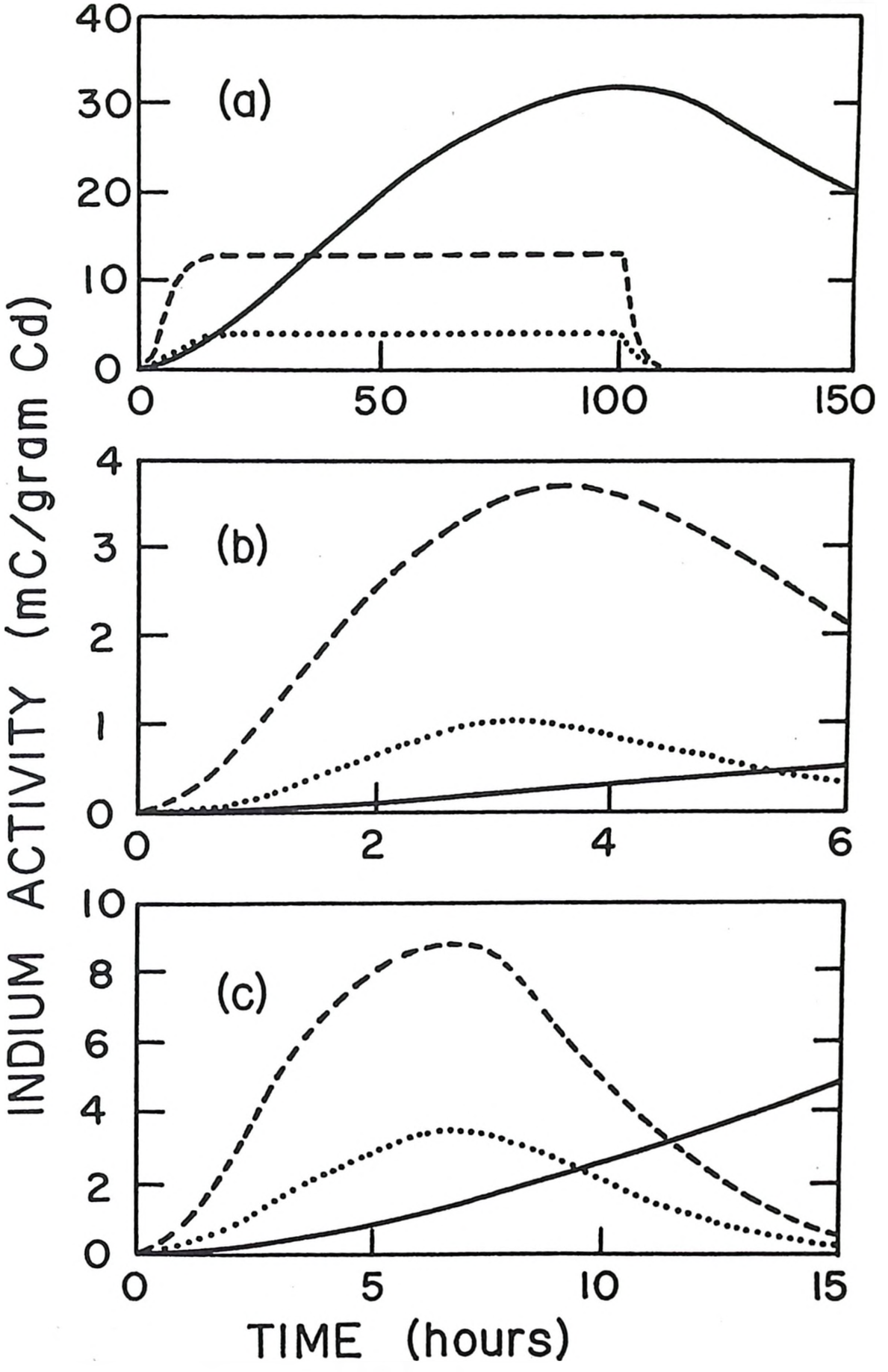
(a)
(b)
(c)
INDIUM ACTIVITY (mC/gram Cd)
TIME (hours)
0
10
20
30
40
50
100
150
1
2
3
4
6
8
5
15

Figure 17

(solid line), In^{117m} (dashed line), and In^{117} (dotted line) are given in millicuries per gram of cadmium with normal isotopic constitution in a neutron flux of 10^{12} neutrons/cm^2 sec.

The methods of production and detection were optimized using the decay schemes of the cadmium and indium isotopes concerned. Considerable data has been accumulated for the mass-115 chain, leading to an unambiguous decay scheme (McGinnis 1960a). This is shown in Figure 18 (a). Much less is known of the mass-117 chain however. Conflicting evidence has been presented relating to the parentage of the two indium isomers. The decay scheme adopted is a slightly modified version of that presented by Gleit (Gleit 1958) and is shown in Figure 18 (b). This differs little with the scheme adopted by the Nuclear Data Group (McGinnis 1960b) but disagrees with that proposed by LeBlanc (LeBlanc 1957). There is relative unanimity insofar as the indium decay to Sn^{117} is concerned.

2. CHEMISTRY

The production of an atomic beam containing the radioactive indium isotopes discussed above requires the separation of these isotopes from the irradiated cadmium and the reduction of the indium, together with stable carrier, to its elemental form. Since the half-lives of the indium isotopes studied are relatively short, the time allowed for the recovery procedure is necessarily small.

There are a number of procedures for the separation of indium from cadmium. The method of ion exchange is suitable for use with small quantities of the elements involved. Scintillation counting techniques were used to study such a separation method. When small amounts of activity were used, indium was separated with no discernable trace of

(solid line), In^{117m} (dashed line), and In^{117} (dotted line) are given in millicuries per gram of cadmium with normal isotopic constitution in a neutron flux of 10^{12} neutrons/cm^2 sec.

The methods of production and detection were optimized using the decay schemes of the cadmium and indium isotopes concerned. Considerable data has been accumulated for the mass-115 chain, leading to an unambiguous decay scheme (McGinnis 1960a). This is shown in Figure 18 (a). Much less is known of the mass-117 chain however. Conflicting evidence has been presented relating to the parentage of the two indium isomers. The decay scheme adopted is a slightly modified version of that presented by Gleit (Gleit 1958) and is shown in Figure 18 (b). This differs little with the scheme adopted by the Nuclear Data Group (McGinnis 1960b) but disagrees with that proposed by LeBlanc (LeBlanc 1957). There is relative unanimity insofar as the indium decay to Sn^{117} is concerned.

2. CHEMISTRY

The production of an atomic beam containing the radioactive indium isotopes discussed above requires the separation of these isotopes from the irradiated cadmium and the reduction of the indium, together with stable carrier, to its elemental form. Since the half-lives of the indium isotopes studied are relatively short, the time allowed for the recovery procedure is necessarily small.

There are a number of procedures for the separation of indium from cadmium. The method of ion exchange is suitable for use with small quantities of the elements involved. Scintillation counting techniques were used to study such a separation method. When small amounts of activity were used, indium was separated with no discernable trace of

Figure 18. Features of the decay schemes of the mass chains (a) A = 115 and (b) A = 117 pertinent to the present experiments.

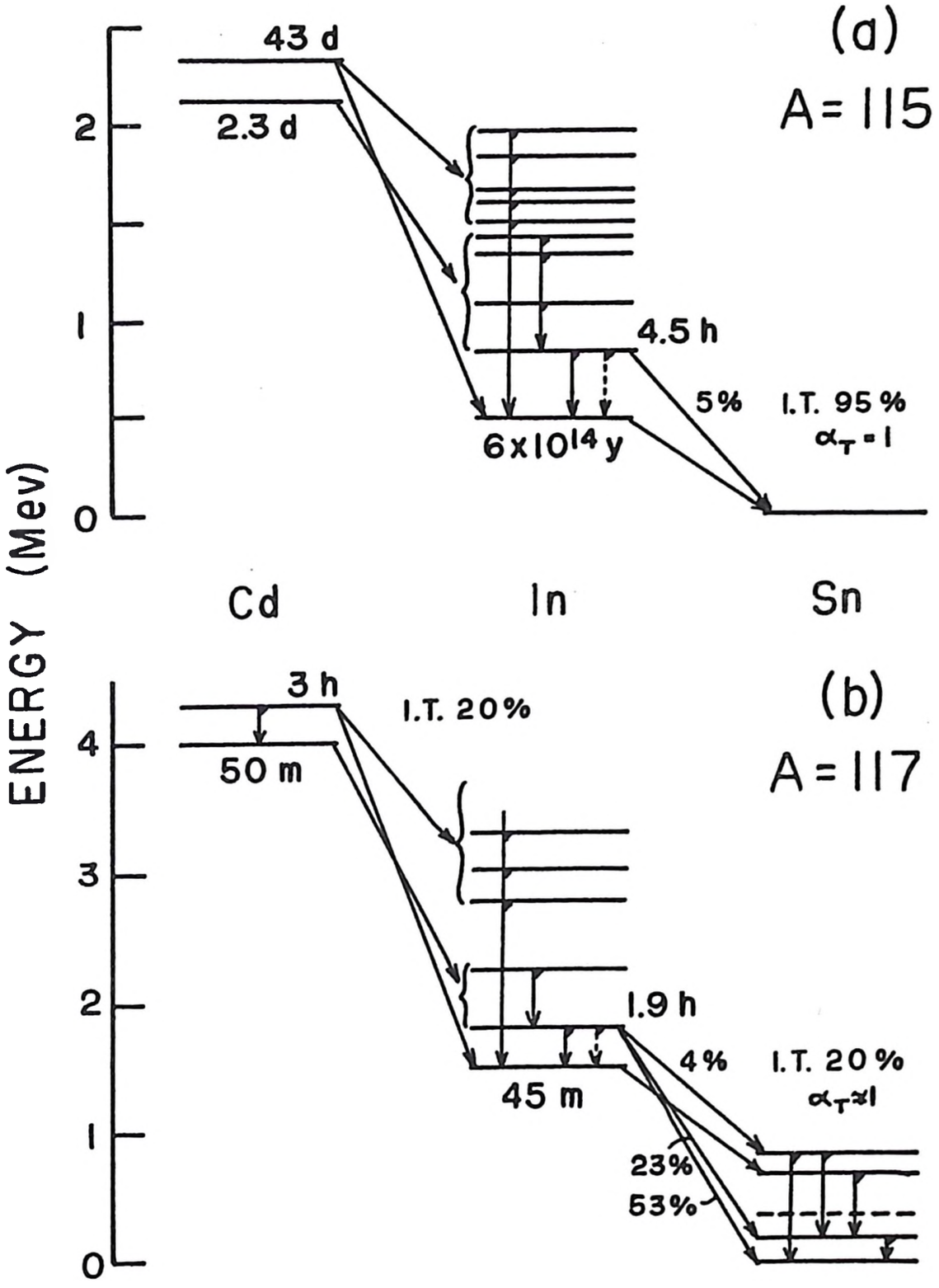
(a)
A = 115
43 d
2.3 d
4.5 h
5%
I.T. 95 %
$\alpha_T = 1$
6×10^{14} y
(b)
A = 117
3 h
I.T. 20%
50 m
1.9 h
4%
I.T. 20 %
$\alpha_T \approx 1$
45 m
23%
53%
ENERGY (Mev)
0
1
2
3
4
Cd
In
Sn

Figure 18

cadmium contamination. However, as the amount of cadmium was increased to the two grams required for the beam experiments, the volume of ion exchange resin rose proportionately and unwieldy volumes of solvent were required. The yield of active indium was found to decrease with the larger columns.

Solvent extraction provides another means of separation of indium from cadmium. However, to handle the two-gram cadmium sample the volume of solvent again proves a difficulty.

The method finally selected is similar to that used in the production refining of indium, although it was devised independently and contains some essential differences. The cadmium, together with 15 to 25 milligrams of indium carrier, is dissolved in a minimum quantity of concentrated nitric acid (about 4 ml) in a 15 ml centrifuge tube. With the addition of ammonia both indium and cadmium hydroxides precipitate. In an excess of ammonia, however, the cadmium forms the soluble ammonium complex $Cd(NH_3)_4(OH)_2$ while the indium hydroxide remains insoluble. Therefore, to effect the separation, the test tube is filled with concentrated ammonium hydroxide and centrifuged. The cadmium fraction is removed and the indium precipitate washed in a further 10 ml of ammonia to remove any residual cadmium. The precipitate is redissolved in hydrochloric acid.

The indium may be recovered as a metal from its acid solution by electrolysis. However, the time required for such a recovery is excessive and the yield is low (Marino 1959). An alternative method was found to be superior. To the weakly acidic solution are added about 75 milligrams of aluminum filings. A spongy black mass of metallic indium is formed, while

most of the excess aluminum dissolves in the acid. The sponge is then lifted from the solution, washed with alcohol, and compressed to remove most of the liquid. The metal is then loaded in the oven and transferred to the atomic beam apparatus.

The procedure outlined above can be carried out in 20 to 30 minutes. Gamma ray spectrum analysis of samples taken at each stage of a typical separation indicated that at least 98 per cent of the cadmium is eliminated. The overall yield of indium is about 70 to 80 per cent, most of the loss occurring in the reduction phase of the process.

3. ENRICHED ISOTOPE SOURCES

As has been pointed out, the use of natural cadmium sources for producing the In^{117} and In^{117m} activities has a decided disadvantage in the search for resonances which might be weak due to the ever-present In^{115m} activity in the background. For the study of the In^{117m} $\Delta F = \pm 1$ transitions and for the work with In^{117}, sources were prepared from cadmium enriched in Cd^{116}. In this way, it was hoped, the analysis of button decay curves would be somewhat simplified. The sample of CdO obtained from the Oak Ridge National Laboratory was of the isotopic constitution shown in Table IV. Since the absorbing effect of the Cd^{113} is now small, the neutron flux in the sample may be assumed to be almost ten times as large as in the natural cadmium samples. The increase by a factor of 12 in the abundance of Cd^{116} gives an overall gain of about 100 in specific activity. Further, the reduction in Cd^{114} improves the 117(m):115 ratio by a factor of 80.

The production of In^{117} and In^{117m} from enriched Cd^{116} provided a further chemical problem, which was that of recovery of the expensive cadmium for re-use. The dissolved cadmium fraction at the excess-ammonia

TABLE IV

Isotopic Analysis of Enriched Cd^{116} Sample

Isotope	Atomic %
106	0.05
108	0.05
110	0.12
111	0.18
112	0.32
113	1.07
114	4.20
116	94.11

stage of the separation may be boiled to dryness to remove most of the ammonia and recover the cadmium as $Cd(OH)_2$. However, a considerable quantity of ammonium nitrate is included in this fraction. It was found easiest to further purify the cadmium fraction by adding more nitric acid to redissolve the cadmium, then to precipitate pure cadmium hydroxide using lithium or potassium hydroxide, which in excess does not redissolve cadmium hydroxide. After centrifugation, the cadmium hydroxide may be dried as a white powder and re-irradiated. This process was found to yield approximately 90 to 95 per cent of the original cadmium.

Since the stable In^{115} carrier used in the separation has a high cross-section to form 1-hour In^{116m}, which might be confused with the 45-minute In^{117} in the beam, it was thought advisable to further clean the cadmium fraction after separation. This was done by carrying through a further "dummy" separation before each irradiation, using thallium or iron as a carrier for any traces of indium which might exist. This was followed by a final recovery of the cadmium hydroxide as outlined above. The overall yield of the three-stage process was in excess of 75 per cent.

4. BEAM PRODUCTION

The vapour pressure of pure indium metal as a function of temperature is given by the relation

$$\log_{10} p = 8.003 - \frac{12180}{T}$$

where T is the absolute temperature and p is the vapour pressure in millimeters of mercury. Thus a vapour pressure of 0.1 mm is attained at a temperature of 1350°K or 1080°C. The temperatures, source masses and run durations are presented in Table V.

TABLE V

Indium Run Data

Isotope	Carrier Mass (mg)	Oven Temperature (°C)	Duration of Run (hours)
In^{115m}	25	1050	2
In^{117m}	20	1100	1
In^{117}	15	1150	1/2

During early experiments with indium beams (King et al. 1961), magnesium metal was used to reduce the indium from the acid solution. In many instances, much of the indium was lost due to the formation at 500 to 600°C of an intense beam of short duration. That this beam was molecular in nature is deduced from the fact that, while bearing the indium activity, it was not affected by the deflecting magnets. With the substitution of aluminum for magnesium during the reduction, this difficulty in beam production was removed and satisfactory beams were obtained with regularity.

Since the fine structure separation ΔE between the $^2P_{1/2}$ ground state of indium and the metastable $^2P_{3/2}$ state is only 2212 cm^{-1}, both will be present in the beam at the source temperatures used. The ratio of the populations is given by

$$\frac{N(^2P_{3/2})}{N(^2P_{1/2})} = \exp\left(-\frac{\Delta E}{kT}\right) \approx 0.10 \quad .$$

The hyperfine structure of both states was studied.

Using the methods described in Chapter IV, the source temperature was held constant to a few degrees near the temperatures indicated in Table V. After the initial rise in oven temperature to the operating level, fluctuations in beam intensity were found to be smaller than 10 per cent. Toward the end of a run, the beam could be maintained by further heating to drive the indium off the cooler parts of the oven, principally the lid. Intensity variations during the course of the runs were measured and allowed for as described in the sections which follow.

5. HOT WIRE DETECTION

The carrier indium beam, as well as the stable sodium calibrating beam, were detected by means of the surface ionizer. The ionization potential of indium, 5.96 volts, is somewhat larger than the work function of pure tungsten, which is 4.5 to 5 volts, depending on the crystal structure. However, by using tungsten wire of high purity, from which the background ion current was very low, it was found possible to detect the indium beam without oxidizing the wire. From the rate of source depletion and the solid angle subtended by the detector at the source, the ionization efficiency is estimated to be about 1 per cent. This is in accord with the efficiency to be expected on the basis of the formula given in Chapter IV, using a tungsten work function of about 5 volts and a temperature of 2500°K. Measured ion currents of 10^{-11} to 10^{-10} amperes were found. This is to be compared with a background current of about 10^{-12} amperes.

Platinum was tried as an ionizing surface for indium, but without success, although its work function is about 6 volts. This failure to detect is attributed to adsorption of indium on the surface at the operating temperature which had to be restricted because of the softening of the wire.

6. DETECTION OF THE RADIOACTIVE BEAM

For the collection of indium, a number of surfaces were tested for high reproducible sticking probabilities. No attempt was made to assess the absolute values of the sticking coefficients, but many relative measurements were made. Some of the materials tested were antimony, brass, copper, indium, lampblack, plastic, platinum, sulphur, and tungsten. Copper was found to be as efficient as any and gave reproducible results when

freshly plated on a clean iron substrate from a slightly acidic solution of cupric sulphate.

The indium isotopes studied decay largely by the emission of either a beta-particle or a conversion electron. Table VI compares the counting efficiencies and background rates of several types of detector for the three isotopes studied. The suitability of the Geiger counting system in each case is clearly indicated, although there was a sacrifice of isotope selectivity. Since no other form of isotope identification was feasible, a measurement of the half-life of the activity of each collected sample must be made.

7. EXPERIMENTAL RESULTS

As has been shown in Chapter III, the nuclear spin and moments of an isotope follow from the way in which its Zeeman and hyperfine transition frequencies vary with field. This field dependence is determined experimentally by obtaining resonances in a series of appropriately selected field strengths. For the study of short-lived isotopes, each run of the series requires a separate source and several hours of counting.

Since the method of radioactive detection does not permit continuous scanning, separate points on the resonance must be obtained by collection of the beam under fixed conditions for a period of time. Subsequent counting of the collected sample establishes the nature and quantity of the activity collected. The resulting counting rates of all the collected samples must then be suitably normalized to allow for radioactive decay. This is accomplished by counting each beam sample at suitable intervals of time to obtain a decay curve. If only a single radioisotope is involved, as in the case of In^{115m}, the curve, after sub-

TABLE VI

Comparison of Counting Methods for Indium Activities

Method	In^{115m}		In^{117m}		In^{117}	
	Efficiency (%)	Background (cpm)	Efficiency (%)	Background (cpm)	Efficiency (%)	Background (cpm)
γ (scin)	10	3	10	5	20 40	2 5
X (scin)	20	1	10	1	-	-
e (scin)	20	2	40	2	30	2
e (G-M)	20	1	40	1	40	1

traction of the constant counter background, is a simple exponential as shown in Figure 19. If more than one activity is collected, a composite curve is obtained which must then be resolved into its pure exponential components. Such a decay curve, obtained with In^{117m}, is shown in Figure 20 resolved into components corresponding to the decay of In^{117m} and In^{115m}. Such an analysis of course introduces more uncertainty into the measurement of the intensities of the isotopes involved than does the single exponential decay.

The intensities of the activities on each of the exposed buttons is then projected to a common time, usually taken near the beginning of the run. This form of decay correction, using only the times of counting and not of exposure, is valid only if the isotopic constitution of the beam is the same as that of the source (cf., for example, Childs and Goodman 1960).

The decay-corrected counting rates must be further normalized to allow for variations in beam intensity from one exposure to the next. If a single activity is present in the beam this is accomplished by periodically monitoring the beam intensity and interpolating in time, assuming a smooth time-dependence of the intensity. Frequent measurements of the source temperature and carrier beam intensity give confidence in this procedure. Monitor buttons are exposed for a short time with the obstacle wire removed so that the fast portion of the beam can reach the detector without the necessity of moment-changing transitions. Such exposures are subject to the same type of decay measurement and correction as are the exposures on the resonance.

Figure 19. Typical decay curves for the activity deposited on the collector buttons. The solid circles are for a monitor exposure, the open circles for an exposure on resonance. Statistical counting errors are less than the size of the circles unless otherwise indicated. The straight lines have been drawn to correspond to a 4.5-hour half-life.

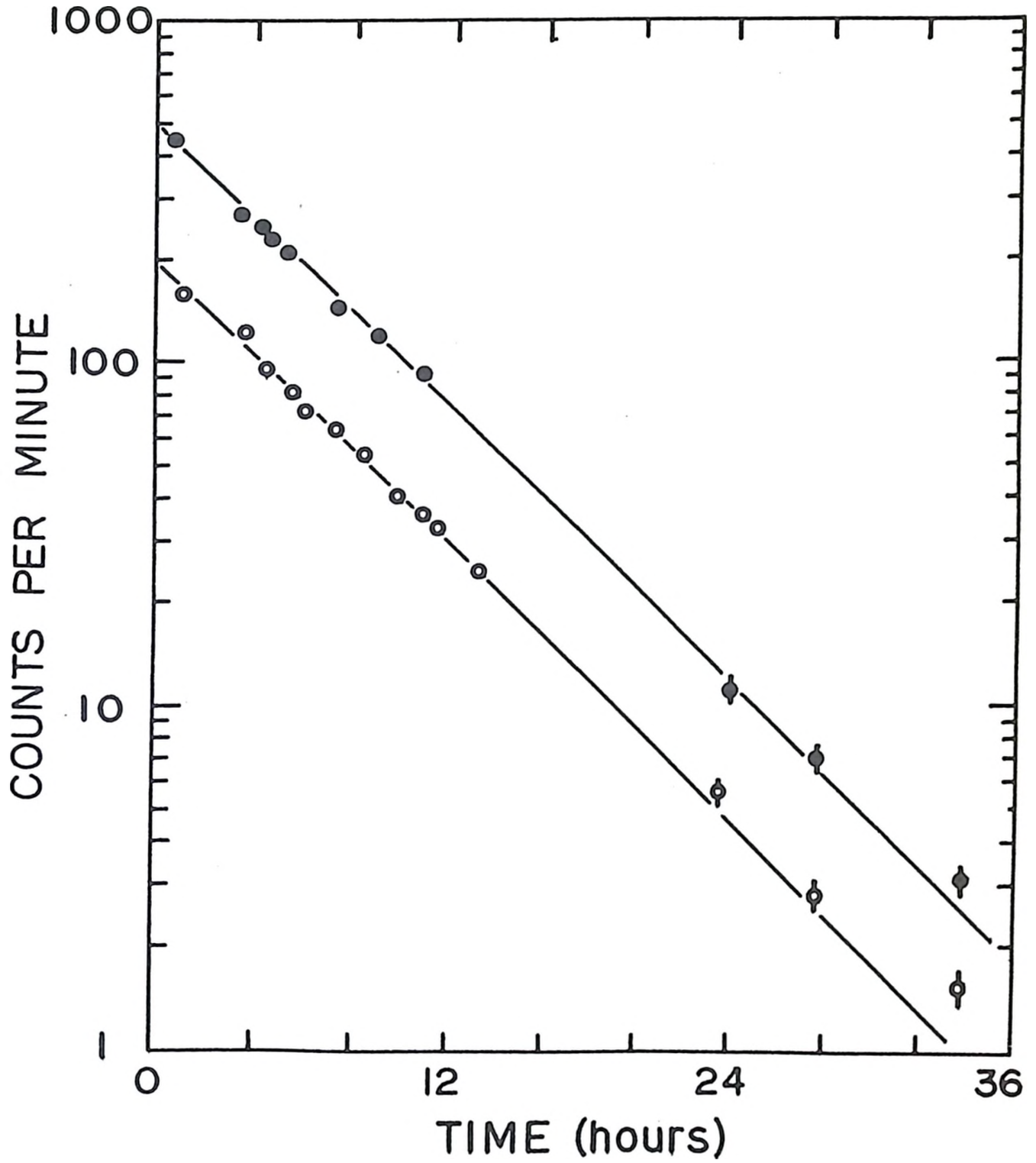

Figure 19

Figure 20. Decay curve of activity collected in an In^{117m} run. The analysis of the composite decay into components with half-lives of 4.5 and 1.9 hours is shown.

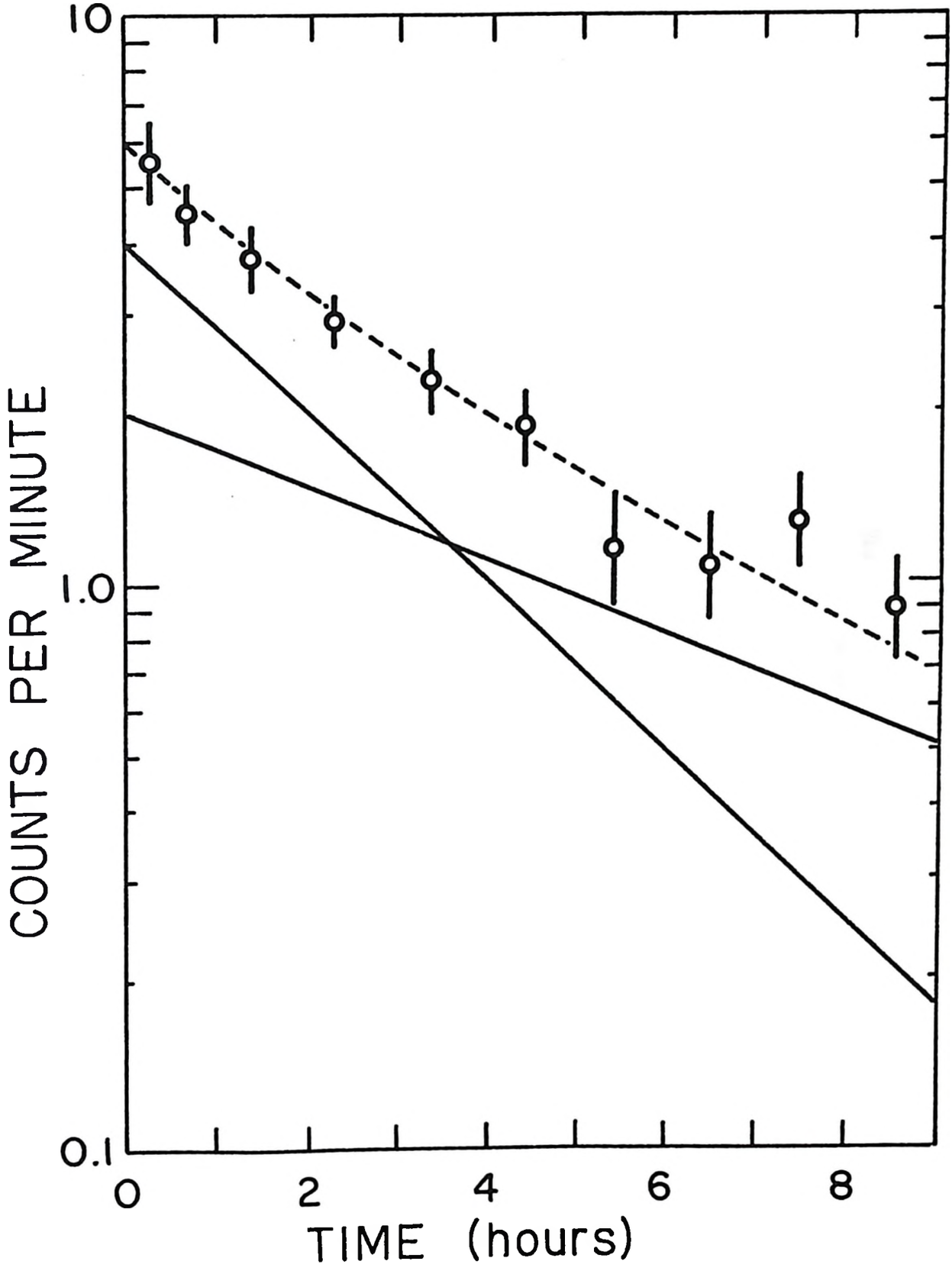

Figure 20

If a second activity is present in the beam, its presence may be used as a monitor of the beam intensity. In this "ratio normalization" technique a resonance in one isotope is observed as an increase in the ratio of its activity to that of the second isotope. This method of course assumes that the resonances in the two isotopes do not occur at the same frequency.

The resonance exposure counting rates, normalized as indicated above for decay and beam intensity, are then plotted against the oscillator frequency at which they were exposed. A smooth curve is fitted to the points and its peak position taken as the resonance frequency.

The C-magnet field was measured before and after each radioactive resonance run and in some cases in the middle of the run. As was indicated previously, this involved placing a sodium-filled oven at the source position and observing the frequency of the Na^{23} resonance using the hot wire detector. In cases where field drifting was observed, smooth variation was assumed and interpolated values of the field, with correspondingly larger uncertainties, were taken. In addition to providing the vital information on C-field strength, the sodium resonance gave a clue to the degree of broadening and distortion to be expected in the radioactive resonance due to field inhomogeneity.

a. In^{115m}

The long half-life of the parent Cd^{115} (54 hours) allows the preparation of beams containing In^{115m} as the only significant activity, as has been previously illustrated.

In an earlier investigation in this laboratory (King 1961) the nuclear spin of In^{115m} was found to be 1/2. The further study of this isotope consisted of following the $\Delta F = 0$ resonance in the $^2P_{1/2}$ electronic

state to high field to determine the value of $a_{1/2}$. After this, observation of transitions between the two hyperfine states in both the $^2P_{1/2}$ and $^2P_{3/2}$ electronic states allowed a precise determination of the interaction constants in these two states.

Resonances corresponding to the transition $(1,1 \leftrightarrow 1,0)$ were obtained at C-magnet fields up to 500 gauss. A representative resonance is shown in Figure 21. The points represent the results for each of the 10-minute button exposures. The statistics shown represent the accumulated uncertainties in the counting, as well as the larger uncertainty due to fluctuations in the beam intensity.

TableVII lists the $\Delta F = 0$ resonances observed in this way. The measured indium resonance frequencies with their estimated uncertainties are given in the first column. The next two columns show the frequencies of the sodium beam field calibrating resonance and the C-magnet fields deduced from them. The fourth and fifth columns give the values of $|a_{1/2}|$ for In^{115m} calculated using the equations of Chapter III and assuming the sign of the nuclear magnetic moment to be positive and negative respectively.

At the highest field used, about 500 gauss, the line width was considerably greater than at lower fields. This is illustrated by Figure 22 which also shows the line shape distortion which was encountered at higher fields. The weighted average of $a_{1/2}$ from these runs is either +901.0 ± 1.1 Mc/sec or -903.5 ± 1.1 Mc/sec. The internal consistency of these data is not sufficient to establish the sign of $a_{1/2}$. It will be recalled from Chapter III that $a_{1/2}$ enters the expression for the frequency ν without its sign, and that the only way in which the sign affects the transition frequency is through the small terms in μ_I.

Figure 21. A $\Delta F = 0$ resonance curve in In^{115m}. If the resonance frequency were a linear function of magnetic field, the maximum would have occurred at ν_0.

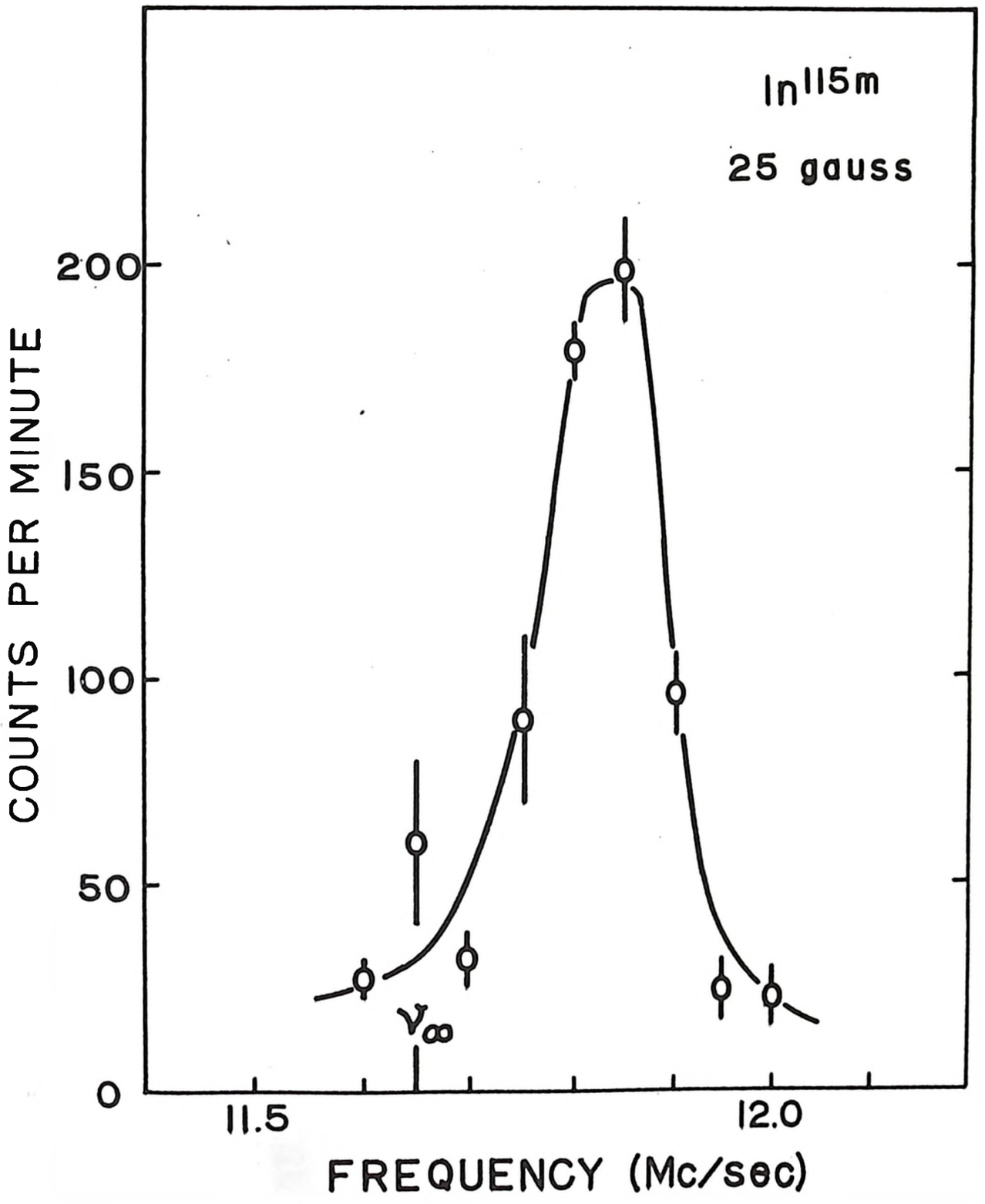
In115m
25 gauss
200
150
100
50
0
COUNTS PER MINUTE
ν_∞
11.5
12.0
FREQUENCY (Mc/sec)

Figure 21

TABLE VII

The $\Delta F = 0$ Transition $(1,1 \leftrightarrow 1,0)$ in $^2P_{1/2}$ In^{115m}

ν_{In} (Mc/sec)	ν_{Na} (Mc/sec)	H (gauss)	$\lvert a_{1/2} \rvert$ (Mc/sec)	
			$\mu_I > 0$	$\mu_I < 0$
7.01 ± .03	10.610 ± .003	14.895 ± .005	680 $^{+600}_{-120}$	720 $^{+940}_{-250}$
11.83 ± .03	18.025 ± .005	25.000 ± .007	750 $^{+120}_{-90}$	790 $^{+135}_{-100}$
21.48 ± .03	33.248 ± .005	45.015 ± .007	860 ± 50	890 ± 55
38.85 ± .07	61.65 ± .04	80.00 ± .06	875 ± 35	890 ± 40
59.37 ± .04	97.11 ± .01	120.00 ± .01	898 ± 10	907 ± 11
65.88 ± .07	108.50 ± .03	132.11 ± .04	868 ± 16	876 ± 16
75.29 ± .05	125.91 ± .02	149.98 ± .02	896 ± 8	903 ± 9
95.05 ± .05	163.35 ± .02	186.15 ± .02	893.9 ± 5.4	900.0 ± 5.6
173.45 ± .10	330.34 ± .01	320.54 ± .01	900.4 ± 3.9	903.6 ± 3.9
173.60 ± .05	330.75 ± .05	320.83 ± .05	901.6 ± 2.6	904.8 ± 2.6
289.32 ± .06	623.17 ± .05	499.60 ± .04	901.5 ± 1.3	903.3 ± 1.3

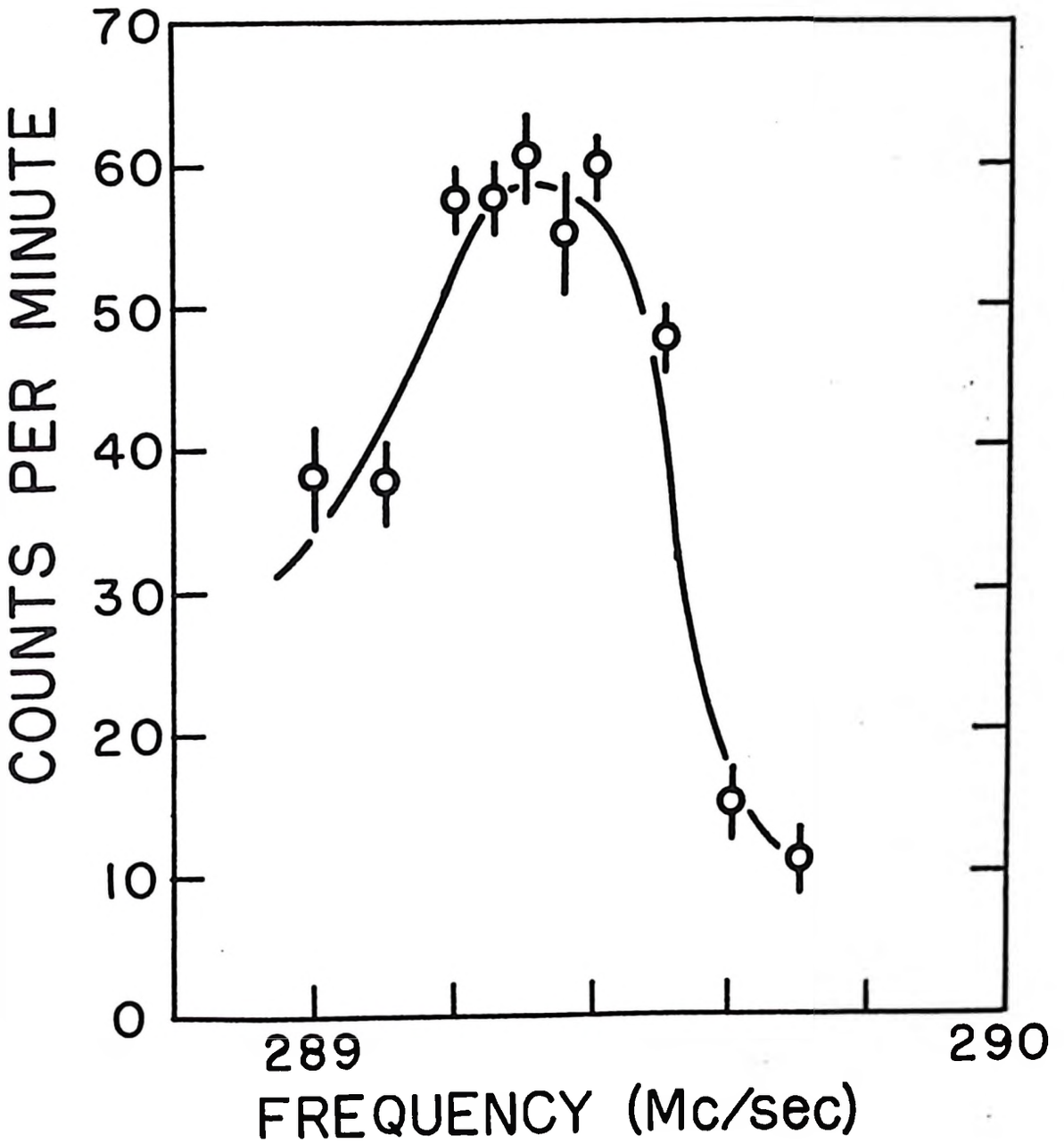
70
60
50
40
30
20
10
0
COUNTS PER MINUTE
289
290
FREQUENCY (Mc/sec)

Figure 22

As a result, when μ_I is small (as it is in this case), experimental errors prevent one from meaningfully deciding which gives a more consistent fit to the resonance data.

A search was made to observe the π transition $(1,1 \leftrightarrow 0,0)$ in the region 906.0 to 910.3 Mc/sec at a C-magnet field of 10 gauss. This corresponds to the range 901.3 to 905.6 Mc/sec for $|a_{1/2}|$. Since it had been observed that the sodium calibrating resonance was quite weak at the higher frequencies, it was not surprising when no clear $\Delta F = \pm 1$ resonance was found.

Using the loop constructed for the purpose (Figure 14b), a search was made for σ transitions in the $^2P_{3/2}$ electronic state. In order to determine the frequency range to be searched, the value of the hyperfine interaction constant in this state, $|a_{3/2}|$, was estimated. It was assumed that the ratio $a_{3/2}:a_{1/2}$ would be approximately the same for In^{115m} as for In^{115} and In^{113}, namely

$$a_{3/2}:a_{1/2} = 0.1061:1 \quad .$$

Accordingly, the estimate of $|a_{3/2}|$ was 95.86 ± 0.12 Mc/sec, and the predicted hyperfine separation in the $^2P_{3/2}$ electronic state

$$\left|\frac{W(2) - W(1)}{h}\right| = 2\,|a_{3/2}| = 191.72 \pm 0.24 \text{ Mc/sec} \quad .$$

The search proceeded and was successful. Due to the weak field dependence of the transition frequency, the lines observed had the theoretical shape calculated in Chapter III. A representative resonance is shown in Figure 23. The large background is contributed mainly by scattered atoms in the $^2P_{1/2}$ state. Table VIII lists the results of four separate examinations

Figure 23. A resonance curve corresponding to the $\Delta F = \pm 1$ σ transition in the $^2P_{3/2}$ state of In^{115m}.

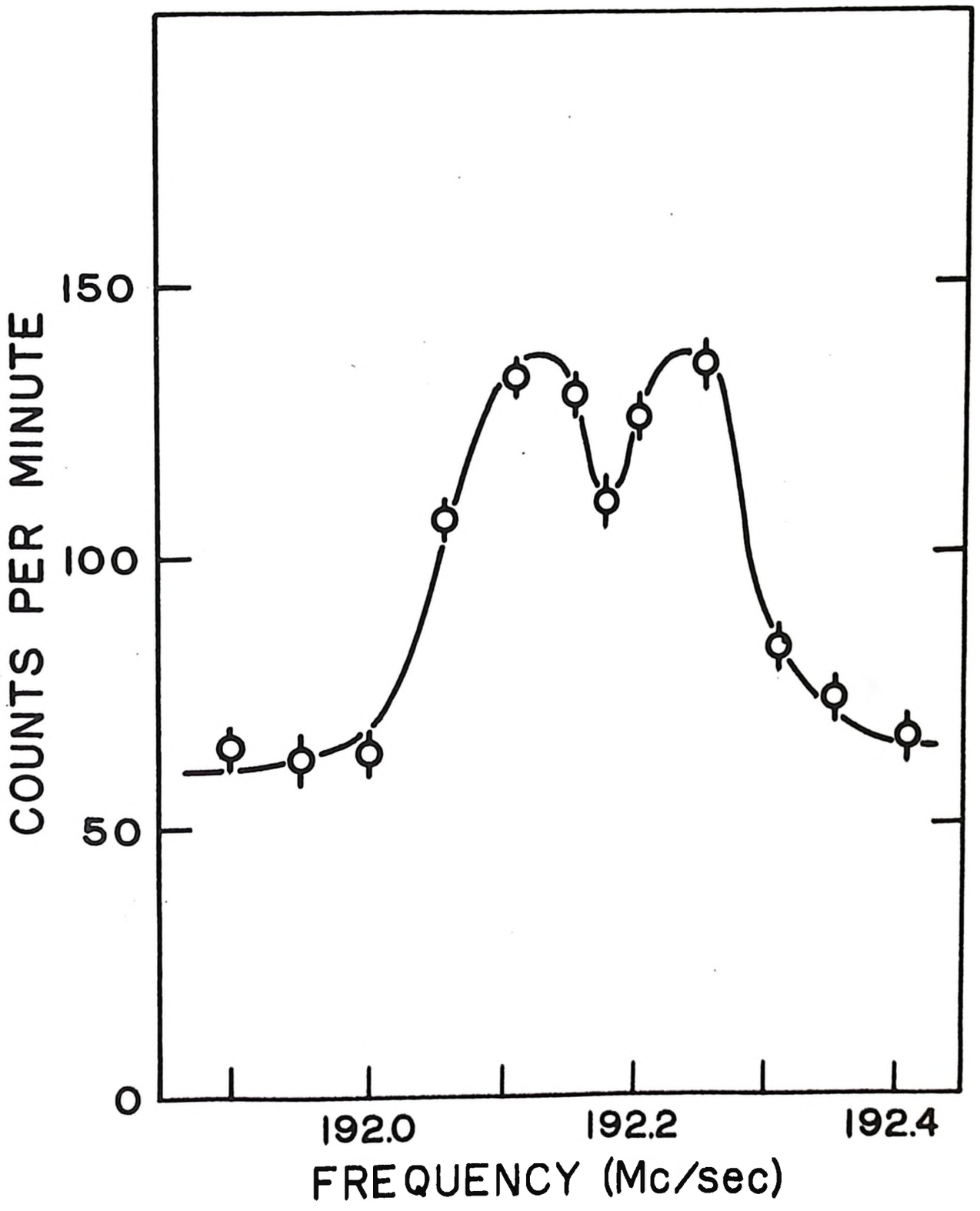
COUNTS PER MINUTE
150
100
50
0
192.0
192.2
192.4
FREQUENCY (Mc/sec)

Figure 23

TABLE VIII

The $\Delta F = \pm 1$ Transition $(2,0 \leftrightarrow 1,0)$ in $^2P_{3/2}$ In^{115m}

ν_{In} (Mc/sec)	ν_{Na} (Mc/sec)	H (gauss)	$\lvert a_{3/2} \rvert$ (Mc/sec)
192.85 ± .05	7.11 ± .02	10.03 ± .03	95.966 ± .025
192.35 ± .01	4.92 ± .01	6.97 ± .02	95.956 ± .010
192.18 ± .01	3.44 ± .02	4.87 ± .03	95.981 ± .010
192.02 ± .01	1.74 ± .02	2.48 ± .02	95.982 ± .010

of this resonance. The values of $|a_{3/2}|$ deduced from them agree reasonably, thus verifying the nature of the transition. Their average value is

$$|a_{3/2}| = 95.973 \pm 0.010 \text{ Mc/sec} .$$

After the shorted coaxial loop (Figure 14c) had been constructed resonances corresponding to the transition $(1,0 \leftrightarrow 0,0)$ in the $^2P_{1/2}$ electronic state could be observed. Their frequencies are shown in Table IX. The average value of $|a_{1/2}|$ deduced from these is

$$|a_{1/2}| = 904.348 \pm 0.016 \text{ Mc/sec} .$$

It is now possible to determine the sign of the interaction constants $a_{3/2}$ and $a_{1/2}$ and therefore of the nuclear magnetic moment. Only for a negative moment are the $\Delta F = 0$ transition frequencies consistent with those of the $\Delta F = \pm 1$ transitions. The final result is therefore

$$a_{1/2} = -904.348 \pm 0.016 \text{ Mc/sec}$$

and

$$a_{3/2} = -95.973 \pm 0.010 \text{ Mc/sec} .$$

The ratio of these measured values is in excellent agreement with those for In^{115} and In^{113} as is shown below:

	In^{113}	In^{115}	In^{115m}
$\frac{a_{3/2}}{a_{1/2}}$	0.106096 ± 0.000039	0.106124 ± 0.000001	0.106124 ± 0.000011

From the values of $a_{1/2}$ for In^{115m} and In^{115}, and using the Fermi-Segrè relationship, the ratio of the magnetic moments for the two isomers is

$$\frac{\mu_{115m}}{\mu_{115}} = -0.044034 \pm 0.0000008.$$

TABLE IX

The $\Delta F = \pm 1$ Transition $(1,0 \leftrightarrow 0,0)$ in $^2P_{1/2}$ In^{115m}

ν_{In} (Mc/sec)	ν_{Na} (Mc/sec)	H (gauss)	$\lvert a_{1/2} \rvert$ (Mc/sec)
904.36 ± .03	3.34 ± .01	4.75 ± .02	904.35 ± .03
904.36 ± .03	2.35 ± .01	3.35 ± .02	904.35 ± .03
904.35 ± .02	1.45 ± .05	2.06 ± .07	904.34 ± .02

Using the value $\mu_{115} = + 5.53441 \pm 0.00066$ nuclear magnetons (Ramsey 1956), it follows that

$$\mu_{115m} = - 0.243707 \pm 0.000026 \text{ nuclear magnetons}$$

where the largest part of the error arises from that in μ_{115}. This in turn depends on the uncertainty in the diamagnetic shielding correction. Since the P-state wave function of the indium atom vanishes at the origin, the hyperfine anomaly due to its overlap with the nucleus is expected to be small. For In^{115} and In^{113}, the anomaly, defined as in Chapter III, is

$$_{115}\Delta_{113} = 0.0014 \quad .$$

Such an anomaly between In^{115} and In^{115m} would lead to a change in the calculated moment value for In^{115m} of only 0.00003 nuclear magnetons.

b. In^{117m}

The first investigations of In^{117m} were carried out using sources prepared from natural cadmium. As a result, the 1.9-hour activity could not be produced without a contamination of In^{115m}. Underlying all the resonances in In^{117m} was a background of In^{115m}, giving rise to the composite decay curves already described and illustrated in Figure 20. In early experiments, both the ratio of the components and the half-life of the short-lived component were treated as adjustable parameters in order to establish the half-life of the short-lived part of the observed signals. Only when this had been determined to be about 2 hours and not 1 hour could one be certain that the observed signals were due to 1.9-hour In^{117m} and not to In^{117}. Henceforth, the decay curves were analyzed into 4.5-hour and 1.9-hour components, only the intercepts remaining to be found.

The presence in the background of the 4.5-hour component had the advantage of allowing ratio normalization of the beam intensity. Initial runs, at low values of the magnetic field, showed no variation in isotopic constitution at resonance. That is, resonances occurred at the same frequencies for the 4.5-hour and 1.9-hour activities. Such resonances were observed in a number of fields at frequencies corresponding to I = 1/2 in the $^2P_{1/2}$ electronic state. The result of one such run is shown in Figure 24. Such a resonance, taken alone, can not definitely be assigned to I = 1/2 since one of the resonances of I = 9/2 in the $^2P_{3/2}$ state (ν_-) occurs at the same frequency. The absence of a large signal at I = 9/2 in the more highly populated $^2P_{1/2}$ state does not clarify the situation since one might expect such a resonance to be greatly attenuated under the experimental circumstances (Goodman and Wexler 1955). However, resonances observed at higher frequencies, corresponding uniquely to I = 1/2 in the $^2P_{3/2}$ state, confirm that for In^{117m} the spin is 1/2. Table X summarizes the observed resonances and Figure 25 shows how they lead to an unambiguous spin assignment.

At higher values of the magnetic field, it was expected that the spin-1/2 resonances of In^{115m} and In^{117m} would separate in frequency due to a difference in their hyperfine structure constants. That this indeed occurred is shown in Figure 26, which gives the results of a run at 150 gauss. Table XI summarizes the data from the high-field runs in which $\Delta F = 0$ resonances were observed in the $^2P_{1/2}$ state of In^{117m}. The average value of $a_{1/2}$ from these is + 930.5 ± 1.3 Mc/sec or - 932.7 ± 1.3 Mc/sec. Again, because of the smallness of the nuclear moment, it is not possible to determine the sign of $a_{1/2}$ from the internal consistency of these data alone.

Figure 24. The results of an In^{117m} spin search in a field of 10 gauss. The half-integers along the top label the predicted positions of resonances for $^2P_{1/2}$ atoms with those spins. The solid circles indicate the observed total activity; the open circles, that which remains after subtraction of the 4.5-hour component.

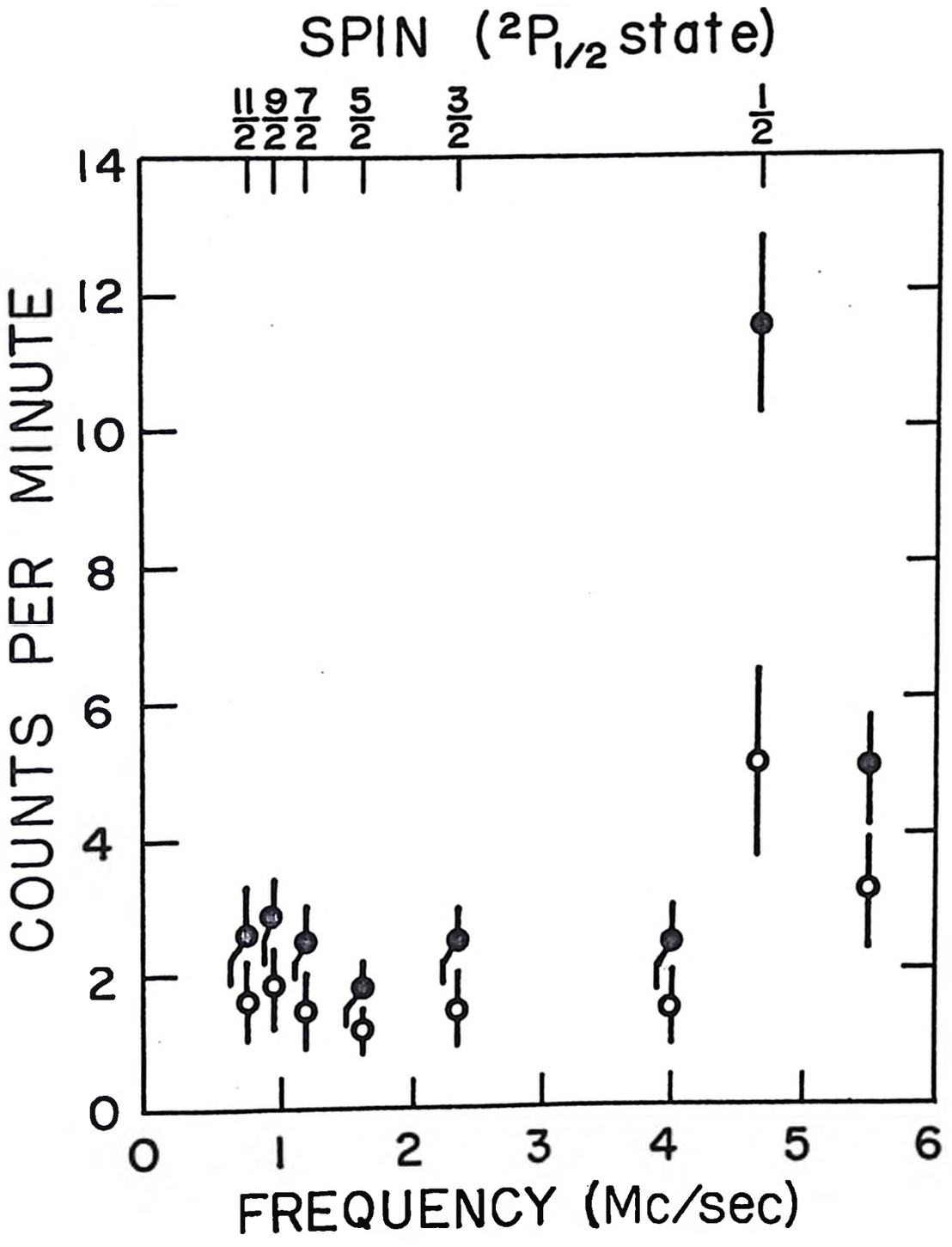
SPIN ($^2P_{1/2}$ state)
11/2
9/2
7/2
5/2
3/2
1/2
COUNTS PER MINUTE
0
2
4
6
8
10
12
14
0
1
2
3
4
5
6
FREQUENCY (Mc/sec)

Figure 24

TABLE X

Zeeman Resonances in In^{117m}

ν_{In} (Mc/sec)	ν_{Na} (Mc/sec)	ν_{In}: ν_{Na}
7.00	10.61	0.660:1
4.66	7.08	0.660:1
2.36	3.54	0.665:1
7.06	3.54	2.00 :1

Figure 25. Nuclear spin dependence of the $\Delta F = 0$ indium resonance frequencies in low magnetic fields for both the $^2P_{1/2}$ and $^2P_{3/2}$ electronic states. The hatched bars represent the observed resonance frequencies of In^{117m}. The only single spin value for which an interpretation of both resonances is possible is $I = 1/2$.

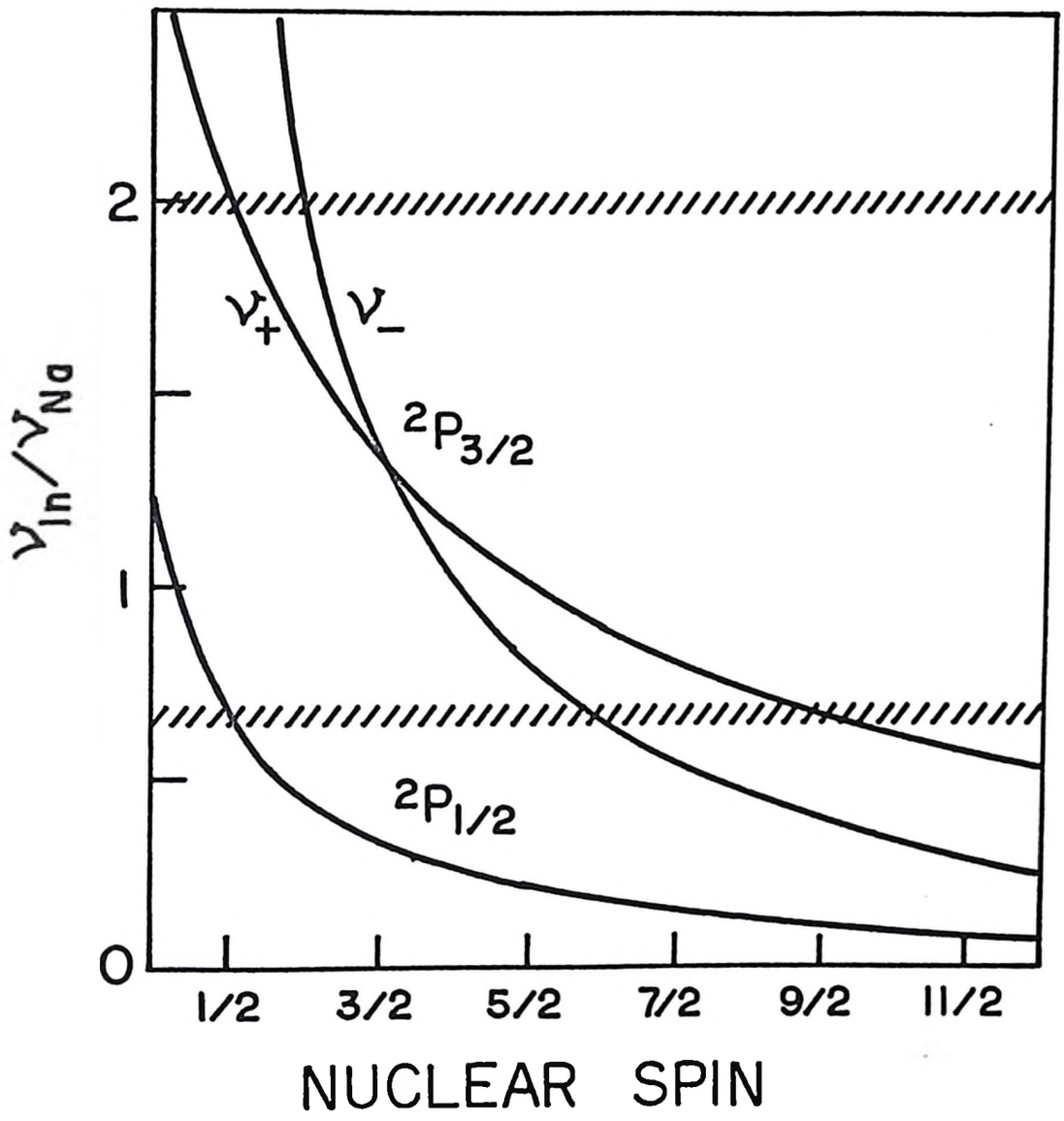

Figure 25

Figure 26. The $^2P_{1/2}$ $\Delta F = 0$ resonance in a field of 150 gauss. The open circles indicate the short-lived activity of each exposure; the solid circles, the 4.5-hour activity.

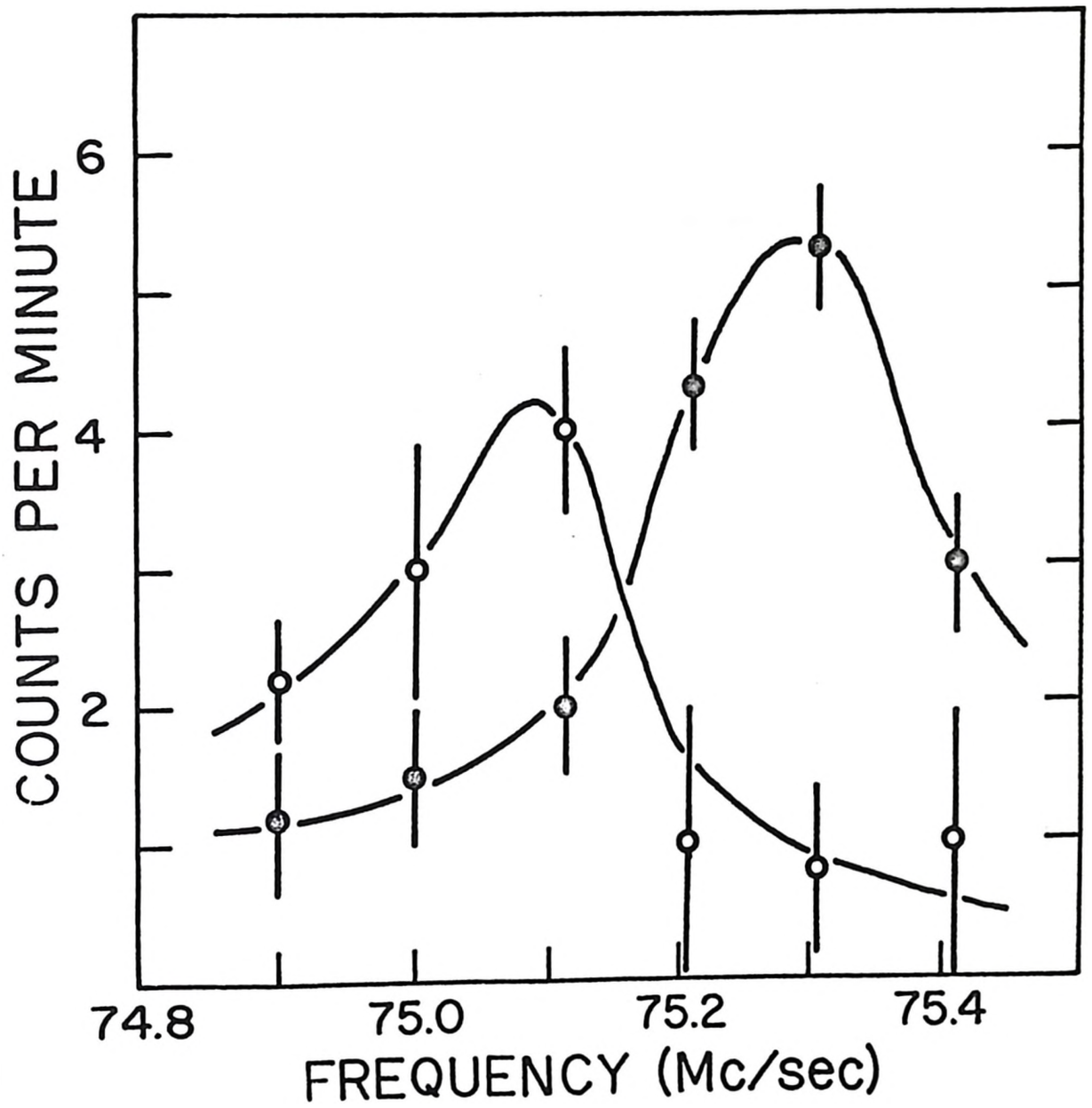

Figure 26

TABLE XI

The $\Delta F = 0$ Transition $(1,1 \leftrightarrow 1,0)$ in $^2P_{1/2}$ In^{117m}

ν_{In} (Mc/sec)	ν_{Na} (Mc/sec)	H (gauss)	$\lvert a_{1/2} \rvert$ (Mc/sec)	
			$\mu_I > 0$	$\mu_I < 0$
75.08 ± .05	125.91 ± .02	149.98 ± .02	931 ± 9	940 ± 9
131.10 ± .08	237.08 ± .01	250.02 ± .01	913 ± 5	917 ± 5
172.90 ± .10	330.62 ± .05	320.74 ± .04	928 ± 4	931 ± 4
287.95 ± .15	623.85 ± .05	499.96 ± .03	930.9 ± 2.5	932.9 ± 2.5
287.90 ± .10	623.65 ± .10	499.85 ± .05	930.6 ± 1.7	932.6 ± 1.7

A search for the $\Delta F = \pm 1$ transitions was undertaken, following the same methods as were used in the study of In^{115m}. However, due to the complicating effect of the In^{115m} background and the low abundance in the beam of atoms in the $^2P_{3/2}$ excited atomic state, no $\Delta F = \pm 1$ resonances were observed in this state. The search range in the $^2P_{1/2}$ state is still too large to make practicable a search for such resonances in that state. It was hoped that sources prepared from cadmium highly enriched in Cd^{116} would allow the $^2P_{3/2}$ hyperfine transition to be observed. However, after a number of unsuccessful searches, the study was terminated due to the high cost of the source material.

Using the known properties of In^{115} and the Fermi-Segrè formula, the magnetic moment of In^{117m} is either

$$+ 0.2508 \pm 0.0003 \quad \text{or}$$

$$- 0.2513 \pm 0.0003 \text{ nuclear magnetons.}$$

Although the experiment does not confirm the sign, nuclear systematics suggest choice of the negative sign.

c. In^{117}

The most elusive indium activity produced in the present study is that of the ground state of In^{117}. Measurement of its properties is always complicated by the unavoidable presence of the more abundant In^{117m}. Even half-life measurements are complicated in this way (McGinnis 1960b). Nevertheless, a preliminary investigation of the isotope was begun concurrently with the study of In^{117m}.

When the spin of In^{117m} was determined to be 1/2, that of the ground state could be strongly inferred. That its spin is large is indicated by the metastability of the spin-1/2 level. In addition, the systematic behaviour of the ground and metastable states of the odd-A indium isotopes

suggests that, as in the cases of In^{109}, In^{111}, In^{113} and In^{115}, the spin of the ground state should be 9/2, the shell model value. It was of interest to confirm the assignment with a direct measurement of the spin. It was also hoped that a measurement of the magnetic moment would follow. The difficulties of source production already mentioned, together with the properties of the hyperfine states, conspire to make such a measurement very difficult.

For nuclei with high spins, there are a large number of magnetic substates in the hyperfine levels, equally populated at all but very low temperatures. Only two of these are useful for producing an observable $\Delta F = 0$, $\Delta m = \pm 1$ resonance. Due to the statistical factor, a resonance at spin 9/2 will be a factor of 5 lower in intensity than one at spin 1/2.

A further difficulty arises because odd-proton nuclei with large angular momenta have associated with them large magnetic moments. As a result the dipole-dipole coupling between the nuclear and electronic spins is very strong. The magnetic field required to decouple the spins is consequently quite large. At the A- and B-magnet field strengths presently available, complete decoupling does not occur in the $^2P_{1/2}$ state and the values of μ_{eff} in the focusing fields are, for some magnetic substates, very much smaller than the electronic moment μ_J. This property causes a partial failure of the focusing system with a resulting decrease in resonance intensity. In the Zeeman region of the magnetic hyperfine structure, it is possible to make multiple quantum transitions to states of high μ_{eff}. The probability of such transitions is, of course, much smaller at low radiofrequency power than that for the single quantum jump.

An alternative possibility is to study the resonances in the $^2P_{3/2}$ electronic state. Here the hyperfine interaction is weaker and the decoupling is almost complete at available focusing field strengths. However, as has been mentioned previously, the population of the $^2P_{3/2}$ state is small at reasonable source temperatures.

A brief study of the low field $\Delta F = 0$ resonances in stable In^{115} indicated that, with the maximum available radiofrequency power in the loop obtained by matching with a tuned air-cored transformer, the intensities of the resonances in the $^2P_{1/2}$ and $^2P_{3/2}$ states were approximately equal at oven temperatures in excess of 1200°C. Conservation of source material, which is a strong consideration in the study of short-lived radioactive isotopes, dictates the use of a lower oven temperature. Therefore it appeared that the examination of multiple quantum transitions in the $^2P_{1/2}$ state would offer the greatest probability of success in the study of In^{117}.

A search was undertaken for the $^2P_{1/2}$ resonance using sources prepared from natural cadmium. Irradiation times were kept at two hours to minimize the In^{115m} contamination. The decay curves of all samples taken were analyzed for any activity of half-life shorter than 2 hours. Runs were made at C-magnet fields of 10, 15 and 20 gauss. When the material enriched in Cd^{116} became available, a fourth measurement was made at 36 gauss. Since little In^{115m} would be formed, an irradiation time of 6 hours was used. The results are accumulated in Figure 27, where the data represent estimates of the short-lived activity, together with the uncertainty in the analysis. For clarity, the results of the separate runs are displaced vertically and normalized frequency abscissae are used.

Figure 27. Summary of the spin search data for In^{117}. The points are "ratio normalized" to correct for variations in beam intensity using the In^{117m} and In^{113m} background.

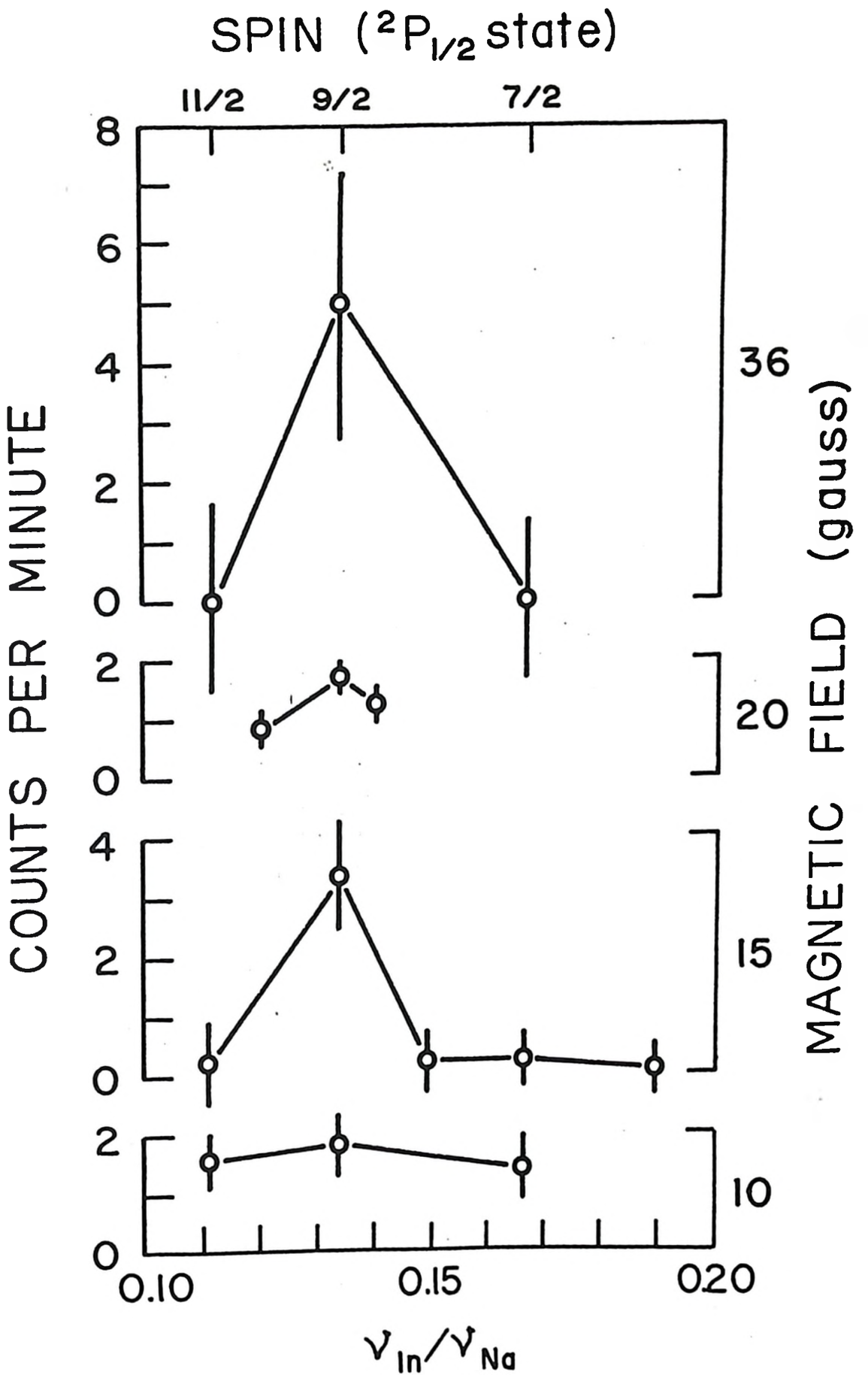
SPIN ($^2P_{1/2}$ state)
11/2
9/2
7/2
COUNTS PER MINUTE
MAGNETIC FIELD (gauss)
8
6
4
2
0
2
0
4
2
0
2
0
36
20
15
10
0.10
0.15
0.20
ν_{In}/ν_{Na}

Figure 27

The frequencies corresponding to $\Delta F = 0$ transitions in the $^2P_{1/2}$ state for spins 11/2, 9/2 and 7/2 are shown at the top. Although the statistical uncertainties are large, in each case there is a slight increase in the short-lived component of the beam at the frequency corresponding to I = 9/2. In the runs at 15 and 36 gauss, the increase is outside the summed errors of the points. It seems justifiable to conclude that the spin of some short-lived component of the beam is 9/2.

A best estimate of the half-life of the short-lived component taken from the data at 15 and 36 gauss, is 1.0 ± 0.3 hours. This is consistent with the measured value of 45 minutes for In^{117}. Since there is no reason to expect any other activity of comparable half-life in the beam, the assignment I = 9/2 is made to that isotope.

Because of the difficulty encountered in the spin determination, even with enriched source material, it is clear that a magnetic moment measurement will be a marginal experiment. With increased radiofrequency power and more counting equipment so full use could be made of the radioactive samples to obtain better counting statistics, it may become feasible.

CHAPTER VI

DISCUSSION OF RESULTS AND CONCLUSIONS

The magnetic moments of In^{115m} and In^{117m} measured in the course of this investigation are in general agreement with the Schmidt moment for a single $p_{1/2}$ proton. This fact confirms the shell model interpretation of the isomerism in the odd-A indium isotopes. The even parity spin 9/2 ground states are assumed to arise from a single hole in the $g_{9/2}$ proton shell since the indium nucleus is just one proton short of the magic number fifty. The metastable isomers are then supposed to be formed by the promotion of a proton from the neighbouring $p_{1/2}$ level to fill the $g_{9/2}$ shell, leaving a single unpaired $p_{1/2}$ proton.

A survey of all the measured $p_{1/2}$ proton moments, however, reveals a small but interesting systematic variation. The measured moments for $g_{9/2}$ and $p_{1/2}$ odd proton nuclei in the range $28 < Z < 50$ are shown in Table XII and illustrated graphically in Figure 28.

Configuration mixing of the type considered by Arima and Horie (Arima and Horie 1954) and discussed in Chapter II is unable to account for the observed variations among the $p_{1/2}$ nuclei. To first order, all corrections to the single particle moment vanish in this case. The deviation of the magnetic moments of the yttrium-rhodium-silver group from the Schmidt value has been attributed to meson quenching effects. However, as Miyazawa has pointed out (Miyazawa 1951), such a quenching, either of the anomalous part of the spin moment, or of the effective charge, is expected

TABLE XII

Magnetic Moments of 9/2+ and 1/2- Odd Proton Nuclei, $28<Z<50$

9/2+		
Nucleus	Magnetic Moment (Nuclear Magnetons)	Reference
Nb^{93}	+ 6.167	Sheriff and Williams 1951
Tc^{99}	+ 5.680	Walchli et al. 1952
In^{109}	+ 5.53	Marino 1959
In^{111}	+ 5.53	Marino 1959
In^{113}	+ 5.523	Proctor and Yu 1951
In^{115}	+ 5.534	Ting and Williams 1953

1/2-		
Nucleus	Magnetic Moment (Nuclear Magnetons)	Reference
Y^{89}	- 0.137	Brun et al. 1954
Y^{91}	(-) 0.164	Petersen and Shugart 1962
Rh^{103}	- 0.089	Walchli 1955
Ag^{105}	(-) 0.101	Ewbank 1959
Ag^{107}	- 0.114	Brun et al. 1954
Ag^{109}	- 0.131	Brun et al. 1954
Ag^{111}	- 0.145	Woodgate and Hollwarth 1956
Ag^{113}	(-) 0.159	Chan and Shugart 1962
In^{113m}	- 0.211	Childs and Goodman 1960
In^{115m}	- 0.244	This Work
In^{117m}	(-) 0.251	This Work

Figure 28. Magnetic moments of the odd-Z spin-9/2 and spin-1/2 nuclei for $28 < Z < 50$. The dashed lines indicate the Schmidt values.

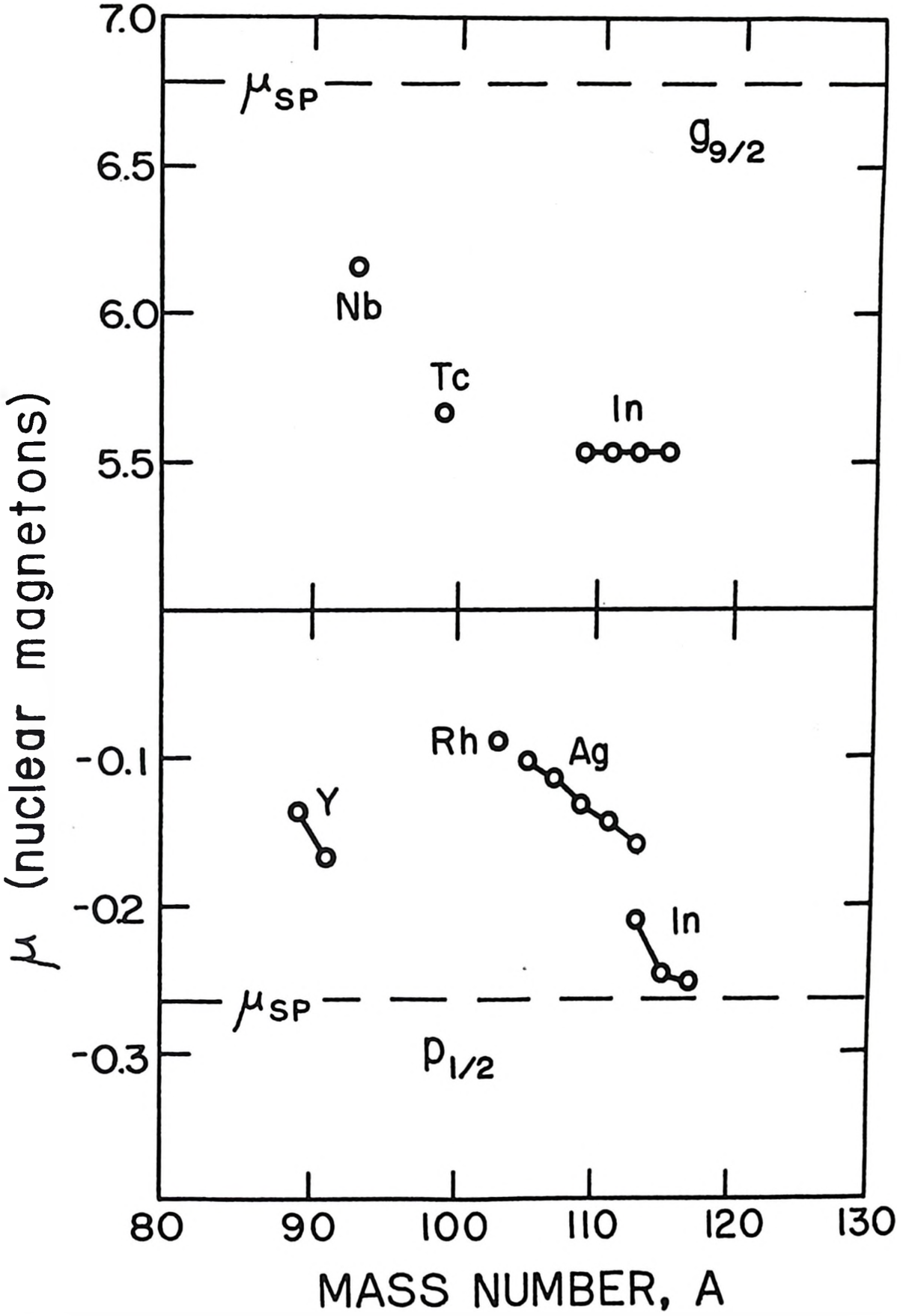
7.0
6.5
6.0
5.5
-0.1
-0.2
-0.3
μ (nuclear magnetons)
μSP
g9/2
Nb
Tc
In
Rh
Ag
Y
In
μSP
p1/2
80
90
100
110
120
130
MASS NUMBER, A

Figure 28

to be almost complete at mass 20 to 30 and to vary only slowly with mass thereafter. This fact reflects the near constant density of nuclear matter. The rapid trend of the magnetic moments of the silver and indium isotopes toward more negative values can not be explained in terms of such a meson theory. It is, nevertheless, known that such mesonic effects exist and must contribute significantly to the static properties of the nucleus. It is therefore meaningful to calculate the change from the single particle moment to be expected in $p_{1/2}$ nuclei. Recent calculations using dispersion theory (Drell and Walecka 1960) indicate a reduction in the anomalous part of the nucleon moment of somewhat less than 10 per cent. Applied to the $p_{1/2}$ proton, this would alter the single particle magnetic moment by + 0.04 nuclear magnetons. Reduction of the effective charge of the proton by 10 per cent would cause a change of - 0.03 nuclear magnetons. With the present state of meson theory, these are no more than order-of-magnitude estimates. In this spirit then, the remainder of the Chapter will be devoted to a search for mechanisms which might cause the observed trends in moments and which require a single particle moment only slightly different from the Schmidt value.

Configurations containing excited states of the normally spherical even-even core can couple with the single particle proton states to give a final configuration of spin 1/2 and odd parity whose magnetic moment may differ considerably from the single particle value. Core configurations of zero angular momentum do not affect the magnetic moment. Those of spin 1 and even parity may couple with the $p_{1/2}$ state directly, or with the spin-orbit partner state $p_{3/2}$ which is only slightly removed in energy within the same major shell. Core states of higher spin and even parity may couple with both the $p_{3/2}$ and the $f_{5/2}$ proton states.

1. CONFIGURATIONS WITH CORE SPIN R = 1

In the nuclei considered here, from yttrium to indium, the neutrons near the Fermi surface are in the first part of the 50 to 82 neutron shell. In the lighter nuclei, yttrium to rhodium, the $d_{5/2}$ and $g_{7/2}$ levels are at the surface, while, for silver and indium, the $s_{1/2}$ and $d_{3/2}$ levels are being filled together with the odd parity $h_{11/2}$ level. Since there is a relatively large energy gap between the $g_{7/2}$ and the $s_{1/2}$ levels, one suspects that excited neutron configurations would be of the type $(d_{5/2}{}^{-1}g_{7/2})_R$ and $(s_{1/2}{}^{-1}d_{3/2})_R$ for the lighter and heavier nuclei respectively.

It is of interest to point out that the states with R = 1 indicated above do give positive corrections to the $p_{1/2}$ proton moment. Such a correction is in fact larger for the $(d_{5/2}{}^{-1}g_{7/2})_1$ configuration than for the $(s_{1/2}{}^{-1}d_{3/2})_1$ configuration. However, the admixture amplitudes required to account in this way for the observed magnetic moments are rather large. The most serious objection comes from the analysis of the level schemes of nearby even-even nuclei. The absence at low energy of any levels which could be assigned the spin and parity 1+ casts serious doubt on the above picture. In order to maintain the 1+ configurations in odd-proton nuclei, even though they are not found among the low-lying levels of the even-even nuclei, one is forced to assume a strong neutron-proton interaction. The strength required of such an interaction would depend on the degree of overlap of the $p_{1/2}$ proton wave function with the core wave functions. No calculations of the effects of the inclusion of a residual neutron-proton pairing force have been carried out for heavy nuclei.

2. CONFIGURATIONS WITH CORE SPIN R = 2

The level schemes of the even-even nuclei in the mass region 100 to 120 are characterized by excited states 2+ and 0, 2, 4+ with large but regular spacing. This behaviour is interpreted as being characteristic of collective quadrupole vibrations of the normally spherical nucleus. It is therefore reasonable to assume that such phonons would modify the single particle wave functions of the ground states of odd-A nuclei and hence alter their magnetic moments. The result of such a calculation using perturbation theory was indicated in Chapter II. No direct coupling of the $p_{1/2}$ particle with the 2+ surface state occurs in 1/2- nuclei. However, interaction with the $p_{3/2}$ and $f_{5/2}$ states gives rise to a magnetic moment change

$$\mu - \mu_{SP} = x^2 \frac{2}{5} (1 - g_R) \left[\left(\frac{\hbar\omega}{\hbar\omega + \Delta_{5/2}} \right)^2 - \left(\frac{\hbar\omega}{\hbar\omega + \Delta_{3/2}} \right)^2 \right],$$

where $\hbar\omega$ is the phonon energy, $\Delta_{5/2}$ and $\Delta_{3/2}$ are the single particle excitation energies from the $p_{1/2}$ state to the $f_{5/2}$ and $p_{3/2}$ states respectively, x^2 is the coupling strength, and g_R is the core gyromagnetic ratio. Using the value

$$g_R = Z/A \approx 0.44$$

and the single particle energies calculated by Nilsson for zero deformation (Nilsson 1955), an expression for $(\mu - \mu_{SP})$ may be obtained. The result increases slowly with $\hbar\omega$ up to a maximum of about 0.2 x^2 nuclear magnetons at $\hbar\omega \approx 2$ Mev, after which it decreases to zero for very large phonon energies.

If the phonon energies are chosen equal to the excitation energies of the first excited states of neighbouring even-even nuclei, a decrease in $(\mu-\mu_{SP})$ is predicted for increasing neutron number through most of the 28-50 proton shell. This can be matched to the observed trend by choosing $x^2 \approx 2$. According to Bohr and Mottelson, such a value would correspond to intermediate coupling between the surface and particle motions. Although the indium isotopes are near the closed shell at Z = 50, intermediate coupling may be justified since the quadrupole moments observed in the $g_{9/2}$ ground states of In^{109}, In^{111}, In^{113} and In^{115} are several times larger than the single particle shell model value. However, to explain these quadrupole moments only requires $x^2 \approx 0.3$ (Bohr and Mottelson 1953).

The calculations of Kisslinger and Sorensen give similar results but indicate a reduction in the coupling of particle to surface from the Bohr-Mottelson calculation (Kisslinger and Sorensen 1960). This would require a further increase in the coupling parameter x^2. At this point, the perturbation approximation is probably no longer valid.

Variations of the magnetic moment which are difficult to calculate arise from changes in g_R. Since the collective vibration is primarily a motion of the nuclear surface, the value of g_R chosen should perhaps be altered somewhat from the value Z/A. In the region of nuclei studied here, relatively few proton holes but many neutrons take part in the surface motion. This would indicate a substantial reduction of g_R. Such an effect should vary rapidly with proton number but only slowly with the number of neutrons. If configurations of neutron pairs with spin 2+ are mixed with the collective motion, their magnetic moments would further modify the value of g_R and hence the magnetic moment predicted by the model.

The positions of the excited levels in the odd proton nuclei may be taken as indicative of the single proton excitation energies $\Delta_{3/2}$ and $\Delta_{5/2}$. The levels in the odd-A indium isotopes should be particularly useful in this regard. However, if the level schemes adopted by the Nuclear Data Group in Washington (McGinnis 1960a, 1960c) are taken seriously, the relative positions of the $f_{5/2}$ and $p_{3/2}$ levels change even within the group of indium isotopes. This variation is presumably an effect of the core motions on the single proton wave function. Since the calculated magnetic moment deviation is sensitive to the difference in these excitation energies, uncertainty in their evaluation makes the calculation very approximate.

3. SUMMARY

The systematic data presently available for $p_{1/2}$ nuclei indicate the need for a critical revaluation of the nuclear theories as they apply to magnetic moments. The values obtained in this investigation for the magnetic moments of In^{115m} and In^{117m}, together with the previous measurements of the magnetic moments of In^{113m} and of the silver, rhodium and yttrium isotopes, show the need for more detailed calculations of the type outlined above. The most fruitful avenue of approach would seem to be the study of the interaction of collective and particle motions. Detailed calculations will require, however, more information about the level schemes of the odd-proton nuclei in the 28-50 shell.

BIBLIOGRAPHY

Arima, A. and Horie, H. 1954. Progr. Theoret. Phys. (Japan) 11, 509.

Baker, F. S. 1960. University of California Lawrence Radiation Laboratory Report UCRL-9364.

Baker, F. S. and Brink, G. O. 1962. University of California Lawrence Radiation Laboratory Report UCRL-6772.

Bellamy, E. H. and Smith, K. F. 1953. Phil. Mag. 44, 33.

Belyaev, S. T. 1959. Kgl. Danske Videnskab. Selskab, Mat.-fys. Medd. 29, No. 16.

Bishop, C. T. 1961. Argonne National Laboratory Report, ANL-6405.

Bloch, F., Hansen, H. and Packard, M. 1946. Phys. Rev. 69, 127; Phys. Rev. 70, 474.

Bohr, A. and Mottelson, B. R. 1953. Kgl. Danske Videnskab. Selskab, Mat.-fys. Medd. 27, No. 16.

Breit, G. and Rabi, I. I. 1931. Phys. Rev. 38, 2082.

Brennan, M. H. and Bernstein, A. M. 1960. Phys. Rev. 120, 927.

Brun, E., Oeser, H., Staub, H. H. and Telschow, C. G. 1954. Phys. Rev. 93, 904.

Case, K. M. 1953. Introduction to the Theory of Neutron Diffusion, Vol. 1 (Los Alamos Scientific Laboratory).

Chan, Y. W. and Shugart, H. A. 1962. Private communication.

Childs, W. J. and Goodman, L. S. 1960. Phys. Rev. 118, 1578.

Drell, S. D. and Walecka, J. D. 1960. Phys. Rev. 120, 1069.

Ehlers, V. J. 1960. University of California Lawrence Radiation Laboratory Report UCRL-9123.

Ewbank, W. B. 1959. University of California Lawrence Radiation Laboratory Report UCRL-8756.

Freed, N. and Kisslinger, L. S. 1961. Nuclear Phys. 25, 611.

Frisch, R. O. and Segre, E. 1933. Z. Physik 80, 610.

Gleit, C. E. 1958. Ph.D. Thesis, Massachusetts Institute of Technology.

Goodman, L. S. 1960. Rev. Sci. Instr. 31, 1351.

Goodman, L. S. and Wexler, S. 1955. Phys. Rev. 100, 1245.

King, H. J. 1960. Ph.D. Thesis, McMaster University.

King, H. J., Cameron, J. A., Eastwood, H. K. and Summers-Gill, R. G. 1961. Can. J. Phys. 39, 230.

Kinslinger, L. S. and Sorensen, R. A. 1960. Kgl. Danske Videnskab. Selskab, Mat.-fys. Medd. 32, No. 9.

Kopfermann, H. 1958. Nuclear Moments (Trans. E. E. Schneider, Academic Press, New York).

Kruse, U. E. and Ramsey, N. F. 1951. J. Math. Phys. 30, 40.

LeBlanc, J. M. 1957. Ph.D. Thesis, University of Michigan.

Lee, T. D. and Yang, C. N. 1956. Phys. Rev. 104, 254.

Majorana, E. 1932. Nuovo cimento 9, 43.

Marino, L. L. 1959. University of California Lawrence Radiation Laboratory Report UCRL-8721.

Mayer, M. G. and Jensen, J. H. D. 1955. Elementary Theory of Nuclear Shell Structure (Wiley, New York).

McGinnis, C. L. 1960a. Nuclear Data Sheets NRC 60-3-104.

McGinnis, C. L. 1960b. Nuclear Data Sheets NRC 60-3-131.

McGinnis, C. L. 1960c. Nuclear Data Sheets NRC 60-2-99.

Miyazawa, H. 1951. Progr. Theoret. Phys. (Japan) 6, 801.

Nilsson, S. G. 1955. Kgl. Danske Videnskab. Selskab, Mat.-fys. Medd. 29, No. 16.

Nordheim, L. 1951. Revs. Mod. Phys. 23, 322.

Petersen, F. R. and Shugart, H. A. 1962. University of California Lawrence Radiation Laboratory Report UCRL-10169.

Proctor, W. G. and Yu, F. C. 1951. Phys. Rev. 81, 20.

Purcell, E. M., Torrey, H. and Pound, R. V. 1946. Phys. Rev. 69, 37.

Rabi, I. I. and Cohen, V. W. 1933. Phys. Rev. 43, 582.

Rabi, I. I., Zacharias, J. R., Millman, S. and Kusch, P. 1938. Phys. Rev. 53, 318.

Ramsey, N. F. 1956. Molecular Beams (Oxford University Press).

Ramsey, N. F. and Purcell, E. M. 1950. Phys. Rev. 78, 807; Smith, J. H., Purcell, E. M. and Ramsey, N. F. Phys. Rev. 108, 120 (1957).

Schmidt, T. 1937. Z. Physik 106, 358.

Schwartz, C. 1955. Phys. Rev. 97, 380.

Sheriff, H. E. and Williams, D. 1951. Phys. Rev. 82, 651.

Stern, O. 1921. Z. Physik 7, 249; Gerlach, W. and Stern, O. Z. Physik 9, 353 (1922).

Ting, Y. and Williams, D. 1953. Phys. Rev. 89, 595.

Walchli, H. E., Livingston, R. and Martin, W. J. 1952. Phys. Rev. 85, 479.

Walchli, H. E. 1955. Oak Ridge National Laboratory Report ORNL-1469, Supplement 2.

Westcott, C. H. 1958. Atomic Energy of Canada Limited, Chalk River Report AECL-670.

Wexler, S. 1958. Revs. Mod. Phys. 30, 402.

Woodgate, G. K. and Hellwarth, R. W. 1956. Proc. Phys. Soc. (London) A69, 511, 588.

Wu, C. S., Ambler, E., Hayward, R. W., Hoppes, D. D. and Hudson, R. P. 1957. Phys. Rev. 105, 1413.

Zacharias, J. R. 1942. Phys. Rev. 61, 270.